INVESTIGATING CYTOSKELETAL REGULATION OF IGE RECEPTOR SIGNALING BY MICROPATTERNED LIGAND ARRAYS

A Dissertation

Presented to the Faculty of the Graduate School

of Cornell University

in Partial Fulfillment of the Requirements for the Degree of

Doctor of Philosophy

by

Alexis J. Torres

February 2010

INVESTIGATING CYTOSKELETAL REGULATION OF IGE RECEPTOR SIGNALING BY MICROPATTERNED LIGAND ARRAYS

Alexis J. Torres, Ph.D.

Cornell University 2010

The high affinity immunoglobulin E (IgE) receptor (FcεRI) is a member of a family of related antigen receptors with conserved structure and similar roles in initiating intracellular signaling in response to an outside stimulus. In mammalian cells, FcεRI is found primarily on the surface of mast cells and basophils. Activation of this receptor by multivalent antigen triggers a series of intracellular signaling events that ultimately lead to the secretion of preformed mediators, such as histamine and serotonin, which are responsible for allergic reactions. Our recent efforts in the study of immunoreceptor signaling have focused on the participation of the plasma membrane and the actin cytoskeleton. However, tools for investigating biomolecular dynamics and interactions that occur within close proximity to the plasma membrane of living cells are somewhat limited.

Micro-fabricated surfaces have been used for applications in cell and tissue engineering, although their full potential has not been explored, particularly in the area of molecular cell biology. We have recently developed a polymer lift-off method for localizing the initial stimulus to micron size patches of antigens such that assembly of signaling components could be visualized with selective fluorescent labeling and confocal microscopy. Employing these technologies we have investigated fundamental mechanisms in immune cell signaling, specifically IgE receptor (FcεRI) signaling involved in allergic responses on mast cells. In past years, our group has observed spatially and temporally resolved responses, including receptor phosphorylation, selective accumulation of Lyn kinase and other membrane components.

In this work, I have applied these tools to investigate functional and structural implications of the actin cytoskeleton regulation of FcεRI signaling and the cytoskeletal dependence of activated receptor internalization. I have shown that particular actin binding proteins, paxillin, talin and vinculin co-redistribute at the patterned antigen and clustered receptors in a similar time course as polymerized actin. These proteins have been extensively characterized in the context of integrin signaling and focal adhesion assembly, but little is known about their involvement in immune cell signaling. Our biochemical data suggests that these proteins have functional relevance in some of the early and late events of the signaling cascade. In addition, I show that the GTPase dynamin 2, which is commonly associated with receptor endocytosis, is selectively recruited to the sites of receptor clustering. Protein knock-down of dynamin 2 decreases the accumulation of F-actin at the clustered receptors, implicating dynamin in the regulation of FcεRI mediated actin redistribution. These results point a possible role for dynamin-actin interactions in regulating activated IgE-FcεRI internalization.

BIOGRAPHICAL SKETCH

Alexis J. Torres was born March 13th, 1981 in San Juan, Puerto Rico. He received the Bachelor of Science in Chemistry from the University of Puerto Rico, Rio Piedras, in 2003. As an undergraduate student, he conducted research as part of Howard Hughes Undergraduate Research Program (2000-2001) and National Institute of Health-Minority Access to Research Careers (NIH-MARC) Program (2001-2003) at the University of Puerto Rico, Rio Piedras. In addition, he participated in Research Experience for Undergraduates (REU) Program at the University Michigan, Ann Arbor in summer 2002. During this time, he received several awards including Warner Lambert Pharmaceutical Honor Scholarship (1999-2000), Robert C. Byrd Honor Scholarship (1999-2003) and Merck and Co. Honors Award (2003). A year prior to his graduate studies, he worked as a research assistant for Dr. Jose A. Lasalde at the University of Puerto Rico, Rio Piedras. He started his MS/PhD studies at the Chemistry and Chemical Biology Department at Cornell University under the guidance of Dr. Barbara Baird in Fall 2004.

To my wife, Jeisa

ACKNOWLEDGMENTS

This work would have not been completed without the mentoring and encouragement of my advisor, Barbara Baird. Her guidance was invaluable to my research and I am truly grateful for that. My gratitude also goes to David Holowka for his help, guidance and support. Special thanks to my committee members, Manfred Lindau and Peng Chen, for their contributions and helpful insights.

Thanks to the Baird-Holowka group members for their friendship and support. Special thanks to Lavanya, Kirsten, Kari and Alice for assisting me in carrying out various experiments. Min Wu was incredibly helpful during my first year in graduate school. She mentored me and shared her knowledge and technical expertise.

I am grateful for the opportunity of being able to collaborate with the Lindau group and Craighead group in the Applied and Engineering Physics Department. Special thanks to Khajak Berberian and Jose M. Moran-Mirabal for working by my side in collaborative research and sharing their expertise.

I want to thank my great friends in Ithaca, Nelson, Felipe, Annie, Karen and Rits, for sharing so many amazing moments with me winter after winter. Thanks to my mother-in-law and sister-in-law, Eva and Yaira, for their enjoyable visits every six months. I deeply thank my parents and brother, Elias, Ivonne and Manuel, without whom I would not be here and for their unconditional support. Finally, I want to thank my beloved wife, Jeisa, for making every day in Ithaca truly wonderful.

TABLE OF CONTENTS

LIST OF FIGURES

LIST OF ABBREVIATIONS

BSA	bovine serum albumin
BSS	buffered saline solution
DNP	2,4-dinitrophenyl
DNP-cap-PE	Dipalmitoyl-*sn*-Glycero-3-Phosphoethanolamine-N-[6-[(2,4-dinitrophenyl)amino]caproyl]
ECM	extracellular matrix
EGFP	enhanced green fluorescent protein
FcεRI	high affinity receptor for immunoglobulin E
FITC	fluorescein isothiocyanate
GFP	green fluorescent protein
ICS	image correlation spectroscopy
IgE	immunoglobulin E
IP_3	Inositol 1,4,5-triphosphate
ITAM	immunotyrosine based activation motif
PBS	phosphate buffered saline
PKC	protein kinase C
PLCγ	phospholipase Cγ
POPC	1-Palmitoyl-2-oleoyl-sn-glycero-3-phosphocholine
RBL	rat basophilic leukemia
TCR	T cell receptor

CHAPTER 1[1]

INTRODUCTION

1.1 Cell biology and the opportunities of nanobiotechnology.

The subject of cell biology covers the hierarchical organizations of diverse biomolecular constituents that enable cells to maintain homeostasis in a particular biological environment and to respond appropriately to external signals. A remarkable example is the receptor (FcεRI) for immunoglobulin E (IgE) on mast cells that operates in the allergic immune response. Multivalent ligand (e.g. an inhaled allergen) binding to and clustering cell surface IgE receptors initiates a transmembrane signal, stimulating intracellular pathways that lead to a number of cellular responses including gene transcription and secretion of chemical mediators. The secreted molecules typically interact with other cells in the surrounding tissues resulting in systemic changes. This example illustrates the remarkable efficiency with which biology integrates response mechanisms over multiple length scales: the nanoscale encounter of allergen and receptor initiates a response that cascades through collective interactions over micrometers in the cell and increasing length scales beyond, ultimately to the macroscale system of the human being. In recent years, many laboratories have investigated signal transduction pathways that are stimulated in a large variety of physiologically relevant cell types, and, by incorporating genetic, biochemical, and physical approaches, key enzymes as well as regulatory structures and mechanisms have been defined. However, the necessary spatial arrangements and regulation are difficult to approach with many current methods. Although advances in genetically encoded fluorescence tags, such as green fluorescent protein (GFP), and

[1] Part of this chapter has been published previously in *Annual Review of Biophysics* ***37***, 265-288.

fluorescence microscopy allow distributions and some dynamics of particular components to be monitored, spatial resolution is limited by the diffraction of light (~ 250 nm) and cellular autoflorescence. Usually more limiting are morphological heterogeneities that confound interpretations of fluorescence images. Other challenges include heterogeneities in the local environment and in properties of the stimuli that tend to increase experimental variables. Micro- and nanofabrication techniques provide spatial and chemical control at the cellular level. Combined with other approaches, these fabrication methods offer a powerfully expanded set of tools for addressing the complexities of cell biology.

Micro- and nanofabrication tools emerged in large part from the realms of electrical engineering and materials science. Photolithography and other methods developed for reducing the size of electronic devices are now able to reach easily into submicron length scales, the same regimes within which biomolecules are organized in cells. Advances in materials science include biocompatible polymers and modified surfaces developed in part for effective engineering of tissues and physiological implants. Together with fabrication methods, materials can be designed with chemical features that resemble spatial cues sensed by cells or, alternatively, can interfere selectively with those cues. The field of nanotechnology usually focuses on materials properties and manipulations corresponding to length scales of 1 - 100 nm. The realm of nanobiotechnology appropriately extends beyond 100 nm and upward to the micron scale, so as to consider biomolecular structures operating collectively within a living cell: the cellular structures are built from biomolecules and provide the relevant context. Thus, the convergence of nanobiotechnology (that includes both fabrication and chemical modification on cellular and biomolecular length scales) with the more standard biochemical and biophysical tools provide exciting new opportunities for cellular investigations.

1.2 Micro- and nano-fabrication for surface patterning.

Modern fabrication technology is based primarily on the principles of lithography: top-down techniques to pattern features on a surface starting from bulk material. Micro and nano-fabrication (reviewed in (*1*)) was particularly advanced by the semiconductor and integrated circuits industry to produce electronic components with designed features of increasingly small size. Photolithography is most amenable to patterning surfaces for spatially controlled interactions with cells that can be visualized and analyzed. Useful feature dimensions range from a few hundred nanometers (as limited by the wavelength of light) to several or tens of micrometers (the size of cells).

The basic photolithographic method generates patterns on a surface (typically a silicon wafer) coated with a photoresist by selectively irradiating the surface with light through a pre-designed mask (figure 1.1a). The mask contains the features of desired shapes and sizes in an opaque material on a transparent background. UV light shining through the transparent regions of the mask changes the chemical composition of the photoresist, making it soluble (positive) or insoluble (negative) to particular organic solvents. After exposure, unprotected sites can be either chemically or dry etched, and subsequent processing steps yield surfaces that have two (or more) patterned regions for distinctive chemical modification or construction of topographical features. Depending on the cell biology application, the fabricated surface regions that provide spatial control need to be selectively modified with materials that are biocompatible and provide chemical control.

The challenge of transforming microfabricated surfaces for effective interfacing with cells has been addressed by adapting the fabrication and the chemical modification schemes. Below we discuss one fabrication approach that has proven particularly useful for investigating cell interactions: polymer lift-off. Other

Figure 1.1: Schematic diagram of methods used in micro-fabrication. a) Conventional Photolothography b) Polymer lift-off c) Microcontact printing.

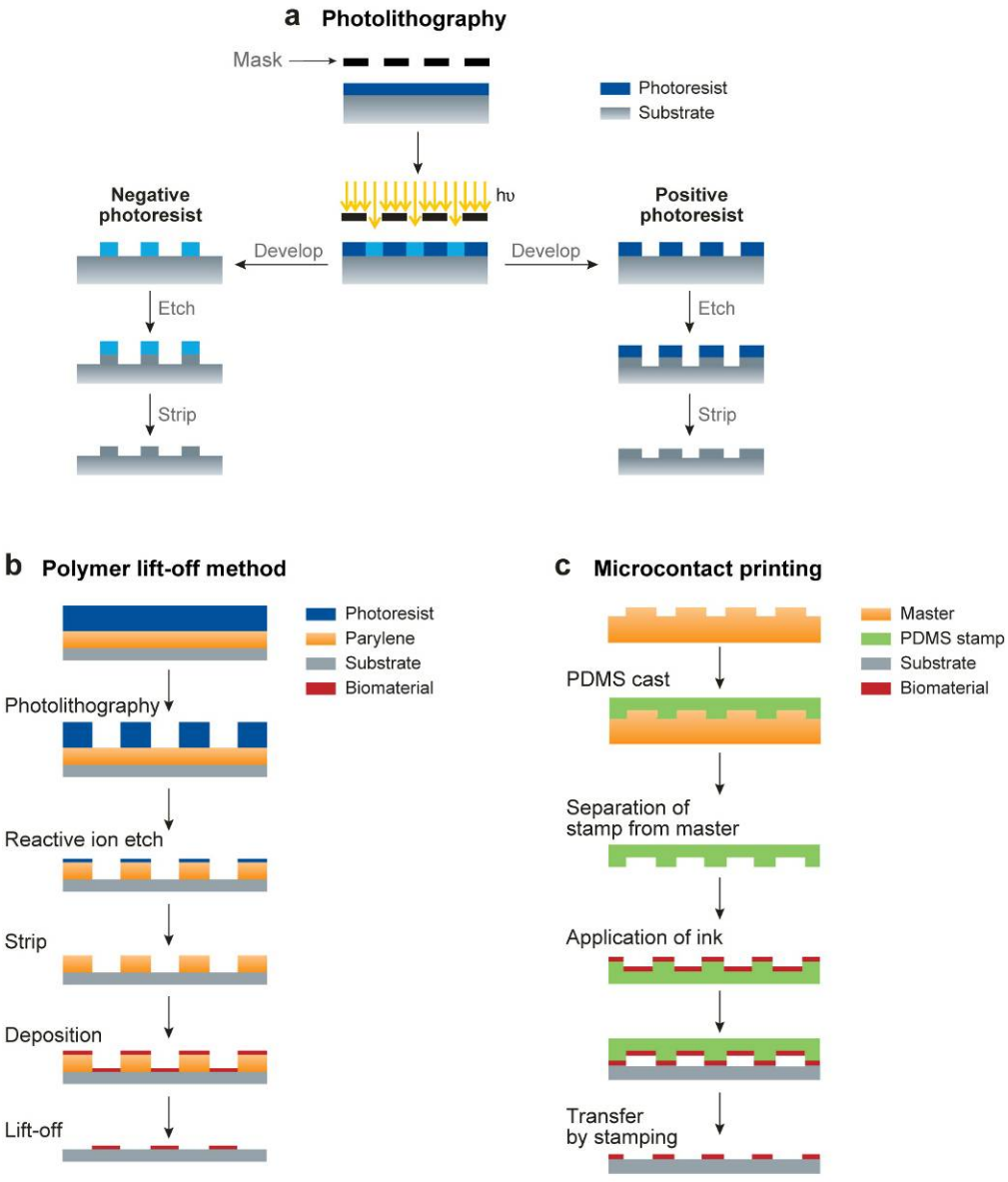
a Photolithography
Mask
Photoresist
Substrate
hυ
Negative photoresist
Positive photoresist
Develop
Develop
Etch
Etch
Strip
Strip
b Polymer lift-off method
Photoresist
Parylene
Substrate
Biomaterial
Photolithography
Reactive ion etch
Strip
Deposition
Lift-off
c Microcontact printing
Master
PDMS stamp
Substrate
Biomaterial
PDMS cast
Separation of stamp from master
Application of ink
Transfer by stamping

techniques (e.g. microcontact printing) have been developed for biological or medical applications, such as patterning proteins or DNA for microarrays. Electron beam (E-beam) lithography, which can pattern features with resolution as small as a few nanometers, is a serial method that requires no mask: the pattern is created by controlling the beam as it scans across a resist-coated substrate. This technique is more difficult and expensive, and it requires a significant amount of time to pattern features over an area of centimeter dimensions.

A versatile approach to biocompatible patterning is polymer lift-off (*2*) (Figure 1.1b). For example, a thin layer (~1μm) of parylene C is deposited over a silica (SiO_2) or glass surface before the addition of the photoresist layer. This substrate is patterned with photolithography to produce the desired features and then subjected to a controlled reactive ion etch that removes exposed regions of parylene down to the silicon dioxide or glass surface. At this stage the sample is transferred to a biologically friendly environment, and the biomaterial is added in aqueous solution to coat the entire surface, before mechanically peeling off the polymer. The revealed pattern is cleanly presented over a bare substrate that can be subsequently modified with a chemically distinctive material.

1.3 Surface interfacing with biomaterials

Surface modification provides chemical control of cell-surface interactions in a patterned array, and minimizing nonspecific interactions can be as critical as selectively engaging receptors or other components in the plasma membrane. Patterned and functionalized surfaces are widely used for biosensor applications, such as antigen-based antibody detection (*3, 4*). However, cells offer more challenges for surface modification, both in terms of the stringency for biocompatibility (cell viability and function) and the capacity for nonspecific interactions (including binding

to surfaces via cellular secretions). Some materials commonly used in cell studies are supported lipid bilayers and carrier proteins containing appropriate ligands. For patterning, these materials can be, for example, stamped onto a prepared surface with μCP (Figure 1.1c) or coated onto a photolithographed polymer, prior to polymer lift-off (Figure 1.1b).

Supported lipid bilayers (reviewed in (*5*)) have been crucial in our investigations of intra-cellular signaling. Bilayers form on glass or silica surfaces by spontaneous fusion of vesicles containing fluid phase lipids (*6, 7*). These planar bilayers have proven useful for microscopic examination of cell-surface or cell-cell interactions (*8, 9*), and they can be stably patterned with micrometer dimensions by μCP (*10, 11*) or polymer lift off (*12*) methods. Lipids are versatile materials; the composition can be varied and the headgroups can be selectively conjugated with small molecules such as fluorophores, small molecule ligands, or other functionalities (e.g., biotin that can bind to avidin in sandwich arrangements). Similarly, proteins can be presented in an oriented and mobile manner in patterned bilayers if they are appropriately lipidated (e.g., by conjugation to glycosylphosphatidylinositol, GPI (*13*)).

1.4 Early application of patterned surfaces: functional consequences of controlled cell adhesion.

Responsive interactions of cells with surfaces are fundamental to physiology, and if disregulated can lead to pathological conditions such as tumor growth. In physiological tissues as well as in plastic culture dishes, adhesion of cells to substrates is primarily mediated by integrins in the plasma membrane binding to extracellular matrix (ECM) proteins. These cell-surface interactions are known to play a critical role in cell cycle regulation leading to proliferation or death (*14, 15*), and they also

modulate receptor-mediated responses to other signals. Surface patterning with microcontact printing made it possible to examine systematically the importance of the spatial dimensions over which these chemical interactions occur. A pioneering study on endothelial cells in the late 1990's (*16*) utilized surfaces coated with "islands" of ECM proteins, (e.g. fibronectin) on a hydrophilic background that resisted nonspecific binding. Cell spreading was thus controlled by cell surface integrins binding ECM, and in this manner, cell size and shape were restricted to the patterned features. The authors could also vary the extent of cell spreading while keeping the direct contact area constant by adjusting the pattern feature sizes and the spaces between them. They correlated the imposed cell shape and spreading with cell cycle regulation, and found that the cellular footprint plays a significant role in switching between cell growth, proliferation and apoptosis.

These and related studies also pointed to the importance of the actin cytoskeleton in mediating these cellular responses through cytoskeletal anchorage to the substrate via integrins in focal adhesion complexes (*17*). In the last several years a large number of studies have taken advantage of patterned surfaces to study spatial control of cell-surface interactions and address specific questions of morphology and adhesion (*18-20*), dendritic branching (*21*), migration (*22*), and mechanotransduction (how cells convert mechanical signals into chemical responses) (*23-29*). As a recent, quantitative example, mechanical interactions were measured between cells and microfabricated surfaces containing needle-like post made of elastomeric PDMS. Cells attached to and deflected multiple fibronectin coated posts, and degree of deflections could be interpreted in terms of the local subcellular distribution of traction forces (*24, 25*).

1.5 Micropatterned lipid bilayers as a tool to investigate FcεRI receptor-mediated signaling.

Cells respond to chemical messages (e.g. antigens, growth factors, and cytokines) in the environment by means of specific cell surface receptors. Binding of these molecular stimuli to receptors stimulates transmembrane and intracellular signaling events that result in a global cellular response. In initial events, supramolecular complexes assemble dynamically at the plasma membrane as the signaling begins to cascade, bringing together the interactive proteins. Spatial and temporal targeting of signaling components in the membrane on micron and sub-micron scales is critical for overall efficiency and regulation of the cellular response. If the environment is engineered, then the spatially regulated response of the cell to defined stimuli can be investigated by monitoring redistributions of selectively labeled components or alterations in signaling pathways. Patterned surface approaches lend themselves readily to signaling that involves specialized regions or interactions such as membrane domains formed by clustered receptors or synapses formed at a cell-cell interface. These are features of immune cell signaling, and studies on IgE receptors and T cell receptors (TCR) are making rapid progress with spatial and chemical control to gain new information about cellular mechanisms.

IgE receptors on RBL mast cells have proven to be a useful model for understanding signaling in hematopoietic cells and the role of the plasma membrane in this process. FcεRI, the high-affinity receptor for IgE, is, like the T cell receptor (TCR), a member of the multisubunit immunoreceptor family that mediates cell activation in response to foreign antigens. IgE binds via its Fc segment to its surface receptors on mast cells or basophils, and the variable domains in the two Fab segments provide specific antigen recognition. As depicted in Figure 1.2, crosslinking of IgE-FcεRI by specific antigens (multivalent ligands) initiates the transmembrane signaling

cascade that leads to the release of preformed mediators (reviewed in (*30*)). Initial steps involve stable association of the clustered receptors with ordered regions of the plasma membrane (commonly called lipid rafts) where they encounter active tyrosine kinases (Lyn, of the Src family) that are anchored by acyl chains to the membrane inner leaflet. Tyrosine phosphorylation of FcεRI subunits by Lyn results in recruitment and phosphorylation of cytoplasmic Syk tyrosine kinase (of the Syk/Zap-70 family) that in turn phosphorylates phospholipase C (PLC) along with several other substrates. Activated PLCγ at the plasma membrane catalyses the hydrolysis of Phosphatidylinositol-4,5-bisphosphate (PtIns(4,5)P_2) to produce inositol- 1,4,5-trisphosphate ($InsP_3$) and diacylglyceraol (DAG). DAG in turn activates protein kinase C (PKC) which regulates degranulation by a yet unidentified mechanism, while $InsP_3$ is responsible for calcium release from the endoplasmic reticulum mediated by $InsP_3$ binding to IP_3 receptors on the ER. This signaling cascade leads to downstream signaling steps, such as subsequent Ca^{2+} mobilization, and results in the targeted release of secretory vesicles (degranulation) and other cellular responses.

Spatial regulation arises early in the signaling process at two stages: 1) ligand dependent crosslinking of the IgE-FcεRI complexes required for cell activation and 2) selective targeting of signaling proteins to the region of the activated receptors. Our collaborative investigations of these questions utilize monoclonal IgE that is specific for the hapten 2,4 dinitrophenyl (DNP). DNP-conjugated ligands can be tested directly for binding to IgE-FcεRI on RBL cells, and the cell activation consequences of crosslinking these receptors can be assessed by monitoring various signaling steps including degranulation.

1.5.1 Membrane compartmentalization of IgE receptor signaling. Spatial targeting of signaling components at the plasma membrane has been a subject of considerable interest and accumulating evidence points to the participation of

Figure 1.2: Minimal scheme for FcεRI-mediated signaling in mast cells. Intracellular signaling is initiated after FcεRI are clustered by cross-linking of bound IgE by multivalent ligand. This clustering drives association with lipid rafts where active Lyn kinase phosphorylates the immune tyrosine activation motifs of the FcεRI β and γ subunits. This results in Syk tyrosine kinase binding and activation by Lyn. Phosphorylation by active Syk is responsible for activation of other downstream signaling molecules such as Lat (linker for activation of T cells) and phospholipase C (PLCγ) Hydrolysis of phosphatidylinositol 4,5-bisphosphate (PIP_2) by PLCγ produces inositol 1,4,5-trisphosphate (IP3) and diacylglycerol, which are responsible for release of Ca^{2+} from endoplasmic reticulum (ER) stores via IP3 receptors and activation of protein kinase C (PKC), respectively. These and other pathways are responsible for mobilization of intracellular Ca^{2+} and consequent degranulation.

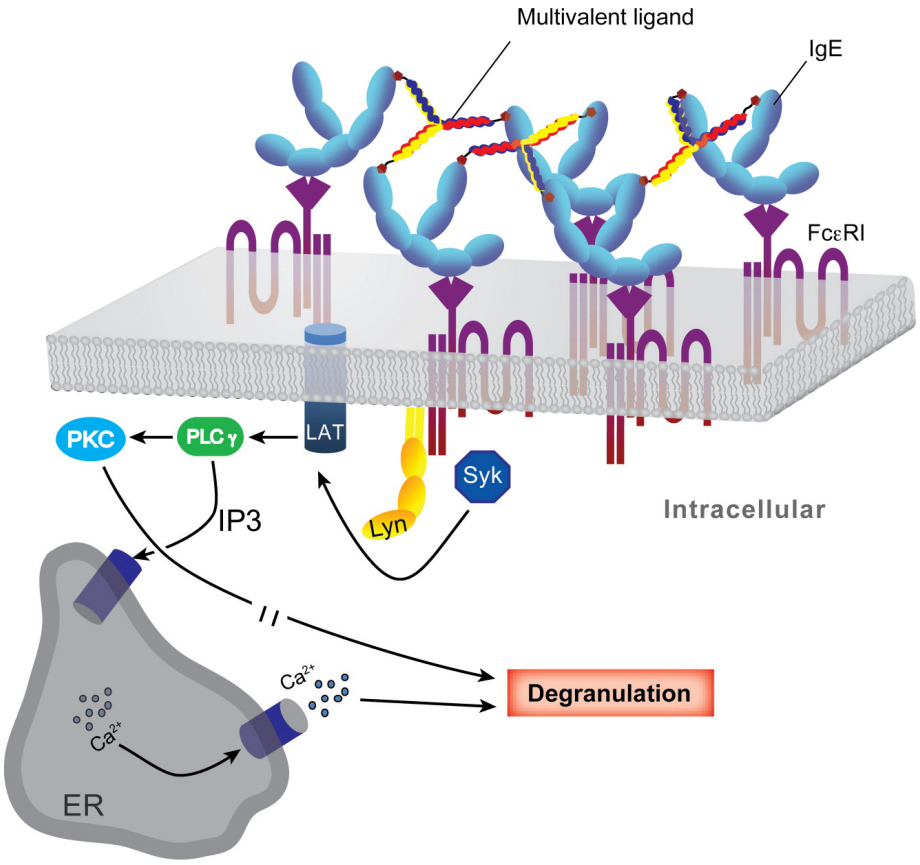
Multivalent ligand
IgE
FcεRI
PKC
PLCγ
LAT
Syk
Lyn
IP3
Intracellular
Degranulation
Ca2+
Ca2+
ER

membrane domains, including lipid rafts (*31-33*). IgE-FcεRI was among the first to be shown to involve lipid rafts in the signaling mechanism, using a number of correlative approaches that related physical properties of these membrane complexes with their biological consequences (reviewed in (*34*)). However, direct methods to investigate spatial rearrangements in the membrane and targeting of components were initially limited by typical heterogeneity of the cells and stimuli, as well as by the diffraction limit of light. For example, we originally observed with fluorescence microscopy that Lyn co-redistributes with antigen-crosslinked receptors in large patches that form after cold incubation for several hours (*35*). By fabricating surfaces that are patterned with receptor-specific ligands we were able to examine labeled cellular components co-redistributing with the receptors clusters in the same pattern, in real time at 37ºC and more physiological conditions (*12, 36*).

Patterned supported lipid bilayers prepared by polymer lift-off for these studies contained, as desired, fluorescent lipid analogues for visualization as well as phospholipids modified with DNP for specific binding of anti-DNP IgE on RBL cells (*12*). Figure 1.3a shows a schematic of cells incubated with patterned bilayers containing specific ligand. Clustering of IgE-FcεRI on the cell surface is visualized with fluorescently labeled IgE as the cells settle on the substrate (Figure 1.3b), and, as expected, cells are activated as observed by their ruffling response and secretory activity. Co-redistribution within the cell of fluorescent membrane probes or GFP-labeled intracellular components can be monitored simultaneously. Intracellular enzyme activities, in particular tyrosine phosphorylation, can also be monitored with the use of labeled antibodies and cells that are fixed at specified time points. We found that intracellular tyrosine kinase activity is visualized (with anti-phosphotyrosine antibodies) within the same few minutes that the cells settle on the patterned substrate and IgE-FcεRI clusters on the cell surface, whereas detectable accumulation of the

Figure 1.3: Patterned lipid bilayers to investigate spatial regulation of FcεRI-mediated signaling. Supported lipid bilayers, patterned by parylene lift-off method contain a fluorophore (for visualization) and DNP conjugated to dioleylphosphatidylethanolamine (for binding anti-DNP IgE). After incubation of RBL cells with these substrates, IgE-FcεRI on cell surface are clustered into the same pattern, and assembly of signaling components within the cell can be visualized with selective fluorescent labeling and microscopy. a) Schematic of IgE-FcεRI clustering on cell surface by the patterned DNP-ligands. b) Confocal micrograph of fluorescently labeled cells interacting with the patterned surface. Co-localization of different GFP-labeled intracellular components (green) with the patterned bilayers (red) occurs at distinctive times; arrows correspond to the approximate time for the first appearance of clustering of the different probes. Concentrated tyrosine phosphorylation (PY) is observed before Lyn kinase accumulates in the patterned regions (87). c) Fluorescence photobleaching recovery in a cell membrane labeled with a GFP construct. In this representative example, cells were labeled with Lyn-GFP. A single spot was bleached in patterned regions where IgE-FcεRI are clustered, and recovery is monitored after the initial bleach. d) Fluorescence photobleaching recovery curves show redistribution of Lyn-GFP and PM-GFP to be dynamic, and the latter has a higher mobile fraction than the former. Alexa488-labeled IgE-FcεRI is immobilized by binding to the patterned ligand and shows no recovery after photobleaching. Scale bar in micrographs corresponds to 10 μm. Adapted from references ((*37*) (*38*) (*36*)).

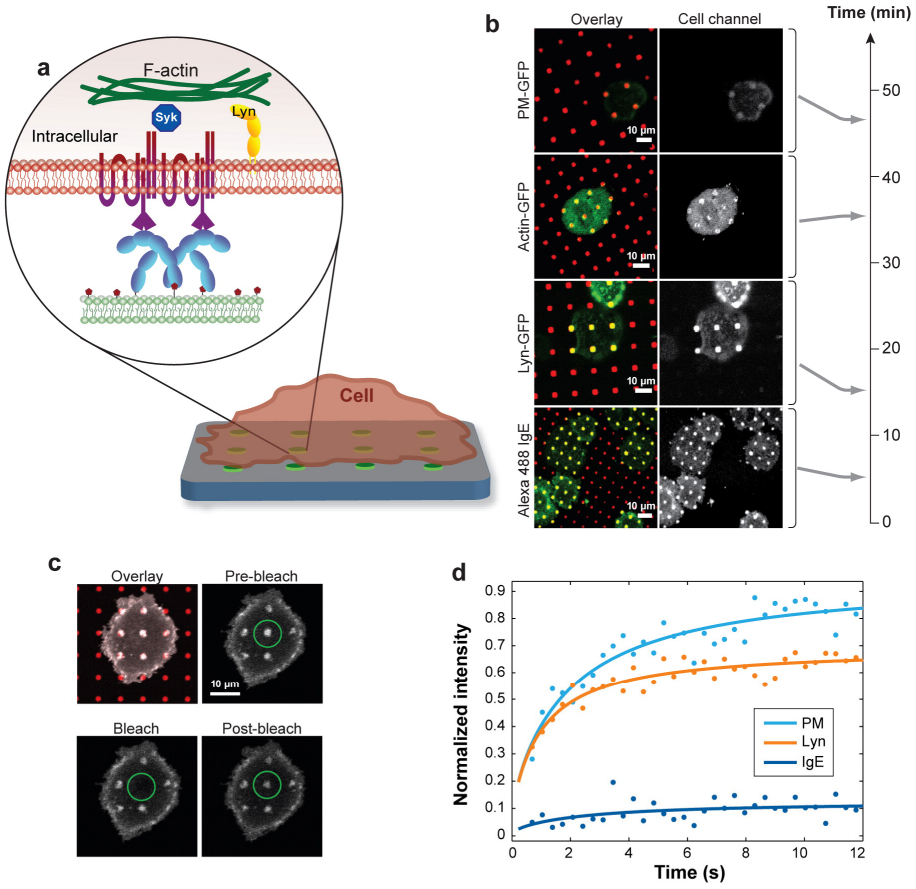
a
F-actin
Syk
Lyn
Intracellular
Cell
b
Overlay
Cell channel
Time (min)
PM-GFP
Actin-GFP
Lyn-GFP
Alexa 488 IgE
10 μm
50
40
30
20
10
0
c
Overlay
Pre-bleach
Bleach
Post-bleach
10 μm
d
Normalized intensity
Time (s)
PM
Lyn
IgE
0
0.1
0.2
0.3
0.4
0.5
0.6
0.7
0.8
0.9
0
2
4
6
8
10
12

Lyn-GFP kinase occurs only after about 15 min (Figure 1.3b). A GFP construct containing only the palmitate/myristate acylated region of Lyn (PM) that anchors it to the membrane also co-redistributes with clustered IgE-FcεRI but at somewhat longer times (~ 45 min). Under these conditions, the inner leaflet lipid phosphatidylinositol 4,5-bis-phosphate (PIP_2) bound to a specific GFP-construct (PH domain of PLCδ) does not co-resdistribute with the clustered IgE-FcεRI, nor do outer leaflet lipid raft markers, including fluorescent lipid $DiIC_{16}$ and fluorescently labeled-cholera toxin B (CTB) bound to ganglioside GM1 (*36*).

The flat surfaces with patterned lipid bilayers lend themselves to other optical measurements, including fluorescence photobleaching recovery. We used this approach to evaluate the dynamic nature of the proteins concentrating in the regions of patterned ligands and clustered IgE-FcεRI. Whereas IgE is immobilized by binding to its ligands, Figure 1.3c and 1.3d show that Lyn-GFP and PM-GFP re-populate the bleached regions, indicating that diffusive exchange occurs for these membrane anchored proteins while the environment that causes their preferential localization is maintained. Interestingly, Lyn-GFP exhibits a mobile fraction that is significantly smaller than that for PM-EGFP. This difference suggests that the SH2 and SH3 protein domains in the Lyn construct (but not in the PM construct) are involved in protein-protein interactions in the region of the clustered IgE-FcεRI, as would be expected for this kinase that phosphorylates FcεRI and other substrates during early stages of signaling.

GFP-actin was also found to co-redistribute with the clustered IgE-FcεRI, pointing to participation of the actin-cytoskeleton in observed co-redistributions with the clustered receptors. Cytochalasin D inhibits actin polymerization, and incubation of cells with this reagent prior to the patterned bilayers prevented detectable GFP-actin, Lyn-GFP, and PM-GFP, but not clustering of IgE-FcεRI or the tyrosine

phosphorylation activity that occurs at early times. These results are consistent with the progressive nature of targeted signaling and our current picture based on these and several other types of data (*39*): initial phosphorylation of clustered IgE-FcεRI by Lyn in ordered membrane domains creates new binding sites for Lyn and assembly of other signaling components, and the actin cytoskeleton further stabilizes and regulates these protein-protein interactions. Overall, these studies demonstrated that patterned lipid bilayers provide new information and insights about spatial (micron-scale) and temporal (minutes) aspects of receptor mediated responses, including phosphorylation activity, selective targeting of signaling components, involvement of the cytoskeleton, and uncoupling of outer and inner leaflet components of lipid rafts. Moreover, the periodicity of the patterns enables reliable and quantitative evaluation of localized receptors and subsequent signaling events.

1.5.2 Cytoskeletal interactions with clustered IgE-FcεRI. The participation of the actin cytoskeleton in FcεRI signaling has been the subject of considerable research. Our current understanding of these processes has been largely based on biochemical characterization of signaling using chemical inhibitors of actin polymerization. Using this approach, several groups have found a direct correlation between inhibition of actin polymerization and increased FcεRI-mediated cellular responses after antigen stimulation (*35, 40-43*). These activated responses include: protein phosphorylation (*35*), calcium influx(*41*) and degranulation(*43*) (*42*). Based on these studies it has been speculated that the actin cytoskeleton functions as a negative regulator of IgE receptor signaling, but the mechanism by with the actin cytoskeleton participates in signaling is still not yet understood. To complicate matters, the actin cytoskeleton is also involved in the internalization of the IgE-FcεRI complex after receptor cross-linking (*44, 45*), and it could potentially function in the down-regulation apparatus of FcεRI signaling by maintaining cell surface receptor

expression. Such a mechanism of regulation is found in both T cell receptor (TCR) (*46*) and B cell receptor (BCR) (*47*) systems where internalized receptors are trafficked to lysosomal compartments for degradation. Interestingly, the timescale of the observed extended phosphorylation lifetime of FcεRI in the presence of cytochalasin D is consistent with impaired receptor internalization. Based on these findings, two potential cytoskeletal regulation mechanisms of FcεRI signaling arise: direct regulation of signaling components by adapter proteins that connect to the cytoskeleton and/or regulation of receptor cell surface expression by endocytosis.

Investigation of IgE receptor signaling is complicated by signaling cross-talk between cytoskeleton dependent cellular processes that participate in signaling from different receptor systems. The actin cytoskeleton and actin binding proteins participate in integrin mediated adherence of cells to substrates via different adhesion complexes. Many different types of adhesion structures that connect the actin cytoskeleton to the ECM have been described: focal adhesions, focal complexes, fibrillar adhesions, podosomes and invadopodia (Figure 1.4). The most characterized adhesion complexes are focal adhesions which are actin rich structures interconnected by several adapter proteins such as vinculin, talin and paxillin. These function as anchor sites to the extracellular matrix (see figure 1.4A and 1.4B) by means of integrin receptors and are necessary for cell migration (*48*). Consistent with studies on T cells that show interplay between integrin/cytoskeletal interactions and receptor-mediated signaling pathways (*49*), RBL mast cells show enhanced levels of stimulated degranulation when they are adherent to ECM (*50*), indicating cross-talk between both pathways (*51, 52*). The picture is complicated by other potentially relevant structural interactions such as that between Lyn and the cytoskeletal adaptor protein paxillin (*53*) or the GTPase dynamin (*54*) as shown by immunoprecipitation studies with cell lysates.

Figure 1.4: Architecture and composition of adhesive structures. (A) Mouse Embryonic Fibroblast (MEF) cells spread on a fibronectin matrix were stained for either β_1 integrin-containing focal adhesions (Fa) and focal complexes (Fx) or fibronectin to localize fibrillar adhesion (Fb). (B) Schematic representation of focal adhesion organization. (C) Baby Hamster Kidney (BHK) cells transfected with cortactin-DsRed and stained for vinculin and paxillin phosphorylated on Y118 (P-Paxillin). Confocal analysis displays a rosette of podosome-type adhesion (PTA). PTA consist of a core surrounded by adhesion proteins (see zoom pictures of an individual structural unit). (D) Schematic representation of the architecture of PTA. Reproduced from reference (62) with permission from Elsevier GmbH.

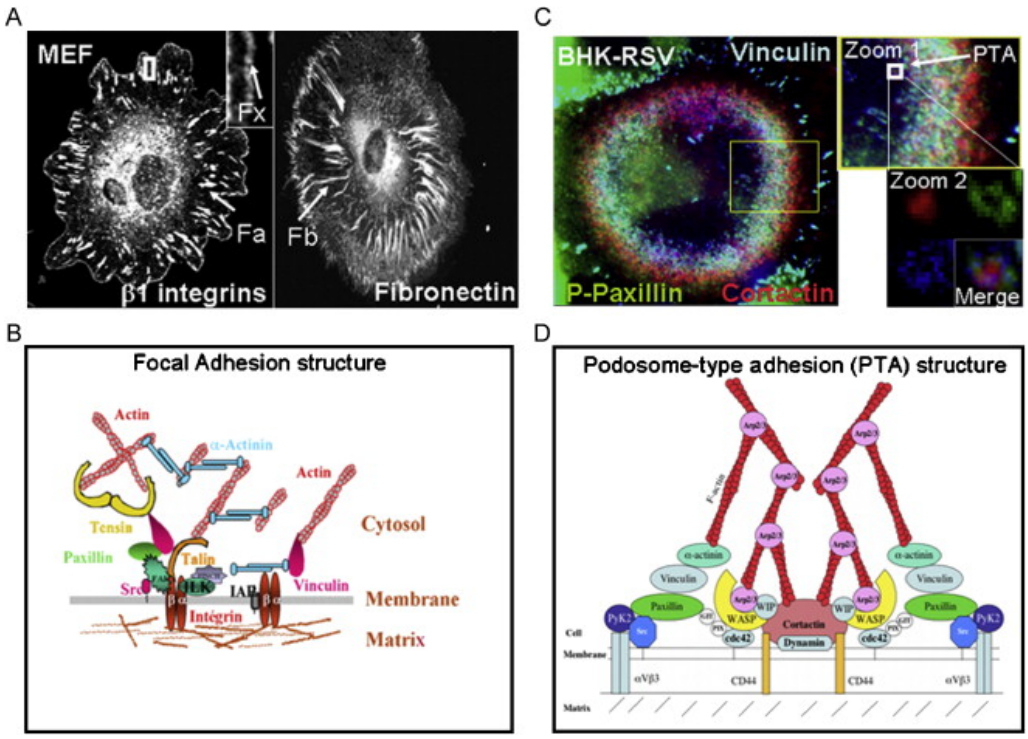
A
MEF
Fx
Fa
β1 integrins
Fb
Fibronectin
C
BHK-RSV
Vinculin
Zoom 1
PTA
Zoom 2
P-Paxillin
Cortactin
Merge
B
Focal Adhesion structure
Actin
α-Actinin
Actin
Tensin
Cytosol
Paxillin
Talin
Src
ILK
IAP
Vinculin
Membrane
Intégrin
Matrix
D
Podosome-type adhesion (PTA) structure
Arp2/3
F-actin
α-actinin
Vinculin
Paxillin
WIP
WASP
Cortactin
Dynamin
cdc42
PyK2
Src
Cell
Membrane
αVβ3
CD44
Matrix

Dynamin 2 is a GTPase that has been mostly studied in the context of receptor endocytosis, where its primary function is believed to be in vesicle scission form the plasma membrane (*55*). More recently, dynamin has been implicated in the regulation of various F-actin dependent structures that also form complexes with focal adhesion proteins. Coordinated interactions between dynamin and cortactin have been shown to control actin dynamics both in-vitro (*56, 57*) and in-vivo (*58, 59*). An illuminating example is the interplay between dynamin, focal adhesion proteins, integrins and the actin cytoskeleton that is found in the formation and regulation of podosomes (*60*) and invadopodia (*61*) which are sites of integrin mediated actin polymerization and matrix degradation (Figure 1.4C and 1.4D). Although podosomes and invadopodia share many similarities with focal adhesion in the structural interplay between integrins and F-actin, they represent distinct cellular processes that are activated by different stimuli and are characteristic of particular cell types (*62*).

Based on our current understanding of these different cellular processes, it is apparent that cells can employ similar networks of protein interactions in different cellular processes that are adapted to the cellular stimuli. Redundancy and cross-talk between distinct signaling pathways complicate interpretation of observed FcεRI activation dependent cellular responses, specifically those dependent on the actin cytoskeleton. The use of patterned bilayers provides a unique opportunity to spatially separate cytoskeletal interactions with integrins from those with clustered IgE-FcεRI, thus dissecting the contributions from each of these pathways. As discussed in the following chapters, using patterned bilayers presenting DNP ligands, we observed that in addition to actin, several focal adhesion proteins such as vinculin and paxillin concentrate in the RBL cells under the clustered anti-DNP IgE-FcεRI. Under the same conditions integrins are excluded from the regions of the antigen-presenting patterned bilayers and preferentially associates with the silica surface between the patterned

features. In addition, consistent with frustrated internalization, we find that dynamin 2 concentrates under the clustered FcεRI receptors and that it functions as a regulator of receptor dependent actin polymerization. Patterned ligand arrays in combination with genetic and biochemical characterization of IgE receptor signaling has provided us with insight into the mechanisms of IgE receptor cytoskeletal regulation.

REFERENCES

1. Voldman, J., Gray, M. L., and Schmidt, M. A. (1999) Microfabrication in Biology and Medicine, *Annual Review of Biomedical Engineering 1*, 401-425.
2. Ilic, B., and Craighead, H. G. (2000) Topographical Patterning of Chemically Sensitive Biological Materials Using a Polymer-Based Dry Lift Off, *Biomedical Microdevices 2*, 317-322.
3. Senaratne, W., Takada, K., Das, R., Cohen, J., Baird, B., Abruna, H. D., and Ober, C. K. (2006) Dinitrophenyl ligand substrates and their application to immunosensors, *Biosensors and Bioelectronics 22*, 63-70.
4. Valsesia, A., Colpo, P., Meziani, T., Lisboa, P., Lejeune, M., and Rossi, F. (2006) Immobilization of Antibodies on Biosensing Devices by Nanoarrayed Self-Assembled Monolayers, *Langmuir 22*, 1763-1767.
5. Boxer, S. G. (2000) Molecular transport and organization in supported lipid membranes, *Current Opinion in Chemical Biology 4*, 704-709.
6. Cremer, P. S., and Boxer, S. G. (1999) Formation and Spreading of Lipid Bilayers on Planar Glass Supports, *J. Phys. Chem. B 103*, 2554-2559.
7. Keller, C. A., Glasmästar, K., Zhdanov, V. P., and Kasemo, B. (2000) Formation of Supported Membranes from Vesicles, *Physical Review Letters 84*, 5443.
8. Kam, L., and Boxer, S. G. (2001) Cell adhesion to protein-micropatterned-supported lipid bilayer membranes, *Journal of Biomedical Materials Research 55*, 487-495.
9. Groves, J. T., and Dustin, M. L. (2003) Supported planar bilayers in studies on immune cell adhesion and communication, *Journal of Immunological Methods 278*, 19-32.

10. Hovis, J. S., and Boxer, S. G. (2001) Patterning and Composition Arrays of Supported Lipid Bilayers by Microcontact Printing, *Langmuir 17*, 3400-3405.
11. Kung, L. A., Kam, L., Hovis, J. S., and Boxer, S. G. (2000) Patterning Hybrid Surfaces of Proteins and Supported Lipid Bilayers, *Langmuir 16*, 6773-6776.
12. Orth, R. N., Wu, M., Holowka, D. A., Craighead, H. G., and Baird, B. A. (2003) Mast Cell Activation on Patterned Lipid Bilayers of Subcellular Dimensions, *Langmuir 19*, 1599-1605.
13. Chan, P. Y., Lawrence, M. B., Dustin, M. L., Ferguson, L. M., Golan, D. E., and Springer, T. A. (1991) Influence of receptor lateral mobility on adhesion strengthening between membranes containing LFA-3 and CD2, *J. Cell Biol. 115*, 245-255.
14. Bijian, K., Takano, T., Papillon, J., Khadir, A., and Cybulsky, A. V. (2004) Extracellular matrix regulates glomerular epithelial cell survival and proliferation, *Am J Physiol Renal Physiol 286*, F255-266.
15. Bourdoulous, S., Orend, G., MacKenna, D. A., Pasqualini, R., and Ruoslahti, E. (1998) Fibronectin Matrix Regulates Activation of Rho and CdC42 GTPases and Cell Cycle Progression, *J. Cell Biol. 143*, 267-276.
16. Chen, C. S., Mrksich, M., Huang, S., Whitesides, G. M., and Ingber, D. E. (1997) Geometric Control of Cell Life and Death, *Science 276*, 1425-1428.
17. Ingber, D. E. (2006) Cellular mechanotransduction: putting all the pieces together again, *FASEB J. 20*, 811-827.
18. Théry, M., Pépin, A., Dressaire, E., Chen, Y., and Bornens, M. (2006) Cell distribution of stress fibres in response to the geometry of the adhesive environment, *Cell Motility and the Cytoskeleton 63*, 341-355.
19. Théry, M., Racine, V., Piel, M., Pépin, A., Dimitrov, A., Chen, Y., Sibarita, J.-B., and Bornens, M. (2006) Anisotropy of cell adhesive microenvironment

governs cell internal organization and orientation of polarity, *PNAS 103*, 19771-19776.

20. Lehnert, D., Wehrle-Haller, B., David, C., Weiland, U., Ballestrem, C., Imhof, B. A., and Bastmeyer, M. (2004) Cell behaviour on micropatterned substrata: limits of extracellular matrix geometry for spreading and adhesion, *J Cell Sci 117*, 41-52.

21. Craighead, H. G., Turner, S. W., Davis, R. C., James, C., Perez, A. M., St. John, P. M., Isaacson, M. S., Kam, L., Shain, W., Turner, J. N., and Banker, G. (1998) Chemical and Topographical Surface Modification for Control of Central Nervous System Cell Adhesion, *Biomedical Microdevices 1*, 49-64.

22. Jiang, X., Bruzewicz, D. A., Wong, A. P., Piel, M., and Whitesides, G. M. (2005) Directing cell migration with asymmetric micropatterns, *PNAS 102*, 975-978.

23. McBeath, R., Pirone, D. M., Nelson, C. M., Bhadriraju, K., and Chen, C. S. (2004) Cell Shape, Cytoskeletal Tension, and RhoA Regulate Stem Cell Lineage Commitment, *Developmental Cell 6*, 483-495.

24. Balaban, N. Q., Schwarz, U. S., Riveline, D., Goichberg, P., Tzur, G., Sabanay, I., Mahalu, D., Safran, S., Bershadsky, A., Addadi, L., and Geiger, B. (2001) Force and focal adhesion assembly: a close relationship studied using elastic micropatterned substrates, *Nat Cell Biol 3*, 466-472.

25. Tan, J. L., Tien, J., Pirone, D. M., Gray, D. S., Bhadriraju, K., and Chen, C. S. (2003) Cells lying on a bed of microneedles: An approach to isolate mechanical force, *PNAS 100*, 1484-1489.

26. Huang, S., Chen, C. S., and Ingber, D. E. (1998) Control of Cyclin D1, p27Kip1, and Cell Cycle Progression in Human Capillary Endothelial Cells by Cell Shape and Cytoskeletal Tension, *Mol. Biol. Cell 9*, 3179-3193.

27. Brock, A. L., and Ingber, D. E. (2005) Control of the direction of lamellipodia extension through changes in the balance between Rac and Rho activities., *Mol Cell Biomech. 2*, 135-144.

28. Dike, L., Chen, C., Mrksich, M., Tien, J., Whitesides, G., and Ingber, D. (1999) Geometric control of switching between growth, apoptosis, and differentiation during angiogenesis using micropatterned substrates, *In Vitro Cellular & Developmental Biology - Animal 35*, 441-448.

29. Parker, K. K., Brock, A. L., Brangwynne, C., Mannix, R. J., Wang, N., Ostuni, E., Geisse, N. A., Adams, J. C., Whitesides, G. M., and Ingber, D. E. (2002) Directional control of lamellipodia extension by constraining cell shape and orienting cell tractional forces, *FASEB J. 16*, 1195-1204.

30. Gilfillan, A. M., and Tkaczyk, C. (2006) Integrated signalling pathways for mast-cell activation, *Nat Rev Immunol 6*, 218-230.

31. Insel, P. A., Head, B. P., Patel, H. H., Roth, D. M., Bundey, R. A., and Swaney, J. S. (2005) Compartmentation of G-protein-coupled receptors and their signalling components in lipid rafts and caveolae, *Biochem. Soc. Trans. 33*, 1131-1134.

32. Allen, J. A., Halverson-Tamboli, R. A., and Rasenick, M. M. (2007) Lipid raft microdomains and neurotransmitter signalling, *Nat Rev Neurosci 8*, 128-140.

33. Zeyda, M., and Stulnig, T. M. (2006) Lipid Rafts & Co.: An integrated model of membrane organization in T cell activation, *Progress in Lipid Research 45*, 187-202.

34. Holowka, D., and Baird, B. (2001) FcεRI as a paradigm for a lipid raft-dependent receptor in hematopoietic cells, *Seminars in Immunology 13*, 99-105.

35. Holowka, D., Sheets, E. D., and Baird, B. (2000) Interactions between Fc(epsilon)RI and lipid raft components are regulated by the actin cytoskeleton, *J Cell Sci 113*, 1009-1019.

36. Wu, M., Holowka, D., Craighead, H. G., and Baird, B. (2004) Visualization of plasma membrane compartmentalization with patterned lipid bilayers, *PNAS 101*, 13798-13803.

37. Wu, M. (2006) Spatial regulation of mast cell signaling by plasma membrane compartmentalization and differential intracellular targeting, p 107, PhD thesis. Cornell University, Ithaca, NY.

38. Wu, M., Baumgart, T., Hammond, S., Holowka, D., and Baird, B. (2007) Differential targeting of secretory lysosomes and recycling endosomes in mast cells revealed by patterned antigen arrays, *J Cell Sci 120*, 3147-3154.

39. Holowka, D., Gosse, J. A., Hammond, A. T., Han, X., Sengupta, P., Smith, N. L., Wagenknecht-Wiesner, A., Wu, M., Young, R. M., and Baird, B. (2005) Lipid segregation and IgE receptor signaling: A decade of progress, *Biochimica et Biophysica Acta (BBA) - Molecular Cell Research 1746*, 252-259.

40. Torigoe, C., Song, J., Barisas, B. G., and Metzger, H. (2004) The influence of actin microfilaments on signaling by the receptor with high-affinity for IgE, *Molecular Immunology 41*, 817-829.

41. Tatsuya, O., Koichi, S., Masatoshi, H., Hiroshi, O., and Hideaki, K. (2002) FcεRI cross-linking-induced actin assembly mediates calcium signalling in RBL-2H3 mast cells, *British Journal of Pharmacology 136*, 837-846.

42. Pierini, L., Harris, N. T., Holowka, D., and Baird, B. (1997) Evidence Supporting a Role for Microfilaments in Regulating the Coupling between

Poorly Dissociable IgE-FcεRI Aggregates and Downstream Signaling Pathways. , *Biochemistry 36*, 7447-7456.

43. Frigeri, L., and Apgar, J. R. (1999) The Role of Actin Microfilaments in the Down-Regulation of the Degranulation Response in RBL-2H3 Mast Cells, *J Immunol 162*, 2243-2250.

44. Ra, C., Furuichi, K., Rivera, J., Mullins, M. J., Isersky, C., and White, K. N. (1989) Internalization of IgE receptors on rat basophilic leukemic cells by phorbol ester: comparison with endocytosis induced by receptor aggregation, *European Journal of Immunology 19*, 1771-1777.

45. Xu, K., Williams, R. M., Holowka, D., and Baird, B. (1998) Stimulated release of fluorescently labeled IgE fragments that efficiently accumulate in secretory granules after endocytosis in RBL-2H3 mast cells, *J Cell Sci 111*, 2385-2396.

46. Liu, H., Rhodes, M., Wiest, D. L., and Vignali, D. A. A. (2000) On the Dynamics of TCR:CD3 Complex Cell Surface Expression and Downmodulation, *Immunity 13*, 665-675.

47. Cheng, P. C., Steele, C. R., Gu, L., Song, W., and Pierce, S. K. (1999) MHC Class II Antigen Processing in B Cells: Accelerated Intracellular Targeting of Antigens, *J Immunol 162*, 7171-7180.

48. Dubash, A. D., Menold, M. M., Samson, T., Boulter, E., García-Mata, R., Doughman, R., Burridge, K., and Kwang, W. J. (2009) Focal Adhesions: New Angles on an Old Structure, in *International Review of Cell and Molecular Biology*, pp 1-65, Academic Press.

49. Smith-Garvin, J. E., Koretzky, G. A., and Jordan, M. S. (2009) T Cell Activation, *Annual Review of Immunology 27*, 591-619.

50. Hamawy, M. M., Oliver, C., Mergenhagen, S. E., and Siraganian, R. P. (1992) Adherence of rat basophilic leukemia (RBL-2H3) cells to fibronectin- coated surfaces enhances secretion, *J Immunol 149*, 615-621.

51. Ra, C., Yasuda, M., Yagita, H., and Okumura, K. (1994) Fibronectin receptor integrins are involved in mast cell activation, *Journal of Allergy and Clinical Immunology 94*, 625-628.

52. Kruger-Krasagakes, Grutzkau, Krasagakis, Hoffmann, and Henz. (1999) Adhesion of human mast cells to extracellular matrix provides a co-stimulatory signal for cytokine production, *Immunology 98*, 253-257.

53. Minoguchi, K., Kihara, H., Nishikata, H., Hamawy, M. M., and Siraganian, R. P. (1994) Src family tyrosine kinase Lyn binds several proteins including paxillin in rat basophilic leukemia cells, *Molecular Immunology 31*, 519-529.

54. Pullar, C. E., Repetto, B., and Gilfillan, A. M. (1996) Rapid dephosphorylation of the GTPase dynamin after FcεRI aggregation in a rat mast cell line, *J Immunol 157*, 1226-1232.

55. Doherty, G. J., and McMahon, H. T. (2009) Mechanisms of Endocytosis, *Annual Review of Biochemistry 78*, 857-902.

56. Mooren, O. L., Kotova, T. I., Moore, A. J., and Schafer, D. A. (2009) Dynamin2 GTPase and Cortactin Remodel Actin Filaments, *Journal of Biological Chemistry 284*, 23995-24005.

57. Schafer, D. A., Weed, S. A., Binns, D., Karginov, A. V., Parsons, J. T., and Cooper, J. A. (2002) Dynamin2 and Cortactin Regulate Actin Assembly and Filament Organization, *Current Biology 12*, 1852-1857.

58. McNiven, M. A., Kim, L., Krueger, E. W., Orth, J. D., Cao, H., and Wong, T. W. (2000) Regulated Interactions between Dynamin and the Actin-Binding Protein Cortactin Modulate Cell Shape, *J. Cell Biol. 151*, 187-198.

59. Cao, H., Orth, J. D., Chen, J., Weller, S. G., Heuser, J. E., and McNiven, M. A. (2003) Cortactin Is a Component of Clathrin-Coated Pits and Participates in Receptor-Mediated Endocytosis, *Mol. Cell. Biol. 23*, 2162-2170.

60. Ochoa, G.-C., Slepnev, V. I., Neff, L., Ringstad, N., Takei, K., Daniell, L., Kim, W., Cao, H., McNiven, M., Baron, R., and De Camilli, P. (2000) A Functional Link between Dynamin and the Actin Cytoskeleton at Podosomes, *J. Cell Biol. 150*, 377-390.

61. Baldassarre, M., Pompeo, A., Beznoussenko, G., Castaldi, C., Cortellino, S., McNiven, M. A., Luini, A., and Buccione, R. (2003) Dynamin Participates in Focal Extracellular Matrix Degradation by Invasive Cells, *Mol. Biol. Cell 14*, 1074-1084.

62. Block, M. R., Badowski, C., Millon-Fremillon, A., Bouvard, D., Bouin, A.-P., Faurobert, E., Gerber-Scokaert, D., Planus, E., and Albiges-Rizo, C. (2008) Podosome-type adhesions and focal adhesions, so alike yet so different, *European Journal of Cell Biology 87*, 491-506.

CHAPTER 2[23]

FOCAL ADHESION PROTEINS CONNECT IgE RECEPTORS TO THE CYTOSKELETON AS REVEALED BY MICROPATTERNED LIGAND ARRAYS.

2.1 Introduction

Cells have evolved to respond to their chemical and physical environment. Chemical stimulants in the form of soluble or surface-bound ligands are recognized by specific cell surface receptors, and physical cues are sensed by integrins that bind to extracellular matrix proteins on surrounding substrates (1). Cross-talk between intracellular signaling pathways that are initiated by integrins and by ligand receptors has been clearly demonstrated, although spatial aspects of these processes have not been defined. Surfaces patterned on the micrometer scale offer the opportunity to separate regions that bind integrins from those that present ligands to cell surface receptors, and thereby delineate respective cytoskeletal connections.

The subject of our study is the IgE receptor (FcεRI), which is a member of the family of multi-subunit immune recognition receptors that includes antigen receptors on B cells and T cells. This family of receptors has conserved structural features and similarly initiate intracellular signaling in response to multivalent ligands (antigens) that activate cells by clustering cell surface receptors. FcεRI receptors are found primarily in mast cells and basophils and are sensitized to a particular antigen by high affinity binding of IgE with the corresponding specificity. Crosslinking of IgE-FcεRI by antigen triggers intracellular signaling events, leading to multiple cellular responses including degranulation to release chemical mediators that cause inflammatory and

[2] This chapter has been published previously in *PNAS* ***105***, 17238-17244.
[3] Lavanya Vasudevan contributed to this work by performing measurements of calcium influx.

allergic reactions. In the earliest signaling events, antigen-induced clustering of IgE-FcεRI causes stable association with ordered lipid domains, wherein the tyrosine kinase Lyn phosphorylates the FcεRI β and γ subunits, resulting in recruitment and activation of tyrosine kinase Syk (2, 3). Activated Syk phosphorylates a series of proteins resulting in Ca^{2+} mobilization and other downstream signaling steps leading to degranulation.

We recently examined spatial relationships during IgE-FcεRI mediated signal transduction using microfabricated ligand arrays. The patterned ligands cause spatially defined clustering of IgE-FcεRI on the cell surface which, because the IgE binds to the ligands, corresponds to the same pattern. These patterned ligands and binding receptors can be visualized with fluorescence microscopy; the periodicity of the patterns enables reliable and quantitative evaluation of localized receptors and signaling components that co-redistribute.

We showed previously with patterned lipid bilayers containing 2, 4-dinitrophenyl (DNP) ligands that tyrosine kinase activity (as visualized with anti-phosphotyrosine antibodies) occurs in the liganded regions on the same time scale that anti-DNP IgE-FcεRI clusters in those regions, and detectable accumulation of the Lyn-GFP kinase occurs after about 15 min. Cytoskeletal F-actin visually concentrates in these regions after about 30 min. Notably, cytochalasin D, which inhibits actin polymerization, prevents the micron-scale accumulation of Lyn but not the initial tyrosine phosphorylation (4), supporting the view that the actin-cytoskeleton becomes involved as signaling progresses.

The present study examines the reorganization and the regulatory role of the actin cytoskeleton during FcεRI-mediated signal transduction, and we focus on participation of several actin binding proteins that have been examined in other signaling pathways. In particular, we investigate ezrin and moesin, which have been

implicated in T cell receptor signaling, and also paxillin, vinculin, and talin, which are known to be involved in focal adhesion complexes and participate in integrin-mediated signaling (5). The adapter protein paxillin has several binding sites for Src kinases that are relevant in immune cell signaling (6).

Previous studies on RBL mast cells showed that paxillin is tyrosine phosphorylated after activation of IgE-FcεRI by multivalent ligand (7). Another study identified paxillin as a protein precipitated by a MBP-Lyn fusion protein only after ligand-mediated clustering of IgE-FcεRI in RBL mast cells, suggesting that this protein is involved in signaling events downstream of the initial phosphosphorylaton of FcεRI (8). Our present study with patterned ligands shows that focal adhesion proteins vinculin, talin, and paxillin co-redistribute with clustered IgE-FcεRI independently from integrins and thereby provide a direct link to the actin cytoskeleton. Moreover, use of short interfering RNA (siRNA) to knock down paxillin expression shows that paxillin plays a regulatory role in IgE-FcεRI signaling. Thus, micropatterned ligand arrays, together with biological manipulation of cellular components, reveals spatially distinctive control of cell signaling by receptors and integrins.

2.2 Materials and Methods

2.2.1 Materials. 1-Palmitoyl-2-oleoyl-sn-glycero-3-phosphocholine (POPC), 1,2-Dipalmitoyl-*sn*-Glycero-3-Phosphoethanolamine-N-[6-[(2,4-dinitrophenyl)amino]caproyl] (DNP-cap-PE) and 1,2-Dioleoyl-*sn*-Glycero-3-Phosphoethanolamine-N-(Lissamine Rhodamine B Sulfonyl) (Lissamine Rhodamine PE) were purchased from Avanti Polar Lipids. Mouse monoclonal anti-2,4-dinitrophenyl IgE was purified as described (9) and fluorescently modified with Alexa 488 (Molecular Probes, Invitrogen Co.) according to the labeling kit instructions.

Cytochalasin D, mouse anti-vinculin (clone hVIN-1), and mouse anti-talin (clone 8d4) antibodies were purchased from Sigma-Aldrich. Alexa 568 phalloidin was purchased from Molecular Probes. Syk kinase inhibitor 3-(1-Methyl-1H-indol-3-yl-methylene)-2-oxo-2,3-dihydro-1H-indole-5-sulfonamide (SI), *trans*-3,3',4,5'-Tetrahydroxystilbene (piceatannol), (-)-blebbistatin, and RGD peptides, GRGDSP and GRGDPT were purchased from Calbiochem (EMD Chemicals Inc.). Monoclonal anti-phosphotyrosine clone 4G10 was obtained from Upstate Cell Signaling Solutions (Millipore Co.), monoclonal anti-alpha tubulin (clone .N.593) from US Biologicals, and monoclonal anti-paxillin clone 349 from BD Biosciences. Rabbit anti-ezrin and anti-moesin antibodies were gifts from Dr. A. Bretscher (Cornell University). Integrin α5-EGFP and avian paxillin-EGFP cDNA constructs were gifts from Dr. A. Horwitz (University of Virginia). Actin-EGFP was a gift from A. Jeromin (Allen Institute, Seattle, WA).

2.2.2 Microfabrication of patterned ligands by polymer lift-off. Surfaces were patterned with 1- 5 μm features as described previously (4, 10), and no significant differences were observed over this length range. A 1μm layer of parylene C polymer was deposited on a 4" wafer with a thermally grown oxide layer by using the PDS-2010 Labcoater 2 parylene deposition system (Specialty Coating Systems, Indianapolis). Then, a photoresist layer was spun on the wafer and exposed through a pre-designed mask using standard photolithography. After chemical development of the exposed photoresist, wafers were subjected to oxygen-based reactive ion etching to remove all of the parylene on the regions unprotected by the photoresist.

Supported lipid bilayers containing (or not) DNP ligands : Small unilamellar vesicles were prepared by sonication. The lipid composition was 10 mol% DNP-cap-PE, 1 mol% Lissamine Rhodamine PE (fluorescent probe), and 89 mol% POPC for experiments with cells labeled with Green Fluorescent Protein (GFP) conjugates.

Lipid composition was 10 mol% DNP-cap-PE and 90 mol% POPC when cellular proteins of interest were visualized by immunofluorescence; in these experiments Alexa 488-IgE marked the clustered IgE-FcεRI because the detergent used to permeabilize the cells destroyed the lipid bilayers. DNP-cap-PE was not included in samples for nonspecificity controls. 10 µl of the vesicle suspension (1 mM lipids) was added to an 8-by-8-mm patterned parylene substrate at 21°C for 10 min. The samples were thoroughly rinsed with deionized water before and after the parylene was mechanically peeled away in solution to yield the patterned lipid bilayers.

Patterns of BSA conjugated to DNP: 6-(2,4-dinitrophenyl)aminohexanoic acid succinimidyl ester (Invitrogen, Molecular Probes) was conjugated to BSA with a yield of ~16 DNP/BSA. DNP-BSA was subsequently conjugated with Cy3 (3-4 Cy3 molecules per BSA) for fluorescence visualization. For patterning of DNP-BSA, substrates containing patterned parylene (same as for the patterned lipid bilayers) were treated with a solution of 2% (v/v) of (3-mercaptopropyl)trimethoxysilane in toluene for 20 min. The silanized substrates were incubated with 2mM of N-succinimidyl 4-maleimidobutyrate (GMBS) for 1h in absolute ethanol. The GMBS acts a cross-linker between the mercaptosilane and the protein to be immobilized. Substrates were rinsed with ethanol and phosphate buffer (0.1M Sodium Phosphate, 0.15M NaCl) and incubated with 50µg/mL of DNP-BSA-Cy3 for 4h in phosphate buffer before mechanically peeling off the palylene polymer. The patterned substrates were then washed and incubated with 10mg/mL BSA (unmodified) overnight to block non-specific sites.

2.2.3 Cell culture and transfection. RBL-2H3 cells were maintained in monolayer cultures and harvested with trypsin-EDTA (Invitrogen, Carlsbad, CA) 3–5 days after passage, as described previously (11). Cells were sensitized by overnight incubation at 37°C with Alexa 488-labeled IgE or unlabeled IgE (0.5 µg/ml). For some

experiments, cells were transiently transfected with specified EGFP constructs by using Lipofectamine 2000 (Invitrogen). Cells were suspended in buffered saline solution (BSS: 135 mM NaCl/5.0 mM KCl/1.8 mM $CaCl_2$/1.0 mM $MgCl_2$/5.6 mM glucose/20 mM Hepes, pH 7.4) containing 1 mg/ml BSA. In some experiments, cells were incubated with specific inhibitors or other agents at 37°C for 5 min prior to and during the time of incubation with the patterned substrates.

2.2.4 Fluorescence microscopy and immunofluorescence. Cells suspended at a concentration of 10^6 cells/ml were added to a patterned substrate (8 by 8 mm) in the center of a 35-mm Petri dish with coverglass bottom (0.16–0.19 mm; MatTek, Ashland, MA). After the specified incubation at 37°C (20-45 min) cells were imaged directly (live cell imaging), or they were fixed with 3.7% formaldehyde in PBS for 10 min followed by quenching with 10 mg/ml BSA in PBS. For immunofluorescence after fixation, cells were labeled with primary antibody at room temperature for 1 h. After washing with PBS/BSA (1 mg/ml), the Alexa 568 labeled secondary antibody was incubated with samples at room temperature for 1 h. Control samples, which had nonspecific mouse IgG as the primary antibody were evaluated to confirm negligible nonspecific label and bleedthrough from the other fluorescence channel. Numerous independent experiments (6-12) were carried out for each fluorescently labeled cellular component (e.g. ezrin, moesin, vinculin and others).

A Bio-Rad confocal head and an Olympus IX 70 inverted microscope were used for confocal microscopy. A 522/DF35 filter set was used for simultaneous or sequential dual-color image acquisition with an oil immersion x63, 1.4 numerical aperture objective. Two milliliters of buffered saline solution/BSA (for live cell imaging) of PBS (for fixed cells) was added into the dish before inverting the chip for microscopy observation. Positive cells showed fluorescent patterns that matched the substrate with intensity in the overlapping patches at least 3x greater than the

background level. Visual and quantitative analysis of the images is detailed in the next section.

2.2.5 Patch recognition and co-localization analysis. The number of cells showing co-clustering with the patterned ligands was quantified by visual scoring. A cell was scored as positive if it exhibited the substrate pattern with defined patches of fluorescence concentrated to at least 3x the background level, and percentage positive of >200 cells observed is reported in the text. For some experiments systematic quantification of co-localization with patterned features was performed by calculating the Pearson's cross-correlation coefficient between the green and red channel similar to the approach used previously (12). The analysis was performed on a series of individual images, where each image contained about 10-15 cells. For this, a mask was created in the channel containing cells by thresholding the image, and the region inside the mask was used for the analysis. Then Pearson's correlation between the two channels was calculated according to:

$$\rho_o = \frac{\sum_i (G_i - \bar{G}) \cdot (R_i - \bar{R})}{\sqrt{\sum_i (G_i - \bar{G})^2 \cdot \sum_i (R_i - \bar{R})^2}}$$

Where G_i and R_i are the intensity values of pixels in the green and red channel respectively and $\bar{G}$ and $\bar{R}$ are the average values of G_i and R_i in the image. We note that under our experimental conditions ρ_o of >0.5 is rare because a large portion of individual cells resides in regions between features, and these regions are taken into account in the analysis.

2.2.6 Knock-down of paxillin with siRNA. Pre-designed On-TARGETplus SMARTpool siRNA (siRNA #1) targeting rat paxillin (Dharmacon, Lafayette, CO) were used to reduce paxillin expression levels in RBL-2H3 cells. The siRNA pool sense sequences were GGAACUUCUUCGAGCGGGAUU,

CCAGAAGGGUUCCACGAGAUU, GGCAAAGCCUACUGUCGGAUU and GCGAGGAGGAACACGUCUAUU. An additional pre-designed siRNA (Ambion, Austin, TX) with the sequence GCUCCAGCACCAAAAAUUC (siRNA #2) was used to confirm the results from the functional assays. A siRNA (ON-TARGETplus siCONTROL, Dharmacon) with the sequence UGGUUUACAUGUCGACUAA was used as the nonspecific (sham knock-down) control. For optimal delivery of siRNA, cells were resuspended in buffer (137 mM NaCl, 2.7 mM KCl, 1 $MgCl_2$, 5.6 mM glucose, 20 mM Hepes, pH 7.4) at a concentration of $1x10^7$ cells/ml and, after addition of 1.5nM siRNA, electroporated using an exponential pulse at 280V and 950 μF. Electroporation was carried out in a 4mm cuvette using a Gene Pulser Xcell electroporator system (BioRad Laboratories). After electroporation, cells were plated in medium at a 25-30 % confluence and incubated at 37°C for 48 hours. Protein knock-down was confirmed by immunoblotting.

2.2.7 Cell lysis and immunoblotting. Whole cell lysates were prepared on ice by suspending cells in lysis buffer (5mM N-ethylmaleimide, 1mM Na_3VO_4, 5mM $Na_2P_2O_7$, 50mM NaF, 2mM iodoacetate, 5mM EDTA, 0.1 % (v/v) Triton X-100, 50mM NaCl, 50mM Tris and 2% protease inhibitor cocktail (Sigma), pH 7.6). Lysates were centrifuged at 15,000 x g for 10 min at 4°C. The supernatant was mixed with Tris-glycine SDS buffer and boiled for 5 min. Samples were resolved on a 12% Tris-Glycine polyacrylamide gel and transferred to an Immobilon-P membrane with a pore size of 0.45μm (Millipore, Billerica, MA) by semi-dry transfer. Immunoblots were visualized with the Enhanced Chemiluminescence method using the appropriate antibodies.

2.2.8 Antigen Stimulated Degranulation. RBL cells (1×10^6 cells/well in a 96-well plate, or $2x\ 10^6$ cells/ml in suspension) were sensitized with anti-DNP IgE as described above. Multivalent ligand DNP-BSA (final concentration 100 ng/ml) was

added as the stimulus, and cellular degranulation was quantified with a β-hexosaminidase colorimetric assay (13). Degranulation was expressed as a percentage of the total β-hexosaminidase released from cells after lysis with 0.1% Triton X-100.

2.2.9 Measurement of intracellular Ca^{2+} mobilization. Cells were loaded with Indo-1 AM (Molecular Probes), and fluorescence was measured on a SML 8100S fluorimeter in a time based acquisition mode as previously described (14). The maximum fluorescence from each sample was measured after lysing cells with 0.1% Triton X-100. Background fluorescence was measured by adding EDTA to the buffer. The Ca^{2+} response was quantified using a normalization factor for each condition as previously described (14).

2.3 Results

2.3.1 F-actin in RBL cells redistributes reversibly with IgE-FcεRI that are clustered by micropatterned ligands. We labeled F-actin with Alexa 568 phalloidin at various time points after incubating anti-DNP IgE sensitized RBL cells with the substrates at 37ºC. Consistent with our previous results obtained with actin-EGFP (4), we observed accumulation of the actin label over the patterned features after 25 min stimulation (Figure 2.1A), and the percentage of cells showing clear actin patches became maximal (typically 70% of the cells) after ~40 min. These patches are observed on top of a diffuse background of cortical actin stain, and some day-to-day variability of detected co-localization with the patterned bilayers is due to this background fluorescence. We investigated the specificity and stability of visibly co-clustered IgE-FcεRI and cytoskeletal actin by adding 20μM DNP-aminocaproyl-L-tyrosine (DCT) 25-30 min after the initial incubation of cells with the patterned

Figure 2.1: Vinculin and talin, but not ezrin and moesin, visibly co-redistribute with clustered IgE-FcεRI. Confocal florescence micrographs show cells incubated at 37ºC with patterned lipid bilayers containing DNP-cap-PE and stained for specific intracellular proteins (red). Clustered IgE-FcεRI on cell surfaces are visualized by Alexa 488-labeled IgE (green). A) F-actin accumulates consistently with the clustered FcεRI-IgE, whereas ERM family members, ezrin and moesin, do not. B) Focal adhesion proteins vinculin and talin redistribute with clustered IgE-FcεRI in absence and presence of fibronectin-RGD peptides (RGDSP or RGDSPT). Intracellular proteins were labeled after ~40 min incubation of cells with substrates, followed by cell fixation and treatment with Alexa 568-phalloidin (F-actin) or specific antibodies (ezrin, moesin, vinculin, talin). Scale bar in all images represents 20 μm.

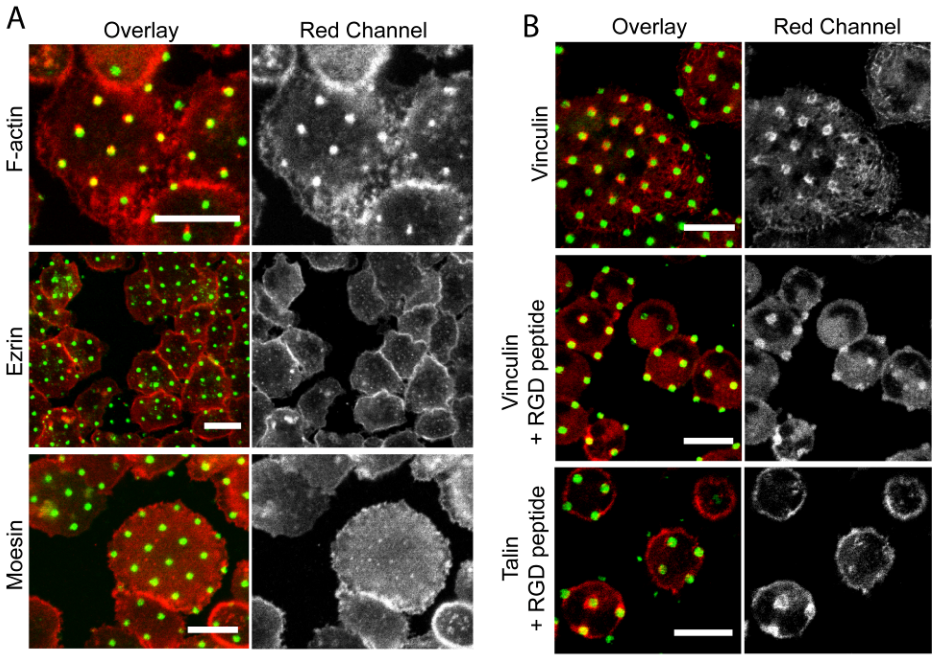
A
Overlay
Red Channel
F-actin
Ezrin
Moesin
B
Overlay
Red Channel
Vinculin
Vinculin
+ RGD peptide
Talin
+ RGD peptide

bilayers. This soluble monovalent DNP-ligand competes with the immobilized DNP-cap-PE in the lipid bilayers and causes the clustered IgE-FcεRI to disperse within 30 min (data not shown). The coincident F-actin stain also disperses on the same time scale as the clustered IgE-FcεRI as monitored in live cells transfected with actin-EGFP (Figure 2.2). These results demonstrate that cytoskeletal actin co-redistribution occurs specifically with clustered IgE-FcεRI and is reversible, pointing to the presence of connecting proteins that sense the state of IgE-FcεRI aggregation.

Pretreatment of cells with inhibitors of actin polymerization such as cytochalasin D prevents co-redistribution of F-actin with IgE-FcεRI that is clustered by patterned ligands, as shown previously (4). In contrast, we find that co-localized IgE-FcεRI and F-actin patches, as reported by actin-EGFP on live cells, are not reversed if cytochalasin D (4μM) is added after these are formed (Figure 2.2). These results indicate the polymerized actin associated with the clustered receptors forms stable structures, probably by means of proteins that crosslink F-actin.

We evaluated members of the ezrin/radixin/moesin (ERM) family that are involved in coupling some signaling components in the plasma membrane with the actin cytoskeleton (15). In particular, ERM adaptors have been implicated in regulation of the immunological synapse in T cells (16). Antibodies specific for either ezrin or moesin were added to cells that had been fixed after incubation with the patterned ligands for periods up to an hour, followed by fluorescent secondary antibody. Although a diffuse membrane stain could be seen, no concentration of anti-ezrin or anti-moesin with the pattern of clustered IgE-FcεRI was detected in numerous experiments of this type (Figure 2.1A).

Figure 2.2: Actin-EGFP clusters are reversed by monovalent ligand (DCT) but not cytochalasin D. Cells transfected with actin-EGFP were incubated for 25-30min. at 21°C before addition of 20μM DCT (A) or 4μM cytochalasin D (CytoD) (B). Confocal images show the same cell prior to addition of respective reagent and 30 min after addition. Arrows indicate locations of the actin clusters that have reversed after 30 min incubation with DCT (A). Scale bars represent 10 μm.

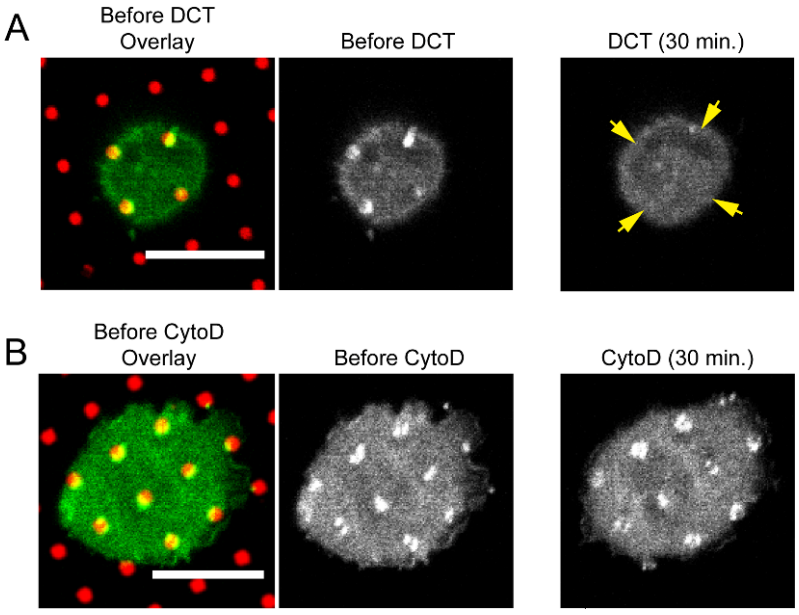
A
Before DCT
Overlay
Before DCT
DCT (30 min.)
B
Before CytoD
Overlay
Before CytoD
CytoD (30 min.)

2.3.2 Focal adhesion proteins co-redistribute with clustered IgE-FcεRI.

Vinculin, talin, and paxillin are involved in complexes associated with focal adhesions that form when integrins bind to extracellular matrix (ECM) proteins, such as fibronectin, and consequently form linkages to the cytoskeleton (5). With antibodies specific for vinculin and talin we observed recruitment of both these proteins to the patches of IgE-FcεRI that form in RBL cells after incubation with the patterned, liganded substrates. The kinetics of this accumulation is very similar to that of F-actin: Resolvable patches of vinculin or talin appear after ~25 min and become maximal after ~40 min (Figure 2.1B). The number of cells with detectable patches of talin, typically 25%, is less than that for vinculin, typically 70%, and this may be due to differences in antibodies or different levels of specific background staining that affects contrast. The stain that concentrates with the patches sometimes appears ring-like, suggesting limited accessibility.

RBL cells adhere to and spread on glass possibly by means of fibronectin or other ECM proteins secreted by these cells, and attached cells labeled with anti-vinculin exhibit structures resembling focal adhesions (Figure 2.3). On substrates patterned with lipid bilayers, the cells adhere in regions in between the patterned features. To test dependence of IgE-FcεRI, vinculin, and talin clustering on integrin engagement and activation we utilized soluble RGD peptides that compete with fibronectin binding sites. We found that addition of 0.5 – 1 mg/ml of GRGDSP or GRGDPT peptides, known to inhibit integrin-mediated cellular attachment (17) causes reduced cell spreading on the substrate, but this treatment does not prevent patches of vinculin and talin in regions of the pattern ligands (Figure 2.1B). On the contrary, we

Figure 2.3: RBL cells exhibit structures resembling focal adhesions after adhering to a silica (glass) surface. Cells were incubated with glass coverslips in BSS for 1h at 37ºC and then fixed and stained for vinculin. Structures resembling focal contacts appear as bright areas, most visible at the cell periphery. Scale bar represents 20 μm.

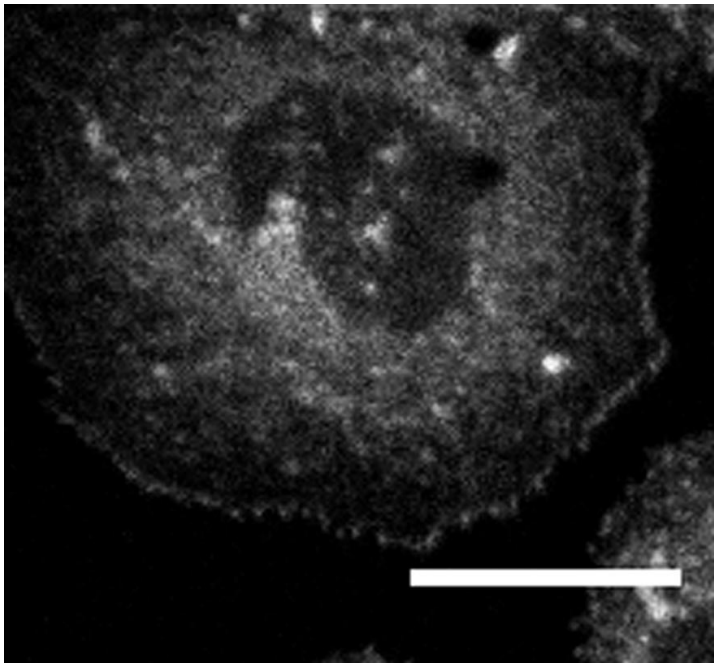

find that this treatment increases the accumulation of these focal adhesion proteins in these regions, probably because they have been released from integrin complexes.

Control experiments and quantitative analyses were carried out. Direct comparison of patterned lipid bilayers containing or not containing the DNP-cap-PE ligand showed that vinculin and talin co-redistribute with IgE-FcεRI only when the specific ligand is present (Figure 2.4). In other experiments patterned lipid bilayers were replaced by patterned bovine serum albumin conjugated to DNP (DNP-BSA) using the same lithographic mask and parylene lift-off method. These substrates were tested with RBL cells sensitized or not with anti-DNP IgE, and vinculin, paxillin, ezrin or moesin were fluorescently labeled. None of these markers clustered with the patterned DNP-ligand for cells without IgE bound to FcεRI, whereas vinculin and paxillin but not ezrin or moesin formed patterned clusters on cells with bound IgE. Cross-correlation analysis provides quantitative confirmation of these results (Figure 2.5)

We investigated whether the association of actin and focal adhesion protein vinculin with clustered IgE-FcεRI is affected by early signaling activities stimulated by these receptors. We treated cells with two different inhibitors of Syk kinase that is activated by clustered IgE-FcεRI after receptor phosphorylation by Lyn kinase (18). Addition of Syk inhibitor SI (1μM) (19) or piceatannol (40uM) prior to and during incubation of cells with liganded substrates had no detectable effect on redistribution of vinculin or actin with the clustered receptors. The same concentrations of these Syk inhibitors reduce antigen stimulated degraunulation by 75-80%. We also tested PP1 (15μM), which inhibits Lyn and other Src family kinases, and this inhibitor reduced

Figure 2.4: Acummulation of vinculin and talin is specific to the clustered IgE-FcεRI. RBL cells were incubated with the patterned bilayers containing 100% POPC (A) or 10% DNP-cap-PE and 90% POPC (B) for 40min at 37°C. A) In absence of DNP-ligand no IgE-FcεRI or vinculin and talin do not accumulate in a defined array as visualized by immunofluorescence, and some cells show exclusion from regions of size and periodicity consistent with a pattern (arrowheads). Patterned substrate is not visualized directly because the detergent (Triton-X 100) used to permeabilize the cells for immunolabeling destroys the bilayer. Cells in (A) were stimulated with soluble DNP-BSA (95 ng/ml) to cause increased spreading similar to cells stimulated by patterned DNP-cap-PE (B). Patterned clustering of IgE-FcεRI and accumulation of vinculin and talin are visualized when DNP-ligand is present in the bilayer (B) as in Figure 1 of the main text. Scale bars correspond to 20μm.

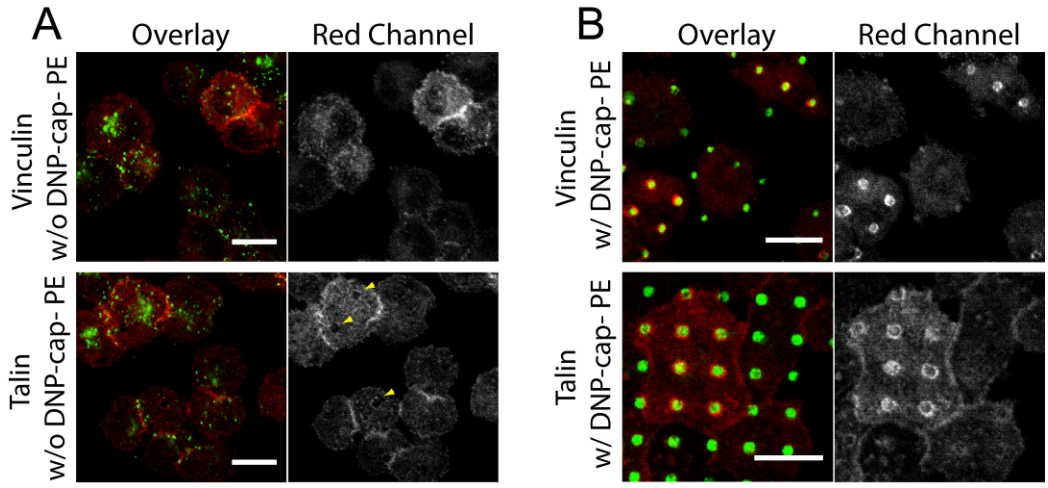
A
Overlay
Red Channel
Vinculin
w/o DNP-cap- PE
Talin
w/o DNP-cap- PE
B
Overlay
Red Channel
Vinculin
w/ DNP-cap- PE
Talin
w/ DNP-cap- PE

by half the percentage of cells showing co-redistribution of actin or vinculin with clustered receptors. Cytochalasin D (2μM) completely abrogates F-actin recruitment, as described above, and this treatment similarly prevents patching of vinculin with clustered receptors. Our results with these inhibitors indicate that vinculin and actin redistribution with clustered IgE-FcεRI depends in part on Src family kinase activity but not on Syk activity.

We considered whether the accumulation of these focal adhesion proteins depends on mechanical tension induced by non-muscle myosin II, a motor protein involved in regulation and distribution of actin filaments such as occurs during formation of stress fibers. As a test, we treated cells with blebbistatin, an inhibitor of myosin II ATPase activity, at a concentration of 50μM prior to and during 40 min incubation of cells with patterned DNP-ligands. This treatment decreased filamentous heterogeneity of fluorescently labeled vinculin or paxillin and enhanced rather than reduced co-redistribution of actin (data not shown), vinculin or paxillin with clustered IgE-FcεRI as compared to samples without blebbistatin (Figure 2.5A, B, and D).

2.3.3 Paxillin co-redistributes with clustered IgE-FcεRI independently of integrins. Paxillin is known to connect vinculin with other binding partners in focal adhesion complexes. We transfected RBL cells with the gene construct for paxillin-EGFP and observed co-redistribution of the expressed protein with clustered IgE-FcεRI after cells were incubated with patterned substrates (Figure 2.6). Clear patches of paxillin-EGFP emerged above the background level in many cells, typically in ~35% after 40 min. In other experiments when anti-paxillin was used as the label, typically 70% of the cells showed co-clustering with IgE-FcεRI (Figure 2.5).

Figure 2.5: Vinculin and paxillin redistribute with patterns of DNP-proteins only when cells are sensitized with anti-DNP IgE, and this redistribution is not prevented by blebbistatin. RBL cells were incubated for 40 min at 37°C on substrates patterned with immobilized BSA conjugated to DNP and fluorophore Cy3. When cells are not sensitized with IgE, no patterns of paxillin (A, upper panel) or vinculin (B, upper panel) are visualized by antibody labeling and immunofluorescence microscopy. IgE sensitized cells show clear clustering of paxillin (A, middle panel) and vinculin (B, middle panel) but not ezrin (C, upper pannel) or moesin (C, lower pannel), and treatment with the non-muscle myosin II inhibitor blebbistatin (50μM) does not prevent co-redistribution of paxillin or vinculin with clustered IgE-FcεRI (A and B, lower panel). Blebbistatin treatment slightly enhances the visibility of vinculin and paxillin accumulation, possibly because the filamentous staining of vinculin and paxillin in stimulated cells, which hinders clarity of pattern, disappears upon blebbistatin treatment (D shows magnified region of B). Scale bars in A, B, and C correspond to 20μm. E) Co-clustering with patterned DNP-proteins of ezrin, moesin, vinculin, and paxillin (the latter two in the absence and presence of blebbistatin) was quantified by measuring the Pearson's cross-correlation coefficient in regions defined by the cells (typically >10) within whole field images and averaged over several (n) images. The legend is as follow: moesin for sensitized cells (MO, n=26), ezrin for sensitized cells (EZ, n=31), paxillin for non-sensitized cells (PAX-C, n=29), paxillin for sensitized cells (PAX, n=26), paxillin, sensitized cells, + 50μM blebbistatin (PAX-BL, n=30), vinculin for non-sensitized cells (VIN-C, n=32), vinculin for sensitized cells (VIN, n=38), vinculin, sensitized cells, + 50μM blebbistatin (VIN-BL, n=29).

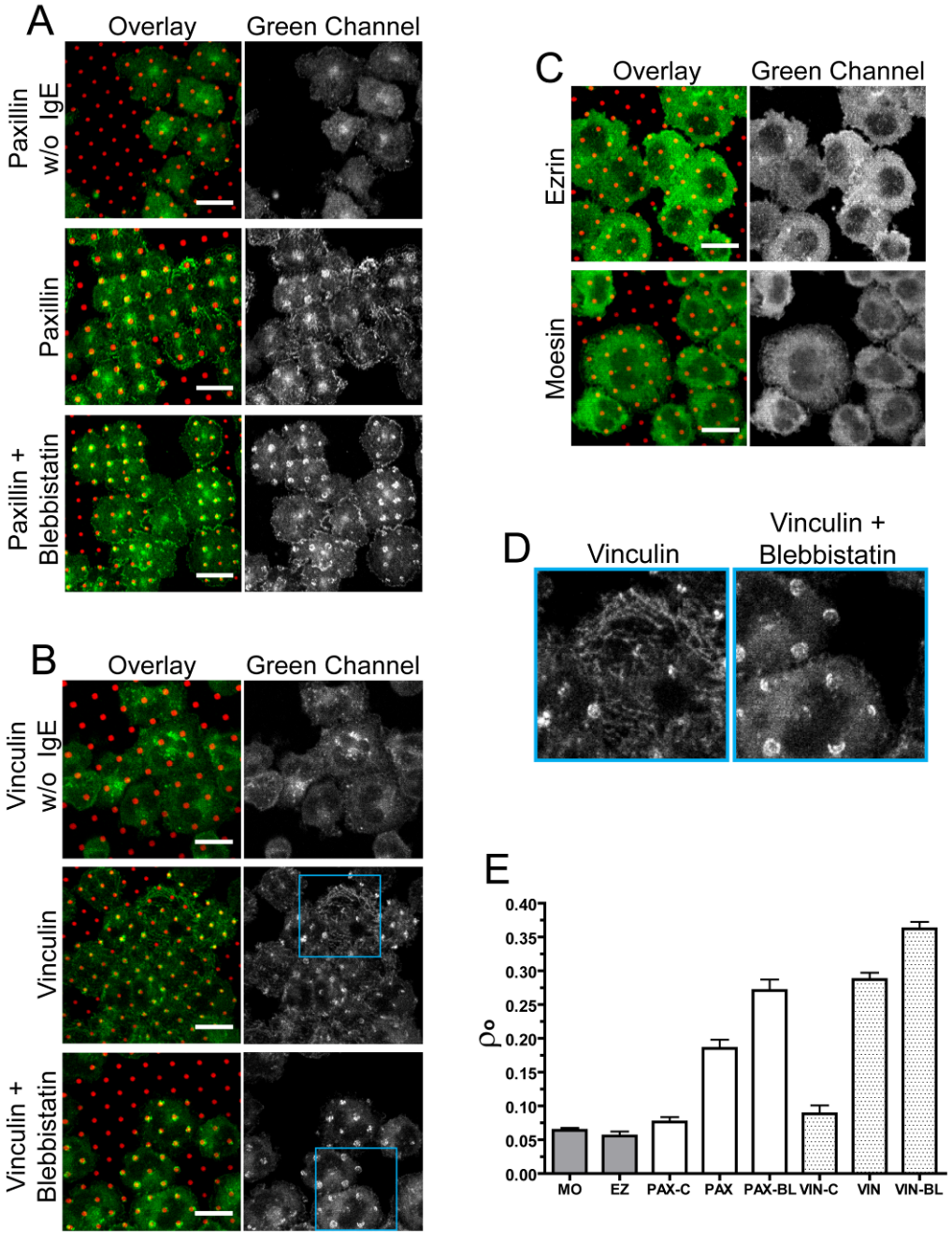
A
Overlay
Green Channel
Paxillin w/o IgE
Paxillin
Paxillin + Blebbistatin
B
Overlay
Green Channel
Vinculin w/o IgE
Vinculin
Vinculin + Blebbistatin
C
Overlay
Green Channel
Ezrin
Moesin
D
Vinculin
Vinculin + Blebbistatin
E
ρo
0.40
0.35
0.30
0.25
0.20
0.15
0.10
0.05
0.00
MO
EZ
PAX-C
PAX
PAX-BL
VIN-C
VIN
VIN-BL

Quantitative analysis of protein co-localization shows a strong accumulation of paxillin to the sites of receptor clustering as determined by fluorescence cross-correlation (Figure 2.5E).

As described in a previous section, we observed that soluble RGD peptides enhanced accumulation of vinculin and talin with clustered IgE-FcεRI (Figure 2.1B). To investigate further whether these interactions of focal adhesion proteins are independent of integrin engagement and signaling, we evaluated RBL cells expressing a GFP construct of α5-integrin and compared these in the same experiment to cells expressing paxillin-EGFP. In contrast to paxillin, α5 integrin resists association with the lipid bilayer regions that contain the specific ligand DNP-cap-PE. This difference is striking in the images and can be quantified with line scans (Figure 2.6). Tested in several independent experiments, as many as 65% of cells expressing the EGFP labeled integrin showed this exclusion, and concentration of this protein was never observed in the patterns. None of the other samples containing IgE sensitized cells with labeled vinculin, talin, or paxillin ever showed this exclusion in many different experiments with the liganded arrays of lipid bilayers. This aversion of α5-integrin to the patterned regions is not caused by clustering and activation of the IgE receptors because the same occurs when the ligand, DNP-cap-PE, is not included in the lipid bilayers (data not shown).

2.2.4 Functional role of paxillin in IgE-FcεRI signaling. Our observation of paxillin clustering with IgE-FcεRI on patterned bilayers, together with previous evidence that paxillin is involved in FcεRI-mediated signaling (see Introduction), prompted us to examine more directly the functional importance of this adaptor

Figure 2.6: Paxillin co-redistributes with clustered IgE-FcεRI and patterned lipid bilayers but integrins avoid these regions. Confocal micrographs show cells expressing paxillin-EGFP or integrin α5-EGFP (green) after incubation for 40 min at 37ºC with patterned lipid bilayers (red) containing DNP-cap-PE and fixation before imaging. A) Paxillin is recruited with IgE-FcεRI in the regions of patterned ligands, and α5-integrin is excluded. Scale bar represents 20μm. B) Intensity line profiles from images in (A) confirm that paxillin accumulation and integrin exclusion correspond exactly to where the patterned bilayers are localized.

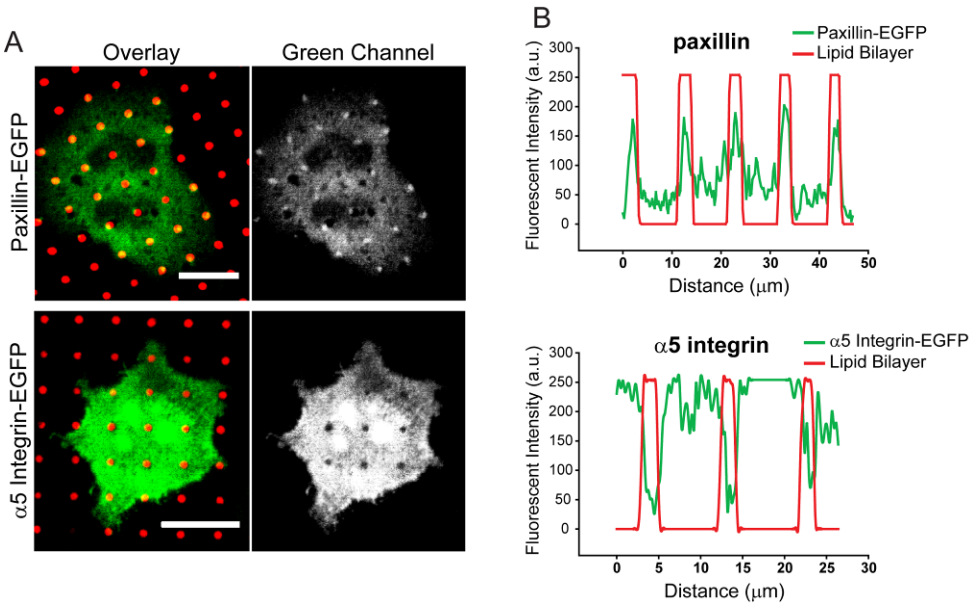
A
Overlay
Green Channel
Paxillin-EGFP
α5 Integrin-EGFP
B
paxillin
Paxillin-EGFP
Lipid Bilayer
Fluorescent Intensity (a.u.)
Distance (μm)
α5 integrin
α5 Integrin-EGFP
Lipid Bilayer
Fluorescent Intensity (a.u.)
Distance (μm)

protein. For this purpose, we used siRNA to knock-down expression of endogenous paxillin. Two different siRNA constructs caused >90% reduction of paxillin (Figure 2.7A). To evaluate participation of paxillin in co-redistribution of F-actin with clustered IgE-FcεRI, we stained knock-down and control cells with Alexa-568 phalloidin after 40 min incubation with the patterned ligands. We detected no differences, indicating that although paxillin may be involved in linking clustered receptors to the cytoskeleton, it is not essential.

Measurements of receptor-mediated cellular responses were carried out on suspended cells to eliminate signaling effects caused by integrin-mediated binding to substrates. We evaluated effects of paxillin knock-down on tyrosine phosphorylation stimulated by IgE-FcεRI by incubating suspended cells with multivalent ligand (DNP-BSA) and immunoblotting cell lysates with an anti-phosphotyrosine antibody. Paxillin knock-down cells yielded a pattern of stimulated tyrosine phosphorylation that was qualitatively similar to control cells treated with nonspecific siRNA (Figure 2.7B). However, the knock-down cells showed a clear and consistent increase in phosphorylation of two bands corresponding to molecular masses of 35kDa (p35) and 50kDa (p50) (Figure 2.7B - D). The p35 band corresponds to FcεRI-β, as demonstrated previously (20); consistent with this assignment the phosphorylation of this band is maximal 3 min after the cells are stimulated with multivalent ligand at 37°C. In contrast, tyrosine phosphorylation of the p50 band is maximal 15 min post stimulation. The time course of phosphorylation of p50 are consistent with the activation and regulation of p50 by Csk, a kinase that negatively regulates Src kinases(21). These results with the knock-down cells suggest that paxillin, possibly by

Figure 2.7: Paxillin knock-down affects phosphorylation stimulated by IgE-FcεRI. A) Immunoblots show that paxillin-specific siRNA cause >90% decrease in paxillin expression levels. To confirm knock-down, the same PDVF membrane was stripped and re-probed with anti-tubulin as a loading control. B) Antigen stimulated phosphorylation was examined in lysates from suspended whole cells ($2x10^6$/ml) 48 h after siRNA delivery, sensitization with anti-DNP IgE, and stimulation with DNP-BSA (50ng/ml) for times indicated. After SDS gel electrophoresis, gels were blotted with anti-phosphotyrosine antibody, 4G10. Boxes indicate 35 kDa (p35) and 50 kDa (p50) bands that are consistently increased after paxillin knock-down in this representative experiment; anti-tubulin bands serve as loading control. C) Densitometric analysis of tyrosine phosphorylation (PY) for p35 band (FcεRI-β) after 3 min stimulation. D) Densitometric plot showing stimulation time course for relative tyrosine phosphorylation of the p50 band. Data in C and D are averaged over five different experiments in which the phosphorylated band was normalized by tubulin band (loading control). The data were further normalized to control (sham knock-down) cells (for C) or to the 15 min time point in the knock-down cells (for D). Significant differences are indicated as ** ($0.01 \leq p < 0.01$) or *** ($p < 0.001$). Error bars indicate standard error of the mean.

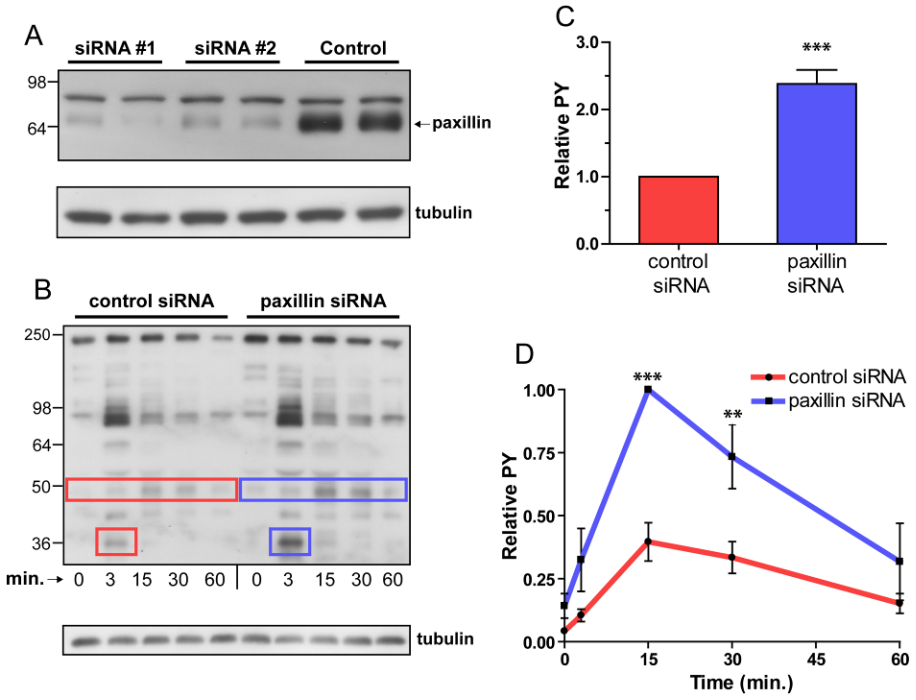
A
siRNA #1
siRNA #2
Control
98
64
paxillin
tubulin
B
control siRNA
paxillin siRNA
250
98
64
50
36
min.→ 0 3 15 30 60 0 3 15 30 60
tubulin
C
3.0
2.0
1.0
0.0
Relative PY
***
control siRNA
paxillin siRNA
D
control siRNA
paxillin siRNA
1.00
0.75
0.50
0.25
0.00
Relative PY
***
**
0
15
30
45
60
Time (min.)

binding to Lyn, plays a negative regulatory role in Lyn phosphorylation of the p35 and p50 substrates.

We also evaluated downstream steps of activation in the paxillin knock-down cells. Stimulated Ca^{2+} mobilization, which follows after initial FcεRI phosphorylation and precedes cellular degranulation, occurs in two phases: release from intracellular stores and influx from extracellular medium. In buffer containing Ca^{2+}, the paxillin knock-down cells show a small but consistent decrease in the Ca^{2+} response (Figure 2.8A). To evaluate separately the stimulated Ca^{2+} release from stores and Ca^{2+} influx, antigen was added in buffer containing no Ca^{2+}, and then Ca^{2+} was added subsequently. Paxillin knock-down resulted in a consistent decrease of ~50% in stimulated Ca^{2+} release from the intracellular stores and a decrease of ~ 10% in the Ca^{2+} influx (Figure 2.8B and C). These results are consistent with a negative regulatory effect of paxillin on Lyn activation that results in an enhancing effect on antigen-stimulated Ca^{2+} release from stores.

2.4 Discussion

The patterned lipid bilayer substrate we employed in this study restricts integrin-mediated adhesion to nonliganded regions, and this spatial separation reveals that actin-binding proteins vinculin, talin, and paxillin interact with ligand-clustered IgE-FcεRI in mast cells, independently of integrins. Our results suggest that these characteristic focal adhesion proteins serve to connect clustered IgE-FcεRI to cytoskeletal actin, which also co-redistributes with these receptors and may regulate receptor-mediated signaling. We and others previously demonstrated the versatility of

Figure 2.8: Paxillin knock-down affects Ca^{2+} mobilization stimulated by IgE-FcεRI. Intracellular Ca^{2+} changes in paxillin knock-down (gray) and sham knock-down (black) cells after stimulation by DNP-BSA (50-200 ng/ml) at 37ºC, in representative (A and B) and summarized (C) experiments. A) Cells were stimulated in buffer containing 2mM Ca^{2+}; release from intracellular stores and influx from the extracellular medium occurs under these conditions. B) Cells were stimulated in the absence of extracellular Ca^{2+} such that only release from stores occurs; after 500 s the Ca^{2+} concentration in the buffer is increased to 2mM (by addition of $CaCl_2$) such that influx occurs. C) Averages over five experiments similar to that shown in (B): The first two sets of two bars correspond to curves prior to and after addition of extracellular Ca^{2+} (2mM), respectively; the last set correspond to both curves additively. In each case changes in intracellular Ca^{2+} concentration were integrated over 500 sec and normalized to the control cell response. Significant differences are indicated as * ($0.01 \leq p < 0.05$) or ** ($0.001 \leq p < 0.01$). Error bars indicate standard error of the mean.

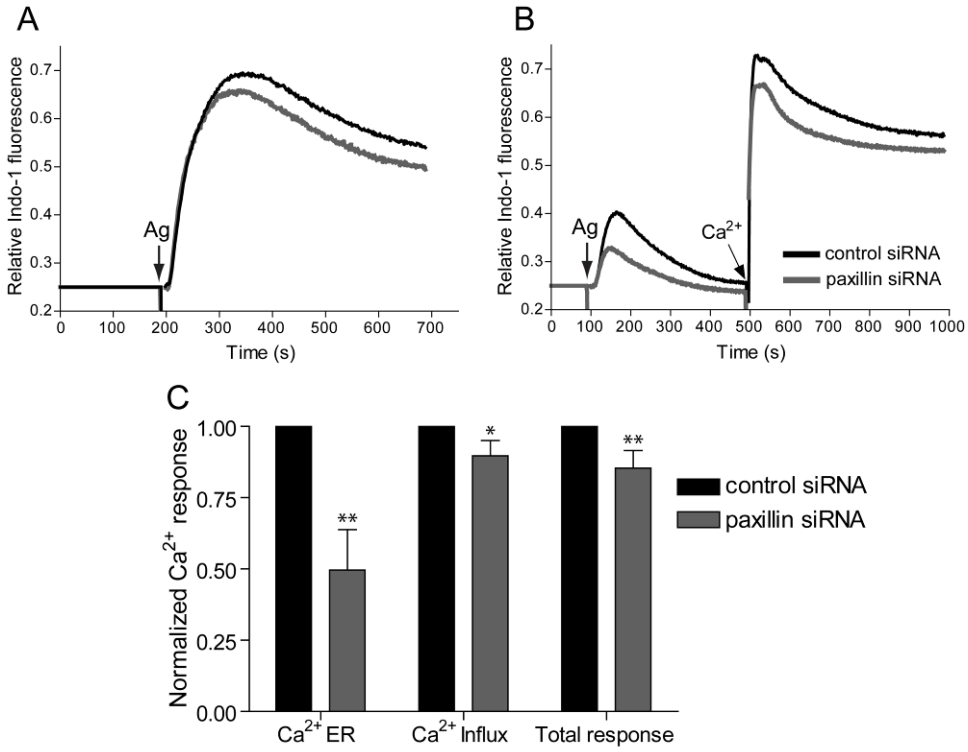
A
Relative Indo-1 fluorescence
Ag
Time (s)
B
Relative Indo-1 fluorescence
Ag
Ca2+
control siRNA
paxillin siRNA
Time (s)
C
Normalized Ca2+ response
control siRNA
paxillin siRNA
Ca2+ ER
Ca2+ Influx
Total response

patterned ligands that confine and activate receptors in micron size regions so that the spatially regulated cellular responses can be monitored (reviewed in (22)). An important feature of patterned lipid bilayers is that proteins do not adhere nonspecifically to the lipid regions: Anti-DNP IgE-FcεRI bind selectively to these regions only because DNP-cap-PE is incorporated in the bilayers (10). In contrast, the most prominent RBL cell integrin (α-5) avoids the regions of the lipid bilayers and binds to the glass surface by means of ECM proteins secreted by the cells. Others also showed previously that supported lipid bilayers are resistive to protein absorption and cell adhesion (23).

Our experiments indicating that characteristic focal adhesion proteins connect antigen-clustered IgE-FcεRI to the cytoskeleton provide new insight to increasing evidence for cytoskeletal regulation of FcεRI signaling (24-27). We showed that F-actin co-concentrates with IgE-FcεRI that is clustered in patches by immobilized DNP-ligands. This co-redistribution is prevented, but not reversed, by cytochalasin D, suggesting stabilization of the polymerized F-actin by actin-binding proteins. In contrast, both IgE-FcεRI clustering and co-concentrating F-actin are reversed by soluble multivalent ligand which competes with the immobilized DNP-ligand. This dynamic, reversible process indicates that the linkage to the cytoskeleton is based on complexes forming stably with FcεRI only after oligomerization by multivalent ligand binding.

To investigate the composition of complexes that connect to the cytoskeleton, we examined several known actin binding proteins. We detected no co-redistribution of ezrin and moesin when sensitized cells are incubated with patterned ligands, in contrast to clear co-redistribution of vinculin, talin, and paxillin. Moreover, these latter proteins accumulate visibly in the same patterns as the clustered IgE-FcεRI with kinetics similar to those observed for F-actin. Interactions between paxillin, vinculin,

talin and actin have been established in the context of integrin-based focal adhesion complexes (5, 28): Vinculin binds directly to paxillin and actin, whereas talin binds actin and vinculin as a result of integrin engagement. The patterned substrates revealed that complexes containing these components form in regions of clustered IgE-FcεRI, even when integrins (as represented by α5) are excluded from these regions.

Our finding that Syk inhibitors, SI and piceatannol, do not inhibit vinculin and actin accumulation whereas the Src family tyrosine kinase, PP1, partially inhibits both suggests that the linkage between FcεRI and the cytoskeleton is enhanced by stimulated Lyn kinase activity and occurs prior to activation of Syk substrates or in parallel signaling pathways. Paxillin is tyrosine phosphorylated after antigen activation in RBL mast cells (7) and has been found to interact with Lyn kinase in this and several other cell types (8, 29, 30), suggesting that paxillin is one of the proteins that provides a link to vinculin, talin and thereby to the actin cytoskeleton.

The observed interactions of focal adhesion proteins with clustered IgE-FcεRI also lends insight to apparent signaling cross-talk between these receptors and integrins. For example, it is known that adherence of RBL-2H3 cells to fibronectin-coated surfaces enhances degranulation and also serves as a co-stimulus for cytokine production (31-33). Similarly, cell activation by antigen mediated clustering of IgE-FcεRI causes increased adhesion and spreading in mast cells (34, 35). We demonstrated competing binding sites for focal adhesion proteins: Soluble RGD peptides compete with immobilized fibronectin and bind integrins, consequently releasing vinculin and talin to increase their concentration with the clustered IgE-FcεRI.

The spatially distinctive information provided by the micropatterned ligand arrays is complemented with cell biological experiments. We found that substantially reducing paxillin in RBL cells with siRNA clearly enhances tyrosine phosphorylation

Figure 2.9: Paxillin knock-down has a small effect on antigen-mediated degranulation. Stimulated degranulation of RBL cells was measured as β-hexosaminidase release. Cells were stimulated with indicated concentration of DNP-BSA for 1h, and total release into supernatant was quantified. Adherent (A) and suspended cells (B) show stimulated degranulation that is similar but slightly less (at higher doses) for paxillin knock-down cells compared to control cells. Data are averaged over multiple experiments (n= 32 and 24 for adherent and suspended cells, respectively).

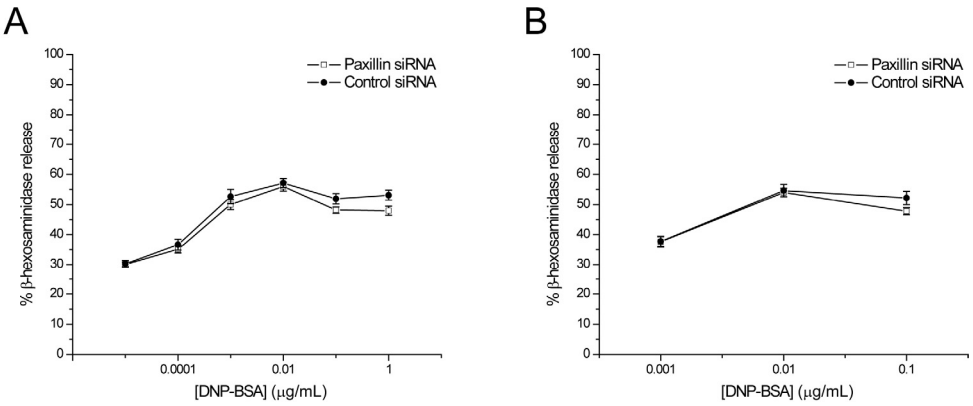
A
Paxillin siRNA
Control siRNA
% β-hexosaminidase release
[DNP-BSA] (μg/mL)
0.0001
0.01
1
B
Paxillin siRNA
Control siRNA
% β-hexosaminidase release
[DNP-BSA] (μg/mL)
0.001
0.01
0.1

of two proteins in response to stimulation by multivalent ligand: The p35 band corresponding to FcεRI β subunit, and the unidentified p50 band. Enhanced phosphorylation of FcεRI β stimulated by antigen was also seen for RBL cells treated with inhibitors of actin polymerization, cytochalasin D and latrunculin (24, 25, 27). These results are consistent with the view that negative regulation of Lyn kinase mediated by paxillin (possibly by linking to the cytoskeleton) occurs during early stages of IgE-FcεRI signaling, when Lyn phosphorylates FcεRI β and γ subunits after antigen-mediated clustering of these receptors (36). This inhibitory effect of paxillin is also evident at later stages due to alterred phosphorylation of the p50 protein. Paxillin regulation may be a consequence of interactions with Csk, an inhibitor of Src family kinases, and its suppression by paxillin results in enhanced downstream signaling (25), as manifested by enhanced Ca^{2+} mobilization.

Paxillin knock-down cells showed only a small inhibitory effect on stimulated degranulation (Figure 2.9), which is one endpoint of the cellular response. This is not surprising because of the relatively modest inhibition of total Ca^{2+} mobilization. It is possible that other proteins compensate for paxillin knock-down or that paxillin plays a larger regulatory role in other stimulated cellular responses, such as cytokine production. In this regard, leupaxin (a member of the paxillin family of adapter proteins) recently was shown to regulate cytokine production resulting from B cell receptor signaling (30). Paxillin knock-down in RBL cells did not detectably affect F-actin co-redistribution with clustered IgE-FcεRI on patterned bilayers, indicating that other proteins are also involved in these linkages, and these may have other regulatory effects. As demonstrated in this study, candidate proteins can now be examined with patterned substrates, pharmacological and genetic manipulation, and biological measurements.

REFERENCES

1. Lock, J. G., Wehrle-Haller, B., and Stromblad, S. (2008) Cell-matrix adhesion complexes: Master control machinery of cell migration, *Seminars in Cancer Biology 18*, 65-76.

2. Kinet, J.-P. (1999) THE HIGH-AFFINITY IgE RECEPTOR (FcεRI): From Physiology to Pathology, *Annual Review of Immunology 17*, 931-972.

3. Holowka, D., Gosse, J. A., Hammond, A. T., Han, X., Sengupta, P., Smith, N. L., Wagenknecht-Wiesner, A., Wu, M., Young, R. M., and Baird, B. (2005) Lipid segregation and IgE receptor signaling: A decade of progress, *Biochimica et Biophysica Acta (BBA) - Molecular Cell Research 1746*, 252-259.

4. Wu, M., Holowka, D., Craighead, H. G., and Baird, B. (2004) Visualization of plasma membrane compartmentalization with patterned lipid bilayers, *PNAS 101*, 13798-13803.

5. Critchley, D. R. (2000) Focal adhesions - the cytoskeletal connection, *Current Opinion in Cell Biology 12*, 133-139.

6. Brown, M. C., and Turner, C. E. (2004) Paxillin: Adapting to Change, *Physiol. Rev. 84*, 1315-1339.

7. Hamawy, M. M., Swaim, W. D., Minoguchi, K., de Feijter, A. W., Mergenhagen, S. E., and Siraganian, R. P. (1994) The aggregation of the high affinity IgE receptor induces tyrosine phosphorylation of paxillin, a focal adhesion protein, *J Immunol 153*, 4655-4662.

8. Minoguchi K, K. H., Nishikata H, Hamawy MM, Siraganian RP. (1994) Src family tyrosine kinase Lyn binds several proteins including paxillin in rat basophilic leukemia cells., *Mol Immunol 31*, 519-529.

9. Subramanian, K., Holowka, D., Baird, B., and Goldstein, B. (1996) The Fc Segment of IgE Influences the Kinetics of Dissociation of a Symmetrical Bivalent Ligand from Cyclic Dimeric Complexes, *Biochemistry 35*, 5518-5527.

10. Orth, R. N., Wu, M., Holowka, D. A., Craighead, H. G., and Baird, B. A. (2003) Mast Cell Activation on Patterned Lipid Bilayers of Subcellular Dimensions, *Langmuir 19*, 1599-1605.

11. Pierini, L., Holowka, D., and Baird, B. (1996) FcεRI-mediated association of 6-micron beads with RBL-2H3 mast cells results in exclusion of signaling proteins from the forming phagosome and abrogation of normal downstream signaling, *J. Cell Biol. 134*, 1427-1439.

12. Hammond, S., Wagenknecht-Wiesner, A., Veatch, S. L., Holowka, D., and Baird, B. (2009) Roles for SH2 and SH3 domains in Lyn kinase association with activated FcεRI in RBL mast cells revealed by patterned surface analysis, *Journal of Structural Biology 168*, 161-167.

13. Naal, R. M. Z. G., Tabb, J., Holowka, D., and Baird, B. (2004) In situ measurement of degranulation as a biosensor based on RBL-2H3 mast cells, *Biosensors and Bioelectronics 20*, 791-796.

14. Pierini, L., Harris, N. T., Holowka, D., and Baird, B. (1997) Evidence Supporting a Role for Microfilaments in Regulating the Coupling between Poorly Dissociable IgE-FcεRI Aggregates and Downstream Signaling Pathways, *Biochemistry 36*, 7447-7456.

15. Bretscher, A., Edwards, K., and Fehon, R. G. (2002) ERM proteins and merlin: integrators at the cell cortex, *Nat Rev Mol Cell Biol 3*, 586-599.

16. Ilani, T., Khanna, C., Zhou, M., Veenstra, T. D., and Bretscher, A. (2007) Immune synapse formation requires ZAP-70 recruitment by ezrin and CD43 removal by moesin, *J. Cell Biol. 179*, 733-746.

17. Gehlsen, K. R., Argraves, W. S., Pierschbacher, M. D., and Ruoslahti, E. (1988) Inhibition of in vitro tumor cell invasion by Arg-Gly-Asp-containing synthetic peptides, *J. Cell Biol. 106*, 925-930.

18. El-Hillal, O., Kurosaki, T., Yamamura, H., Kinet, J. P., and Scharenberg, A. M. (1997) syk kinase activation by a src kinase-initiated activation loop phosphorylation chain reaction, *PNAS 94*, 1919-1924.

19. Lai, J. Y. Q., Cox, P. J., Patel, R., Sadiq, S., Aldous, D. J., Thurairatnam, S., Smith, K., Wheeler, D., Jagpal, S., Parveen, S., Fenton, G., Harrison, T. K. P., McCarthy, C., and Bamborough, P. (2003) Potent small molecule inhibitors of spleen tyrosine kinase (Syk), *Bioorganic & Medicinal Chemistry Letters 13*, 3111-3114.

20. Sheets, E. D., Holowka, D., and Baird, B. (1999) Critical Role for Cholesterol in Lyn-mediated Tyrosine Phosphorylation of FcεRI and Their Association with Detergent-resistant Membranes, *J. Cell Biol. 145*, 877-887.

21. Honda, Z.-i., Suzuki, T., Hirose, N., Aihara, M., Shimizu, T., Nada, S., Okada, M., Ra, C., Morita, Y., and Ito, K. (1997) Roles of C-terminal Src Kinase in the Initiation and the Termination of the High Affinity IgE Receptor-mediated Signaling, *J. Biol. Chem. 272*, 25753-25760.

22. Torres, A. J., Wu, M., Holowka, D., and Baird, B. (2008) Nanobiotechnology and Cell Biology: Micro- and Nanofabricated Surfaces to Investigate Receptor-Mediated Signaling, *Annual Review of Biophysics 37,* 265-288.

23. Kam, L., and Boxer, S. G. (2001) Cell adhesion to protein-micropatterned-supported lipid bilayer membranes, *Journal of Biomedical Materials Research 55*, 487-495.

24. Frigeri, L., and Apgar, J. R. (1999) The Role of Actin Microfilaments in the Down-Regulation of the Degranulation Response in RBL-2H3 Mast Cells, *J Immunol 162*, 2243-2250.

25. Holowka, D., Sheets, E. D., and Baird, B. (2000) Interactions between Fc(epsilon)RI and lipid raft components are regulated by the actin cytoskeleton, *J Cell Sci 113*, 1009-1019.

26. Oka, T., Sato, K., Hori, M., Ozaki, H., and Karaki, H. (2002) FcεRI cross-linking-induced actin assembly mediates calcium signalling in RBL-2H3 mast cells, *136*, 837-846.

27. Torigoe, C., Song, J., Barisas, B. G., and Metzger, H. (2004) The influence of actin microfilaments on signaling by the receptor with high-affinity for IgE, *Molecular Immunology 41*, 817-829.

28. Ziegler, W. H., Liddington, R. C., and Critchley, D. R. (2006) The structure and regulation of vinculin, *Trends in Cell Biology 16*, 453-460.

29. Rathore, V. B., Okada, M., Newman, P. J., and Newman, D. K. (2007) Paxillin family members function as Csk-binding proteins that regulate Lyn activity in human and murine platelets, *Biochem J 403*, 275-281.

30. Chew, V., and Lam, K.-P. (2007) Leupaxin Negatively Regulates B Cell Receptor Signaling, *J. Biol. Chem. 282*, 27181-27191.

31. Ra C, Y. M., Yagita H, Okumura K. (1994) Fibronectin receptor integrins are involved in mast cell activation, *J Allergy Clin Immunol 94*, 625-628.

32. Kruger, K., Grutzkau, Krasagakis, Hoffmann, and Henz. (1999) Adhesion of human mast cells to extracellular matrix provides a co-stimulatory signal for cytokine production, *Immunology 98*, 253-257.

33. Hamawy, M. M., Oliver, C., Mergenhagen, S. E., and Siraganian, R. P. (1992) Adherence of rat basophilic leukemia (RBL-2H3) cells to fibronectin- coated surfaces enhances secretion, *J Immunol 149*, 615-621.

34. Wyczolkowska J, D. J., Slusarczyk A, Kolago B. (1994) Relations between FcεRI crosslinking-induced mast cell activation and adhesion to fibronectin., *J Physiol Pharmacol 45*, 501-516.

35. Dastych, J., Wyczólkowska, J., and Metcalfe, D. D. (2001) Characterization of α5-Integrin-Dependent Mast Cell Adhesion following FcεRI Aggregation, *Int Arch Allergy Immunol 125*, 152-159.

36. Odom, S., Gomez, G., Kovarova, M., Furumoto, Y., Ryan, J. J., Wright, H. V., Gonzalez-Espinosa, C., Hibbs, M. L., Harder, K. W., and Rivera, J. (2004) Negative Regulation of Immunoglobulin E-dependent Allergic Responses by Lyn Kinase, *J. Exp. Med. 199*, 1491-1502.

CHAPTER 3

DYNAMIN 2 REGULATION OF FcεRI RECEPTOR-MEDIATED REDISTRIBUTION OF ACTIN: IMPLICATIONS IN RECEPTOR INTERNALIZATION.

3.1 Introduction

The high affinity receptor for immunoglobulins E (IgE), FcεRI, is a member of a family of cell surface immune receptors that share a common activation mechanism: Receptor aggregation induces phosphorylation of immunoreceptor tyrosine-based activation motifs (ITAMs) by Src family kinases, and subsequent signal propagation (*1, 2*). FcεRI, which is primarily found in mast cells and basophils, serves as a gate keeper for the release of chemical mediators that causes inflammatory and allergic reactions upon exposure to foreign molecules (*3, 4*). IgE-FcεRI clustering and activation by multivalent antigen initiates a series of biochemical signaling steps that lead to different cellular responses including: changes in cell morphology, cytokine production, secretion of chemical mediators and endocytosis. Although the mechanisms of biochemical signaling have been well characterized (*4, 5*), less is known about the accompanying steps that lead to receptor internalization under physiological conditions.

Levels of signaling required for an optimal cellular response are determined by different mechanisms that include not only kinase and phosphatase regulation but also receptor internalization (*6, 7*). Although FcεRI receptor endocytosis has been the focus of recent investigation (*8-11*), the mechanism by which cross-linked receptors are internalized are not yet fully understood. Different pathways for internalization are available for regulation of receptor surface expression, and redundancy may exist

allowing different pathways to work simultaneously (*12*). In addition, the dimension of the receptor clusters seems to be important in promoting either endocytosis or phagocytosis of activated receptor in some cell types (*13, 14*).

Among the different available modes of endocytosis, clathrin mediated endocytosis has been the most widely characterized. More recently, it has become clear that numerous clathrin independent mechanisms are largely responsible for internalization of a variety of receptor systems, demonstrating the complexities of receptor internalization and trafficking. For example, the cytokine receptor gamma chain has been shown to internalize via a mechanism dependent on cortactin-dynamin 2 interactions but independent of clathrin (*15*). These studies have also shed light on the importance of the actin cytoskeleton in endocytosis, which has been difficult to investigate due to the fact that clathrin mediated endocytosis for many systems does not depend on actin polymerization (*16*).

Several studies based on electron microscopy imaging have concluded that FcεRI is endocytosed via clathrin-coated pits based on the proximity of gold labeled, cross-linked receptors to morphological structures resembling clathrin coated pits (*17-19*). In contrast to these observations, a recent report (*9*) showed that knock-down of several components of the clathrin endocytic machinery does not prevent crosslinking-dependent IgE receptor endocytosis. They also demonstrated a role for dynamin 2 in FcεRI receptor internalization by using a dominant negative mutant of dynamin, suggesting a clathrin-independent, dynamin-dependent mechanism. An established role of dynamin in receptor mediated endocytosis is to promote membrane fission of clathrin coated vesicles from the plasma membrane (*20, 21*). However, dynamin 2 has been implicated in numerous clathrin-independent (*15, 22*), modes of receptor internalization and in several actin-dependent processes such as: actin tails (*23*), podosomes(*24, 25*) and phagocytosis (*26*). The proline rich domain (PRD) of dynamin

is known to bind to several actin regulating proteins such as profilin (*27*), cortactin (*28*) and Abp1(*29*), and these interactions are thought to play a role in filamentous actin remodeling (*30, 31*) and regulation of various aspects of clathrin-mediated endocytosis(*28, 32*).

To investigate the role of dynamin 2 in IgE receptor internalization and/or signaling, we characterize IgE receptor clustering and activation by different stimuli that induce distinct cellular responses. We also employ micropatterned ligand arrays to spatially cluster and activate receptors while preventing receptor internalization. We have already established this technique as a tool to investigate spatial regulation of IgE receptor signaling (reviewed in (*33*)) and we have found that several signaling proteins accumulate under the activated IgE-FcεRI, including Lyn kinase, F-actin and actin related proteins (*34, 35*). Using this approach we show local recruitment of dynamin 2 to the clustered receptors under conditions that prevent vesicle formation and fission. Moreover, by using siRNA to reduce the expression levels of dynamin-2 we find evidence to suggest a role for dynamin 2 in regulation of actin interactions important for receptor internalization.

3.2 Materials and methods

3.2.1 Materials. 1-Palmitoyl-2-oleoyl-sn-glycero-3-phosphocholine (POPC) and 1,2-dipalmitoyl-sn-glycero-3-phosphoethanolamine-N-[6-[(2,4-dinitrophenyl)amino]hexanoyl] (16:0 DNP-cap-PE) were purchased from Avanti Polar Lipids. Mouse monoclonal anti-DNP IgE was prepared as described elsewhere (*36*) and conjugated to Alexa Fluor 488 (Molecular Probes, Invitrogen) or fluorescein isothiocyanate (FITC) as described previously (*37*). Goat anti-mouse IgG1 Alexa 568, goat anti-rabbit Alexa 568 (H+L) and Alexa Fluor 568 phalloidin were purchased from Molecular Probes (Invitrogen). Cytochalasin D and the Rho kinase inhibitor Y-

27632 were purchased from Calbiochem (EMD Chemicals). Mouse anti-Rho (clone 55), mouse anti-Rac1 (clone 102), mouse anti-dynamin 1 (clone 41) and mouse anti-clathrin heavy chain (clone 23) were purchased from BD Biosciences. Polyclonal anti-dynamin 2 raised against a synthetic peptide corresponding to residues 760-779 from human dynamin 2 was purchased from Abcam. Mouse anti-cortactin (clone 4F11) was purchased from Millipore, rabbit anti-HS1 (rodent specific) from Cell Signaling Technologies, and monoclonal anti-α-tubulin (clone .N.593) from U.S. Biologicals. Mouse anti-clathrin heavy chain (X-22) was a generous gift from Frances Brodsky (University of California, San Francisco). Dynamin 2-EGFP (*38*) and Dynamin 2 K44A –EGFP (*39*) cDNA were obtained from Mark McNiven (Mayo Clinic). DNP-conjugated beads were prepared by conjugation of 4μm aliphatic amine latex beads (Invitrogen) with 6-(2,4-dinitrophenyl)aminohexanoic acid (DNP-X) succinimidyl ester (Invitrogen) and followed by extensive washing with 70% ethanol to remove excess DNP.

3.2.2 Cell culture and transfection. RBL-2H3 cells were maintained in monolayer cultures and harvested with trypsin-EDTA (Invitrogen) 3–5 days after passage, as described previously (*36*). For internalization experiments, cells were sensitized for 1h at 37°C with FITC-IgE prior to fluorescence measurements and excess IgE was removed by 3 consecutive steps of centrifugation and resuspension in buffered saline solution (BSS) composed of 135 mM NaCl, 5.0 mM KCl, 1.8 mM $CaCl_2$, 1.0 mM $MgCl_2$, 5.6 mM glucose and 20 mM Hepes (pH 7.4). For image correlation spectroscopy (ICS) experiments, cells were plated at 0.5 x 10^6 cells/mL in media on a glass bottom culture dish (MatTek Co., MA) and sensitized by incubating with 4μg/mL Alexa 488 IgE for 1h at 37°C. In other experiments, cells were sensitized overnight with unlabeled or Alexa Fluor 488 IgE. In experiments involving chemical inhibitors, cells were incubated with specific inhibitors or other agents at

37°C for 5 min before and during the time of the experiment. Transfection of cells was obtained by electroporation with specified EGFP constructs. Electroporation was carried out by resuspending cells in buffer [137 mM NaCl, 2.7 mM KCl, 1 $MgCl_2$, 5.6 mM glucose, 20 mM Hepes (pH 7.4)] at a concentration of 1×10^7 cells per ml and electroporating ~0.025 μg/mL of the DNA construct by using an exponential pulse at 280 V and 950 μF. Electroporation was performed in a 4-mm cuvette by using a Gene Pulser Xcell electroporator system (Bio-Rad). After electroporation, cells were plated in medium for 24 hours.

3.2.3 Fluorescence microscopy and immunofluorescence. For experiments involving patterned ligand arrays, cells suspended in BSS at a concentration of $0.5x10^6$ cells per ml were added to a patterned substrate (8 × 8 mm) in the center of a 35-mm Petri dish with coverglass bottom (0.16–0.19 mm; MatTek). After the specified incubation time at 37°C, cells were fixed with 3.7% formaldehyde in PBS for 10 min followed by quenching with 10 mg/ml BSA in PBS. For immunofluorescence after fixation, cells were labeled with primary antibody at room temperature for 1 h. After washing with PBS/BSA (1 mg/ml), the Alexa Fluor 568-labeled secondary antibody was incubated with samples at room temperature for 1 h. Cells were imaged using a Bio-Rad-MRC600-confocal head coupled with a Zeiss Axiovert 10 inverted microscope. A 522/DF35 filter set was used for simultaneous or sequential dual-color image acquisition with an oil-immersion 63x/1.4NA objective. Two milliliters of PBS was added into the dish before inverting the chip for microscopy observation. Cells scored as positive showed fluorescent patterns that matched the substrate with intensity in the overlapping patches at least three times greater than the background level.

Cells used for image correlation spectroscopy (ICS) were rinsed with BSS after sensitization with Alexa 488-IgE and stimulated with 500 ng/mL DNP-BSA for

various times. After stimulation, cells were fixed with 3.7% forlmaldehyde for 10 min followed by incubation with 10 mg/mL BSA in PBS to quench the reaction. Cells were stored in PBS for imaging. Images of the botton surface of the cell (at the interface between the glass and the plasma membrane) were collected with a Zeiss LSM 510 META confocal laser-scanning microscope on an Axiovert200M motorized frame. An analog photomultiplier tube was used for detection. Samples were excited with the 488 nm line of the 20 mW air-cooled argon ion laser (set at 40% of its maximum power) under the control of an AOTF set at 7% transmission. The excitation light was directed to the sample via a dichroic mirror (HFT 488) and a Zeiss Plan-Apochromat 63x/1.4NA oil immersion objective. The fluorescence light was directed through the DC and a LP505 emission filter to the photomultiplier detector. The pinhole size was set to 1 Airy unit. The image size was 1024 × 1024 pixels and the zoom factor was set to 4 (0.03 μm/pixel) to ensure that the point spread function (PSF) contained a sufficiently large number of pixels. The $1/e^2$ ($\omega \sim 0.37$ μm) waists of the PSF was approximated by performing a z-stack on 175 nm fluorescent beads (PS-Speck microscope point source Kit, Molecular Probes) and fitting the obtained intensity profiles in xy-direction and in z-direction with a Gaussian profile.

3.2.4 Protein siRNA knock-down. siRNA was electroporated into cells using the same conditions as those described above for DNA transfection. For optimal delivery, the siRNA concentration and the number of successive electroporation was varied depending on the siRNA used. For clathrin knock-down two different siRNAs with sequences UAAUCCGAUUCGAAGACCAAU and AAUGGAUCUCUCUGAAUACGG were pooled and electroporated by three successive electroporations of 1μM siRNA every 24 h. Experiments were performed after 72 h from the initial electroporation. For simultaneous knock-down of cortactin and its homolog HS1, siRNA for cortactin with sequence

CCGAGAGAGCUCAGCGGAU (ON-TARGETplus, Dharmacon) and HS1 with sequence UAGAAGAGCCAGUGUACGA (ON-TARGETplus, Dharmacon) were pooled and electroporated by two consecutive electroporations of 2.5 μM siRNA with an interval of 24 h. Experiments for these cells were carried out 48 h after initial electroporation. The sequence used for dynamin 2 knock-down was GACAUGAUCCUGCAGUUUA, and optimal knock-down was achieved by two consecutive electroporations of 1.5 μM siRNA. Experiments were performed after 72 hours of initial electroporation. A siRNA with the sequence UUAACCUUACCGAGGGUCGAA was used as a mock in all experiments. Protein knock-down was confirmed by immunoblotting with appropriate antibodies.

3.2.5 Cell lysis and immunoblotting. Whole-cell lysates were prepared on ice by suspending cells at ~$3.5x10^5$ cells/mL in lysis buffer [5 mM *N*-ethylmaleimide, 5 mM EDTA, 0.5% (vol/vol) Triton X-100, 50 mM NaCl, 50 mM Tris, 1X Halt Protease Inhibitor Cocktail (Pierce, Thermo Fisher) and 1X Halt Phosphatase Inhibitor Cocktail (Pierce, Thermo Fisher), pH 7.6]. Lysates were centrifuged at 15,000 x g for 10 min at 4°C. The supernatant was mixed with 5X Tris-glycine SDS buffer (Pierce, Thermo Fisher) and boiled for 5 min. Samples were resolved on a 12% Tris-glycine polyacrylamide gel and transferred to an Immobilon-P membrane with a pore size of 0.45 μm (Millipore) by semidry transfer. Immunoblots were visualized with the Enhanced Chemiluminescence method by using the appropriate antibodies as described previously (*35*).

3.2.6 Detection of clustered receptor internalization by fluorescence quenching. For each experiment 2 ml of FITC-IgE-labeled cells (at $1x10^6$ cells/mL) were placed in a 10x10x40 mm acrylic cuvette and stirred continuously in a thermostatic sample chamber at 37°C. Cells were equilibrated for 5 min in the chamber at 37°C before being stimulated with 500 ng/mL DNP-BSA. In some

experiments inhibitors were added prior to the stimulating ligand, and equilibrated for 5 min at 37°C. Fluorescence measurements were made with an SLM 8000 fluorescence spectrofluorometer operated in ratio mode. FITC was excited at 490 nm, and emission was monitored at 520 nm. To account for day to day variations, a control sample (untreated with chemical inhibitor) was always performed on the same day as treated samples and used to normalize the data from each independent experiment. Fluorescence quenching of FITC labeled IgE occurs in two phases, the first phase is due to rapid binding of the DNP-BSA and the second slower phase is due to acidification of internalized receptors in the intracellular compartments. The second phase of the curve was used to compare the degree of internalization between different samples.

3.2.7 Analysis of internalization of clustered IgE-FcεRI by flow cytometry. Flow cytometry quantification of receptor internalization was performed as described previously (*9*). Briefly, IgE sensitized cells were re-suspended in BSS at 1×10^6 cells/ml and incubated with 500 ng/mL DNP_{22}-BSA for 30 min at 37°C to cross-link FcεRI receptors. Internalization was stopped by placing cells at 4 °C and washing with ice-cold PBS. Cells were incubated with 1mg/mL BSA for 15 min at 4 °C on ice before labeling with fluorescent anti-IgE to reduce non-specific binding. Cell surface receptors were labeled by incubation with FITC-labeled rat anti-mouse IgE (clone R35-72, BD Biosciences) for 30 min on ice. FITC anti-IgE binding was quantified using flow cytometry on a LSRII Flow Cytometer (BD-Biosciences).

3.2.8 Image correlation spectroscopy analysis. Image correlation spectroscopy (ICS) has been described previously (*40, 41*) and was performed following the guidelines presented in reference (*42*). ICS is based on the analysis of spatial fluorescence intensity fluctuations in images collected on a confocal laser-

scanning microscope. The normalized intensity (i(x,y)) fluctuation spatial autocorrelation function of the image is given by:

$$r(\xi,\eta)=\frac{\langle \delta i(x,y)\,\delta i(x+\xi,y+\eta)\rangle}{\langle i(x,y)\rangle^2}$$

where the brackets denote spatial averaging over the image, and ξ and η are spatial lag variables corresponding to pixel shifts of the image relative to itself in the *x* and *y* directions. The autocorrelation function can also be computed by Fourier methods that minimizes computation time by using:

$$r(\xi,\eta)=\frac{F^{-1}\left[F\left(i(x,y)\right)F^{*}\left(i(x,y)\right)\right]}{\langle i(x,y)\rangle^2}-1$$

where F denotes the 2 dimensional (2D) spatial Fourier transform, F^{*} is the complex conjugate of this transform, and F^{-1} is the inverse 2D spatial Fourier transform. The correlation function, g(ξ,η), is then fitted to the 2D Gaussian function:

$$g(\xi,\eta)=g(0,0)e^{(\xi^2+\eta^2)/\omega^2}+g_0$$

where ω is the e^{-2} radius of the laser beam, $g(0,0)$ is the amplitude of the autocorrelation function upon extrapolation of ξ and η to zero and g_0 is a constant that accounts for the incomplete decay of the autocorrelation function. The zero-lag amplitude of the autocorrelation function, $g(0,0)$, is inversely proportional to the average number of independently distributed particles in the beam area, and the average number of independent fluorescent particles per μm^2 (cluster density, CD) at the cell membrane can be calculated as:

$$CD=\frac{1}{g(0,0)\pi\omega^2}$$

To determine if the detected clusters are present as monomers, dimers or oligomers, further information about the system is needed. The average intensity of an

image, $\langle i(x,y)\rangle$, is proportional to the average number of fluorescent molecules in the area illuminated by the laser beam, and this relation can be used to quantify the relative number of proteins per cluster, defined as the degree of aggregation (DA). The degree of aggregation is proportional to the average number of proteins monomers ($\bar{N}_m$) in the protein aggregate divided by the average number of independent particles (clusters), $\bar{N}_p$, and is calculated according to:

$$DA = \left\langle i(x,y) \right\rangle g(0,0) = c\frac{\bar{N}_m}{\bar{N}_p}$$

The constant *c* accounts for instrumental and experimental parameters (e.g. efficiency of collection of the confocal microscope, number of fluorophores per protein, etc.). These parameters are constant for a given set of experimental conditions. If the constant, c, is determined, we can calculate the number of proteins per cluster (in our case, # IgE/cluster). The number of proteins per cluster is then the DA divided by the value of c. In this work, the constant *c* was determined for each experiment by calculating the autocorrelation function from unstimulated cells in which it is assumed that the detected particles represent single receptors and $\bar{N}_m / \bar{N}_p = 1$. Data analysis was performed in a custom MATLAB R2008a (MathWorks) routine.

3.2.9 Microfabrication of patterned ligands by polymer lift-off. Surfaces were patterned with 1.5 to 4μm features and functionalized with supported membranes containing 2,4-dinitrophenyl (DNP) ligands as described previously(*43, 44*), and no significant differences were observed over this length range. Small unilamellar vesicles were prepared by sonication. The lipid composition was 10 mol% DNP-cap-PE, and 90 mol% POPC. In some experiments, Alexa 488-IgE marked the clustered IgE-FcεRI. For control experiments, DNP-cap-PE was not included in the samples. Ten microliters of the vesicle suspension (1 mM lipids) was added to an 8 by 8 mm patterned Parylene substrate at room temperature for 10 min. The samples were rinsed

thoroughly with filtered water, and Parylene was mechanically peeled away in solution to yield the patterned lipid bilayers.

3.3 Results

3.3.1 IgE-FcεRI clusters of less than 200 IgEs are formed after receptor cross-linking. In a recent report, small receptor clusters of at least three IgE-FcεRIs per cluster were found to be mobile and signaling competent, whereas larger aggregates that form at high valency and doses of antigen (as those used in this report) produce large immobile clusters that correlate with internalization (*45*). Since it has been shown that particle size is an important factor in determining the mechanism of internalization in other receptor systems (*13*), we characterized the size and density of IgE receptor clusters formed at high doses of multivalent antigen (DNP_{22}-BSA) using image correlation spectroscopy. For ICS, cells were allowed to spread on a glass surface for > 1h at 37°C while being sensitized with fluorescently modified IgE (Alexa 488 –IgE) because ICS requires flat surfaces for accurate results. After stimulation with DNP_{22}-BSA for different amounts of time, cells were fixed and imaged as described in the methods section. We found that as the stimulation time increases, the density of aggregated IgE-FcεRI clusters near or at the plasma membrane decreases, in part as a result of internalization. However, these clusters become more distinctive and brighter with longer stimulation times, indicating a larger number of cross-linked receptors per cluster (Figure 3.1A). The autocorrelation function of 128x128 pixel regions (4 regions per cell) was computed (Figure 3.1B) and the cluster density and degree of aggregation was calculated as described in the methods section. The number of receptors per cluster of unstimulated cells was assumed to be one. This is a reasonable assumption based on the measured distribution of gold labeled IgE receptors in resting cells (Chiang et al., submitted for publication)

and although the density of receptors in resting cells is close to the limit that can be accurately calculated with ICS, we obtained reasonable densities when compared to SEM imaging of gold labeled receptor distribution (~200 receptors/μm^2) (Chiang et al., submitted for publication). The calculated degree of aggregation (DA) from resting cells was used to obtain the proportionality constant necessary for correcting the data and obtain values of numbers of IgE receptors per cluster (#IgE/cluster). Although at the time scale of these experiments some of the receptor clusters are already internalized or in endocytic structures, we can establish an upper bound in the number of IgE receptors per cluster. As shown in Figure 3.1C the # of IgE/cluster increases with stimulation time until it reaches a plateau of about an average of 146 ± 7 receptors per cluster. Most of the formed clusters are smaller than ~500 nm and appear as Gaussian particles because of the laser beam profile. Inhibition of actin polymerization by treatment with 2μM cytochalasin D (CytoD) prior to DNP_{22}-BSA addition had a small effect of the number of IgE/cluster (Figure 3.2) indicating that the actin cytoskeleton participation does not strongly influence this parameter. These results suggest that initial clustering of receptors is largely driven by IgE receptor diffusion. Inhibition of actin polymerization prevents endocytosis of the clustered receptors (see below), and the modest difference between CytoD treated and untreated cells indicates that most of the clusters are at the plasma membrane. However, this analysis cannot distinguish whether the clusters are in endocytic structures at the plasma membrane that have not yet pinched off, or whether actin is necessary for the formation of endocytic structures.

3.3.2 IgE receptor internalization is dependent on Syk kinase propagation of signaling and the actin cytoskeleton. In several cells types, both constitutive and activation-dependent receptor endocytosis are found to be insensitive to disruption of the actin cytoskeleton (*13, 16*). This cytoskeleton-independent and clathrin-dependent

Figure 3.1: ICS analysis reveals distinctive IgE-FcεRI aggregates of < 200 receptors per cluster. A) Confocal micrograph showing formation of receptor cluster at different time points after stimulation with 500 ng/mL DNP_{22}-BSA. B) Example of cells used for ICS analysis; a region of 128x128 pixels is used to calculate the autocorrelation function (right plot). The autocorrelation function was fitted to a Gaussian function as described in the methods section. The fitted plot is shown as a darker mesh (one quarter of the plot facing out) superimposed in the raw autocorrelation function. C) Plot for the calculated diffraction limited cluster density and corrected DA (#IgE per cluster) for different time points after stimulation. Four regions were averaged per cell and the number of cells (37 for unstimulated cells, 30 for 5 min, 35 for 1 5min 45 for 30 min and 38 for 45 min stimulation) was used to calculate the standard error (SEM). Scale bar in (a) and (b) represents 20 μm.

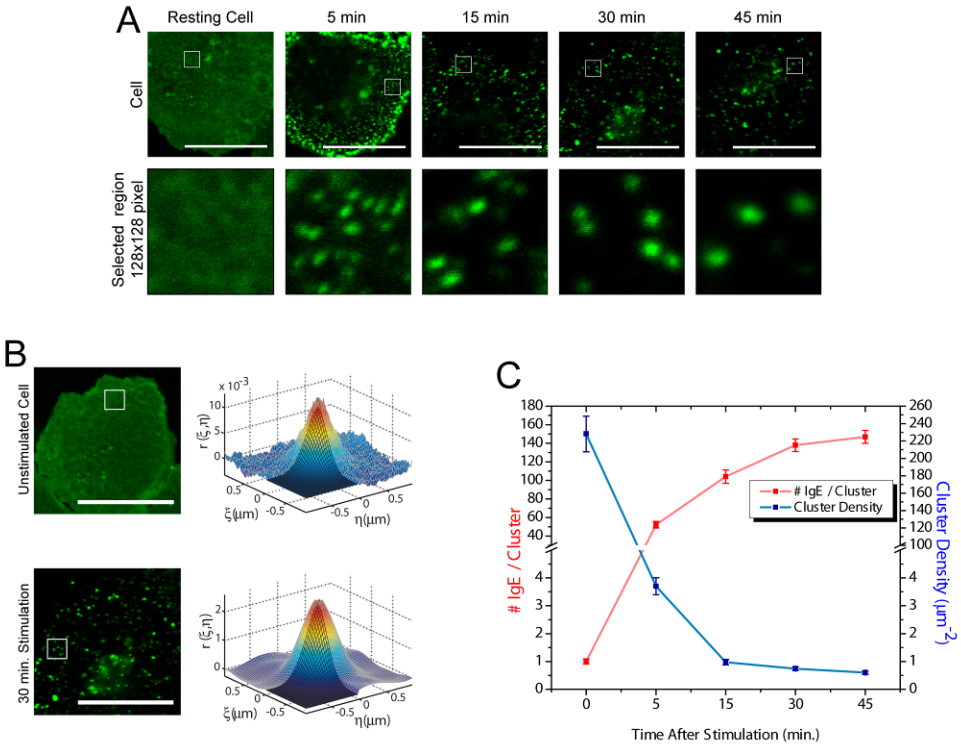
A
Resting Cell
5 min
15 min
30 min
45 min
Cell
Selected region
128x128 pixel
B
Unstimulated Cell
30 min. Stimulation
x 10-3
r (ξ,η)
ξ(μm)
η(μm)
C
IgE / Cluster
Cluster Density
Cluster Density (μm-2)
Time After Stimulation (min.)

Figure 3.2: Effect of actin polymerization inhibition on the relative number of receptors per cluster after stimulation with multivalent antigen. A) Confocal images of cells stimulated with antigen at 37°C. Adherent cells were treated with 2μM Cytochalasin D (CytoD) during and prior to stimulation with 500 ng/mL DNP_{22}-BSA. Both untreated (control) and cytochalasin treated cells were stimulated for 15 min at 37°C before fixation. Scalebar corresponds to 20μm. B) The degree of aggregation, which is proportional to the number of receptors per cluster, was calculated for each treatment group. A modest decrease (~20%) in the relative number of IgE-FcεRI was detected in cyochalasin treated cells. The calculated DAs were not corrected; hence DAs do not represent # IgE/cluster. Error bars correspond to standard error where the indicated number of replicates (n) is the number of cells analysed, and the DAs obtained from two different regions were averaged per cell. Asterisk (*) correspond to a p-value less than 0.05.

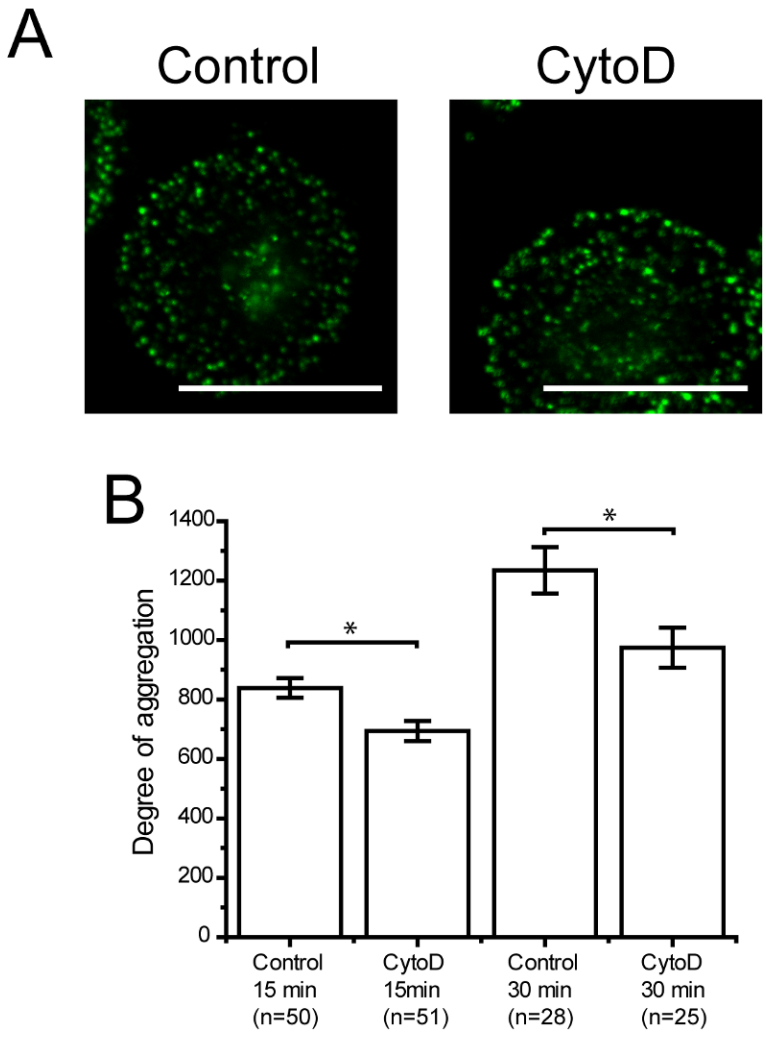
A
Control
CytoD
B
Degree of aggregation
1400
1200
1000
800
600
400
200
0
*
*
Control
15 min
(n=50)
CytoD
15min
(n=51)
Control
30 min
(n=28)
CytoD
30 min
(n=25)

mechanism is used by the Fcγ receptor (*13*), which resembles FcεRI in both activation and signaling mechanisms and the capacity to promote phagocytosis of large particles. However, there are many examples where the cytoskeleton, through regulation of Rho GTPases (*46*) and other adapter proteins, plays an essential role in endocytosis mainly through clathrin independent mechanisms. The role of the actin cytoskeleton was investigated by monitoring fluorescence quenching of FITC labeled IgE after receptor cross-linking (*47*). After IgE receptors are endocytosed and intracellular compartments containing the receptors acidify, the fluorescence intensity decrease is followed in real time to determine the kinetics of receptor internalization at 37°C (Figure 3.3A).

During cell stimulation, DNP_{22}-BSA binding to the FITC-IgE causes an initial quenching of FITC fluorescence (*48*) that is completed within ~1 min. After ~2 min subsequent quenching occurs due to acidification of internalized vesicles (*47*), and this quenching follows an exponential decay that can be fitted to characterize the kinetics and degree of receptor endocytosis. Using this approach we determined that receptors are internalized within minutes of stimulation by antigen with a half-time of 4.0 ± 0.3 min. RBL cells deficient in Cdc42 and Rac1 activation (B6A4C1 cell line) (*49, 50*) or RBL cells treated with 10 μM Rho kinase (ROCK) inhibitor Y-27632 did not show any reduction in receptor endocytosis. As previously reported (*48*), treatment of RBL cells with 2μM cytochalasin D caused a prominent decrease of endocytosis (Figure 3.3B-C), and the additional quenching visualized in these cells is likely due to residual binding of DNP_{22}-BSA. The effects of inhibition of actin polymerization on IgE receptor endocytosis were confirmed by flow cytometry. In this assay, cells were stimulated for 30 min at 37°C with DNP_{22}-BSA, and the remaining exposed cell surface receptors were labeled with FITC anti-IgE. Consistent with the previous results, disruption of the actin cytoskeleton by either 2μM cytochalasin D or 2μM Latrunculin-A causes a decrease in receptor endocytosis as reported by the increase

Figure 3.3: Real time internalization of clustered IgE-FcεRI followed by fluorescence quenching of FITC-IgE reveals a role for Syk kinase and the actin cytoskeleton in IgE receptor endocytosis. A) Fluorescence quenching of FITC-IgE after antigen (500 ng/mL DNP_{22}-BSA) addition at 37°C occurs in two phases. The first phase corresponds to rapid binding of DNP_{22}-BSA to the receptor and the second, slower phase corresponds to receptor internalization (red box). To quantify the amount of receptor endocytosis, quenching curves beginning 2 min after antigen addition were fitted to a single exponential decay, $y = Amplitude*\exp(-t/\tau) + y_0$. The initial points (2 min after antigen addition) of the curves were shifted to start at ($t = 0$, $y = 1$) for visualization purposes. Because of these shifted values, the calculated amplitudes of the curves are equivalent to $1-y_0$. Blowout plot shows data fitted to an exponential decay. B) Shifted fluorescence quenching curves beginning 2 min after antigen addition for control RBL cells and cells treated with 2 μM cytochalasin D, 15 μM Y-27632 (ROCK inhibitor) or mutant cells deficient Cdc42 and Rac1 activity or cell deficient in Syk kinase. C) Quantification of the normalized (divided by the control value) amplitude of the fitted curves show a significant reduction of activated receptor endocytosis in cells deficient in Syk kinase and cells treated with cytochalasin D. Error bars correspond to standard deviation (SD) for n replicates, and asterisk correspond to p-value <0.05.

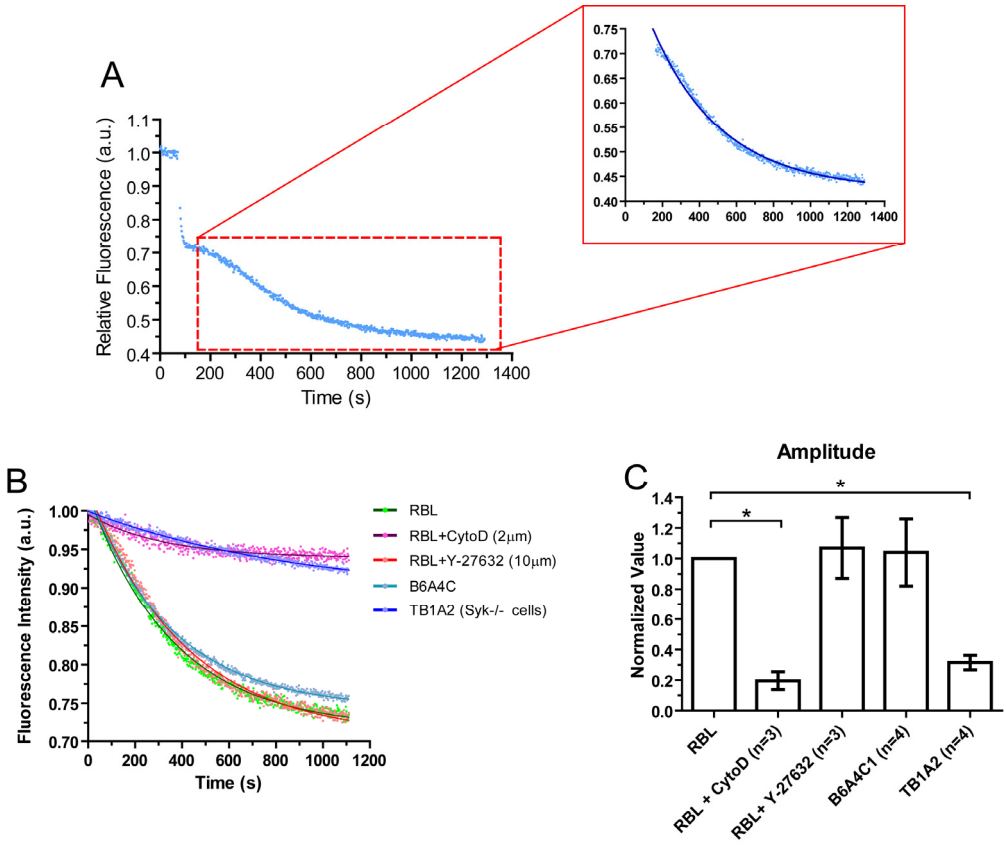
A
Relative Fluorescence (a.u.)
Time (s)
B
Fluorescence Intensity (a.u.)
Time (s)
RBL
RBL+CytoD (2μm)
RBL+Y-27632 (10μm)
B6A4C
TB1A2 (Syk-/- cells)
C
Amplitude
Normalized Value
RBL
RBL + CytoD (n=3)
RBL+ Y-27632 (n=3)
B6A4C1 (n=4)
TB1A2 (n=4)

cell surface receptor labeling as compared to control (untreated) cells (Figure 3.4). These effects on cell surface receptor exposure are less dramatic as compared to those obtained in Figure 3.3. Contrary to the fluorescence quenching assay that follows the acidification of receptors once they reach intracellular compartments, the latter correlates the accessibility of the IgE-FcεRI (to the anti-IgE antibody added in solution) to the number of receptor clusters remaining at the surface.

These effects of inhibition of actin polymerization are consistent with a role for the actin cytoskeleton in activated IgE receptor endocytosis (*51*) that is independent of Rho GTPase regulation. In contrast, 4μm DNP coated latex beads are phagocytosed by RBL cells, and this process is impaired in B6A4C1 cells and is also inhibited by Cytochalasin D (Figure 3.5). Treatment with 100 nM wortmanin (PI3-K inhibitor) prevented phagocytosis of 4μm beads (Figure 3.5) but had no effect in receptor endocytosis of soluble DNP_{22}-BSA (data not shown) as reported by the FITC quenching assay, demonstrating a difference in the mechanisms required in each process.

There have been contradicting reports for the role Syk kinase in activated receptor internalization. For example, it was found that IgE receptor endocytosis is reduced in Syk deficient cells as measured by flow cytometry (*11*) while others report no effect on receptor internalization (*10*) using the same Syk deficient cell line and the same assay. We found that both endocytosis of DNP_{22}-BSA clustered receptors (Figure 3.3B-C) and phagocytosis of 4um DNP containing beads (Figure 3.5) are significantly reduced in RBL cells deficient in Syk kinase (TB1A2 cell line) (*52*), indicating an important role for Syk mediated signal propagation in cell surface receptor down-regulation through internalization. Because quenching of the FITC-IgE occurs due to acidification of intracellular compartments, our results cannot

Figure 3.4: Disruption of the actin cytoskeleton prevents activated FcεRI receptor internalization as determined by reduced epitope accessibility to fluorescently modified anti-IgE. A) Schematic illustrating the flow cytometry assay. Receptors at the cell surface (stage I) are easily accessible to the fluorescently modified anti-IgE and this binding is correlated to the number of receptors remaining at the plasma membrane. Epitope accessibility may be reduced at stage II depending on the degree to which the vesicle has formed with constricted opening. Accessibility is completely hindered at stage III when receptors are in intracellular vesicles. The actin cytoskeleton may be involved in the initial formation of an endocytic structure (stage II) or the fission of the formed vesicle from the plasma membrane (stage III). B) Quantification of remaining cell surface receptors as measured by fluorescence anti-IgE binding to the clustered IgE-FcεRI. After antigen stimulation for 30 min at 37°, cells treated with Cytochalasin D or Latrunculin-A show higher levels of available receptors as compared to control untreated cells. The reduced level of cell surface receptors in control cells is caused by rapid endocytosis of the activated receptors. Intensity values from control cells incubated at 4°C (to prevent receptor internalization) were used to normalize the data and these values (from 4°C control cells) are assumed to represent 100% of initial receptor expression. Error bars correspond to standard deviation for n replicates.

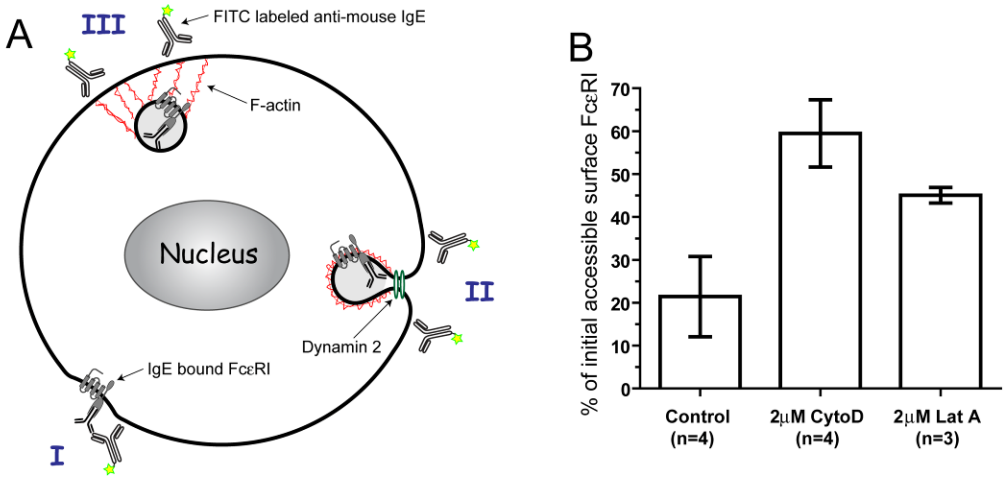
A
III
FITC labeled anti-mouse IgE
F-actin
Nucleus
II
Dynamin 2
IgE bound FcεRI
I
B
% of initial accessible surface FcεRI
70
60
50
40
30
20
10
0
Control
(n=4)
2μM CytoD
(n=4)
2μM Lat A
(n=3)

Figure 3.5: FcεRI phagocytosis is dependent on the actin cytoskeleton, phosphatidylinositol 3-kinase and Syk kinase. Alexa 488-IgE sensitized cells were incubated with 4μm beads for 30 min at 37°C with the respective inhibitor. Several internal beads are visualized on untreated RBL cells but phagocytosis of the beads is prevented by treatment with 2μM Cytochalasin D and 10nM wortmanin. Cells deficient in rac-1 and CdC42 activation or deficient in Syk kinase do not show internalization of DNP conjugated beads. Data shown is representative from more than 50 cells imaged under these conditions. Control (untreated) cells typically showed 3-4 internalized beads per cell. Yellow arrows represent beads that are bound to the membrane but are not internalized. Scale bar corresponds to 20μm.

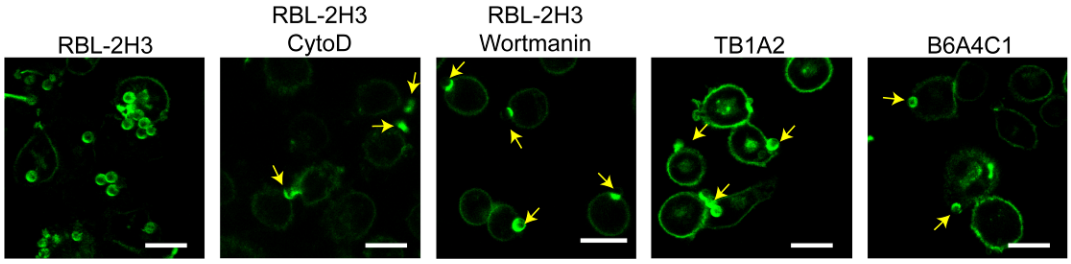
RBL-2H3
RBL-2H3
CytoD
RBL-2H3
Wortmanin
TB1A2
B6A4C1

distinguish whether the formation of endocytic structures (forming vesicles attached to the membrane) or acidification of endosomes are prevented on the Syk deficient cell.

3.3.3 Activated FcεRI receptor internalization is reduced by dynamin 2 knock-down but not by clathrin, cortactin or HS1 knock-down. Several reports have implicated interactions between the actin binding protein cortactin and dynamin in both clathrin mediated (*28, 53*) and clathrin independent endocytosis (*15*). To address the role of these proteins in activated IgE-FcεRI endocytosis we employed siRNA to selectively knock-down dynamin 2, clathrin heavy chain, cortactin and the cortactin homolog HS1 (Hematopoietic lineage cell specific protein 1, also known as hematopoietic cell-specific Lyn substrate 1). As shown in Figure 3.6A, we detect >95% knock-down of dynamin 2, clathrin and HS1, and ~75% knock-down of cortactin, as detected by immunoblotting. Cortactin and HS1 were knocked-down simultaneously because of the possible functional redundancy between these two closely related homologs (*54*). Dynamin 2 expression levels were detected by immunoblotting with an anti-dynamin 1 antibody that cross-reacts with dynamin 2. Given that no dynamin is detected under these conditions, it is likely that dynamin 2 is the principal isoform of dynamin expressed in these cells. While knock-down of clathrin heavy chain, cortactin, or HS1 did not cause any detectable decrease in receptor endocytosis (Figure 3.6B-C) or in the kinetics of internalization after antigen stimulation (as determined by the kinetics of FITC-IgE quenching; Figure 3.6C), knock-down of dynamin 2 caused a reduction of endocytosis monitored by vesicle acidification of ~35% (Figure 3.6C), consistent with a role for dynamin 2 in endocytosis of activated receptors as previously detected (*9*). It is very interesting that >95% knock-down of dynamin 2 caused only a 35% decrease of total signal whereas Cytochalasin D caused a reduction of > 80%. This result suggests that a component of IgE receptor endocytosis is dynamin 2-independent or that there are redundant

Figure 3.6: Dynamin 2 but not clathrin, cortactin or HS1 knock-down causes a reduction in activated receptor endocytosis. A) Representative experiment of protein knock-down evaluated by immunoblotting and densitometry. Upper bands represent the protein of interest and the lower band was used as a loading control (tubulin or nonspecific anti-cortactin band of ~50 kDa). B) Fluorescence quenching of FITC-IgE shows a decrease of endocytosis for dynamin 2 knock-down cells as compared with cells electroporated with control siRNA, while no significant reduction is detected for clathrin heavy chain knock-down cells or cells with simultaneous knock-down of cortactin and HS1. C) Quantification the normalized (divided by control value) time constant (τ) and amplitude obtained from fitting to a single exponential decay. Only Dynamin 2 knock-down cells showed a significant decrease in the amplitude but no statistically significant difference was observed for the time constant values in any treatment group as compared to control cells. Asterisk (*) correspond to a p-value <0.05 and error bars are SD for n replicates.

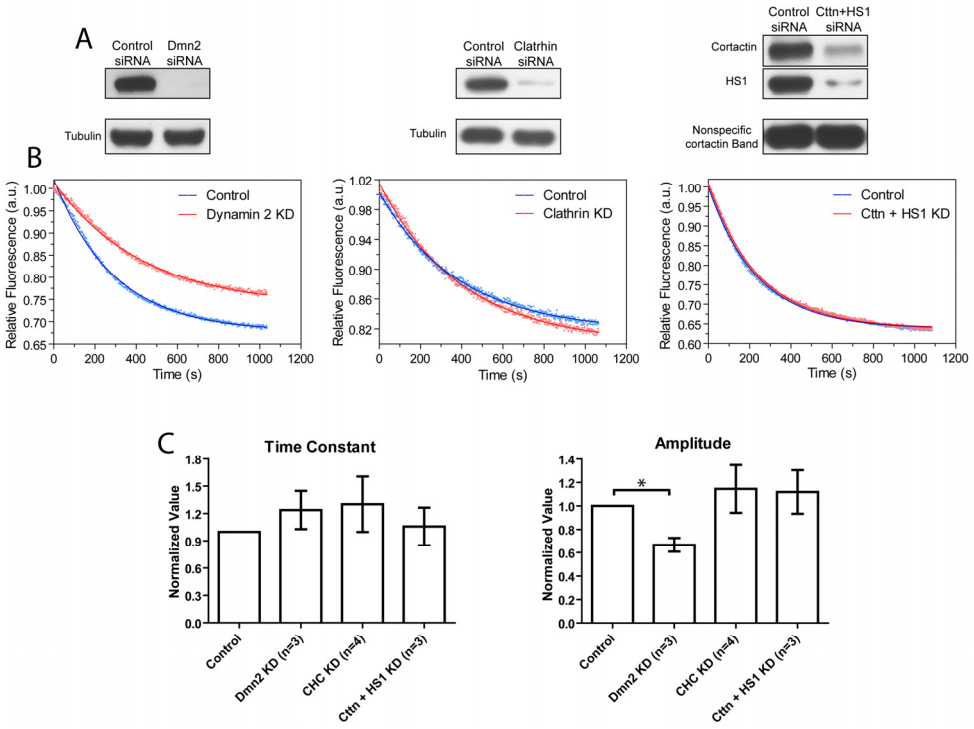
A
Control siRNA
Dmn2 siRNA
Tubulin
Control siRNA
Clatrhin siRNA
Tubulin
Control siRNA
Cttn+HS1 siRNA
Cortactin
HS1
Nonspecific cortactin Band
B
Relative Fluorescence (a.u.)
Time (s)
Control
Dynamin 2 KD
Control
Clathrin KD
Control
Cttn + HS1 KD
C
Time Constant
Normalized Value
Control
Dmn2 KD (n=3)
CHC KD (n=4)
Cttn + HS1 KD (n=3)
Amplitude
*
Normalized Value
Control
Dmn2 KD (n=3)
CHC KD (n=4)
Cttn + HS1 KD (n=3)

pathways that may be activated upon dynamin knock-down. These alternative mechanisms do not seem to need dynamin 2 for vesicle scission and suggest the prescence of other proteins capable of performing this function.

3.3.4 Dynamin 2 and clathrin are recruited to clustered receptors under conditions that prevent receptor internalization. We reported previously that by using micropatterned ligand arrays to spatially cluster and activate IgE receptors we could visualize selective recruitment of signaling components by fluorescence microscopy (*34, 35*). Because ligands are immobilized at the surface, no internalization of the receptor occurs and accumulation of other components can remain stable for relatively long times (up to 1 hour). Using this approach we found that dynamin 2 (by immunofluorescence labeling) is recruited to the clustered receptors (up to 70% cells show dynamin accumulation) and this accumulation becomes maximal at ~30 min, similar to that observed for F-actin (Figure 3.7B-C), and remains stable for at least 45min (longest time investigated). Dynamin 2-EGFP (Figure 3.7C) and the dominant negative mutant Dynamin 2 K44A-EGFP (data not shown) also show recruitment to the clustered receptors. Moreover, this selective recruitment of dynamin is not prevented by addition of 2μM Cytochalasin D (Figure 3.7B) or 100nM wortmanin (data not shown), indicating that this recruitment to the sites of clustered receptors is not dependent on actin polymerization or phosphatidylinositol 3-kinase (PI3-K).

Dynamin 2 is most commonly thought to be involved in the latter stages of the formation and scission of the endocytic vesicles (*20, 21*) but these data suggest that activated receptors can elicit signals that recruit dynamin to the sites of activated receptors at the plasma membrane in the absence of internalization. Moreover, under the same conditions we detect accumulation of clathrin in only about 15-20% of the cells (Fig. 3.7B).

Figure 3.7: Micropatterned DNP ligand array reveals selective accumulation of dyamin 2 and clathrin under the clustered IgE-FcεRI. A) Schematic cartoon showing cells activated by the patterned lipid bilayers containing DNP-Cap-PE and selective accumulation of signaling components (modified from (*33*)). B) Selective accumulation of dynamin 2 (~70% cells scored positive) and clathrin (15-20% cells scored positive) but not Rac1 (0% cells scored positive) is observed under the cluster receptors on Alexa 488-IgE (green) sensitized cells after 30 min incubation with the patterned surface at 37°C. Treatment with 2 μM Cytochalasin D does not prevent accumulation of dynamin 2 to the clustered receptors. Red channel represents protein of interest labeled by immunofluorescence. C) IgE sensitized cells show accumulation of dynamin 2-EGFP (green) to the patterned receptors that coincides to F-actin (red) accumulation. Scalebar corresponds to 20 μm.

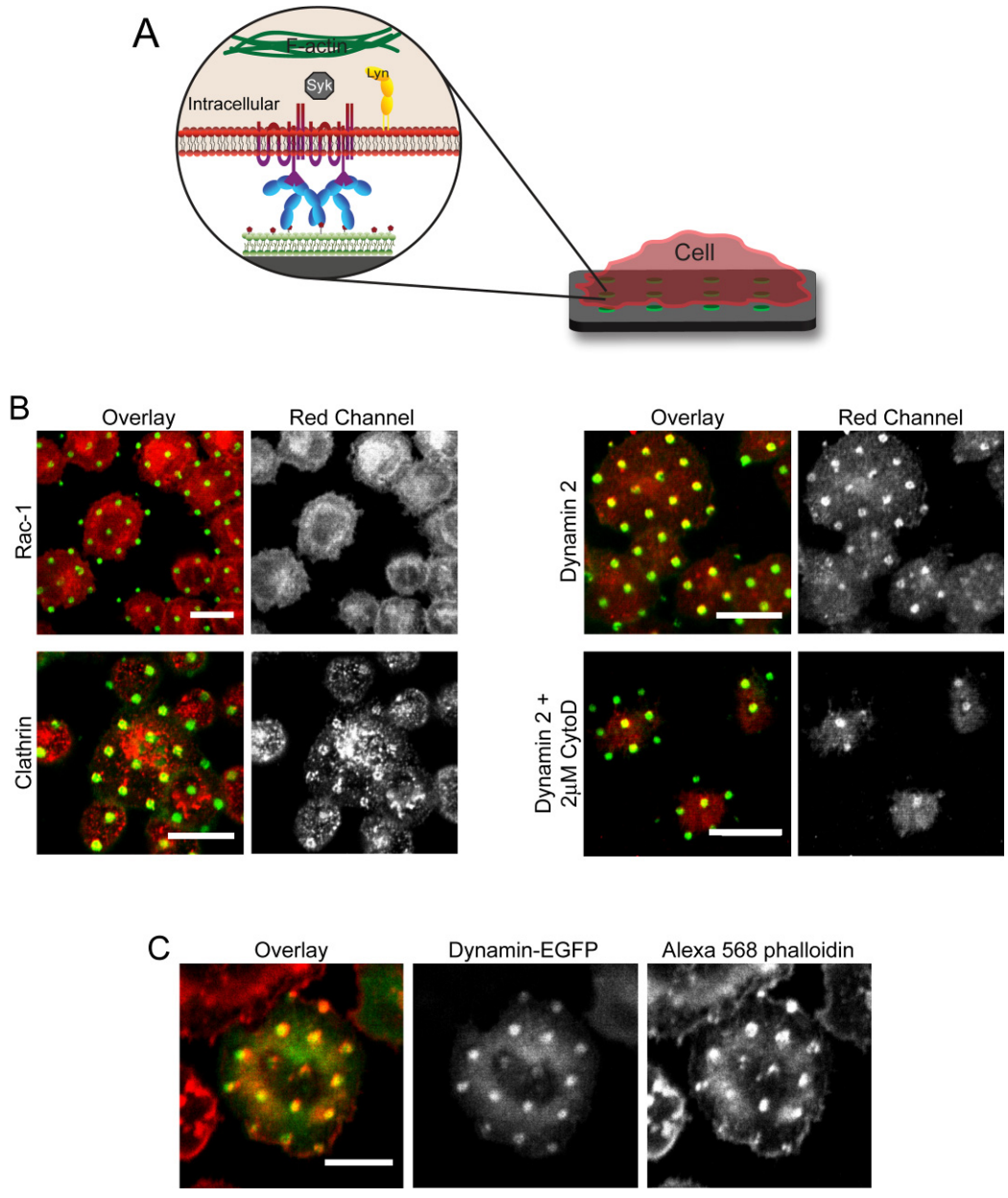
A
F-actin
Syk
Lyn
Intracellular
Cell
B
Overlay
Red Channel
Rac-1
Clathrin
Overlay
Red Channel
Dynamin 2
Dynamin 2 +
2μM CytoD
C
Overlay
Dynamin-EGFP
Alexa 568 phalloidin

3.3.5 Dynamin 2 knock-down reduces accumulation of F-actin to clustered receptors. Several actin regulation proteins such as profilin (*27*) and cortactin (*28*) have been show to interact directly with dynamin 2, and interaction between these and other adapter proteins with dynamin have been found to be important in several cellular processes including formation of podosomes (*24*) and actin polymerization at the immunological synapse (*55*). We previously showed selective accumulation of F-actin and other actin binding proteins, including vinculin, paxillin and talin to the clustered receptors in the absence of integrin activation (*35*), suggesting an active role for the actin cytoskeleton in IgE receptor signaling. To test whether dynamin 2 is important for the accumulation of F-actin to the clustered receptors, we compared F-actin accumulation with and without knock-down of dynamin 2. As shown in Figure 3.8, actin accumulation to the patterned receptor clusters is reduced in dynamin 2 knock-down cells suggesting a role for dynamin in this process. Regulation of the actin cytoskeleton by dynamin could be modulated in coordination with cortactin, Abp1 other actin binding proteins that interact directly or indirectly with dynamin.

We previously observed that chemical inhibition of Syk kinase by Piceatannol did not prevent accumulation of F-actin to the clustered receptors (*35*). However, using the Syk deficient mutant cell line we never detected any accumulation of actin over the patterned receptor clusters (data not shown). These results are consistent with a requirement for Syk dependent signaling propagation for activation of components necessary for FcεRI mediated actin redistribution and vesicle scission.

3.3.6 Phagocytosis of large particles is not dynamin 2 dependent. Previous reports implicate a necessary role for dynamin 2 in Fcγ receptor phagocytosis in macrophages (*13, 26*). As shown in Fig 3.9 and 3.10, we find that neither dynamin 2 knock-down nor over-expression of the dominant negative mutant dynamin 2 K44A-EGFP have a detectable effect on phagocytosis mediated by FcεRI in RBL mast cells.

Figure 3.8: Dynamin 2 knock-down causes a reduction in actin accumulation under the clustered IgE-FcεRI. A) Cells electroporated with control or dynamin 2 siRNA were sensitized with Alexa 488-IgE overnight. Cells were incubated with the micropatterned supported lipid bilayers containing 10% DNP-Cap-PE for 30min at 37°C. Cells fixed and stained with Alexa 568 phalloidin to label actin filaments. B) The number of cells showing visible accumulation of actin to the clustered receptors was quantified and a significant reduction was observed on dynamin 2 knock-down cells. The percentage of cells scored as positive obtained from >100 cells per independent experiment from 3 different experiments were averaged (n=3). Error bars represents SD and asterisk (*) correspond to a p-value less than 0.05.

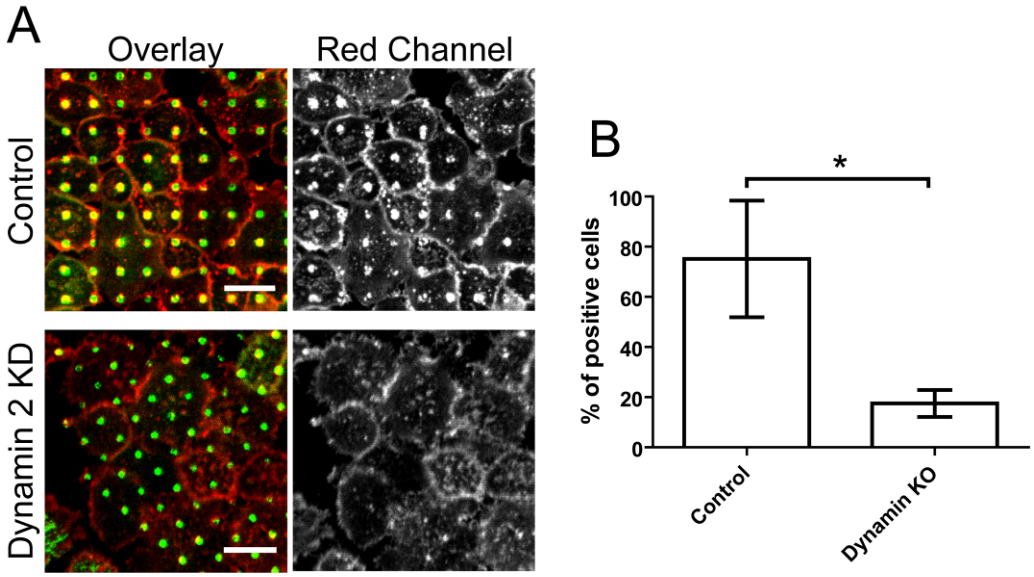
A
Overlay
Red Channel
Control
Dynamin 2 KD
B
*
% of positive cells
100
80
60
40
20
0
Control
Dynamin KO

IgE senstitized cells were incubated with DNP modified 4μm beads at 37°C in BSS for 30 min. After the appropriate incubation time, cells were washed with BSS, fixed and labeled for F-actin or Rac1.We found that dynamin knock-down had no significant differences in the number of internalized particles per cell or the number of cells showing internalized beads (Figure 3.9). Cells over-expressing dynamin 2-EGFP or dynamin 2 K44A-EGFP showed accumulation of dynamin at the bead contact interface, and this accumulation is usually found to colocalize with F-actin (Figure 3.10). Dynamin 2 and F-actin co-accumulation at the phagocytic cup is transient and becomes maximal at 5-10 min and decreases again before the particle is completely internalized. In addition, dynamin knock-down does not reduce actin accumulation to nascent phagosome (data not shown). These results suggest that dynamin 2 does not play a necessary role for particle internalization during phagocytosis mediated by FcεRI in RBL cells.

3.4 Discussion

Dynamin 2 is a GTPase protein that is essential for both clathrin dependent and independent endocytosis in several cellular systems. The GTPase activity of this protein has been well characterized and shown to be involved in vesicle fission from the plasma membrane (*20*), but less is known about the function of dynamin 2 in other cellular processes that depend on the actin cytoskeleton. Dynamin 2 has been found in several actin rich structures including actin comets (*56*), podosomes (*24*), invadopodia (*57*) and is involved in the formation of the immunological synapse (*55*). However, the functional role of dynamin 2 in these actin dependent processes is not yet clear, and is complicated by the variety of different cellular processes that it appears to regulate. To investigate the role of dynamin 2 in IgE receptor internalization we have used siRNA technologies to probe the functional consequences of protein knock-down and

Figure 3.9: FcεRI-mediated phagocytosis of DNP conjugated beads is insensitive to dynamin 2 knock-down. A) Unsensitized (upper panel) or sensitized cells with Alexa 488-IgE (green) were incubated with 4μm DNP conjugated beads for 30min at 37°C. Cells were fixed and labeled with anti-Rac1 (red) to label the cytoplasm and visualize internalized beads. Both cells electroporated with control or dynamin 2 siRNA show phagocytosis of several particles while cells unsenzitized with IgE do not phagocytosed the DNP conjugated beads. The number of cells showing active phagocytosis (B) and the number of internalized beads per cell (C) was quantified in all three treatment groups and no statistically significant difference was observed between control and dynamin knock-down cells on cells sensitized with Alexa 488-IgE. The percentage of cells scored as positive obtained from >100 cells from 3 different experiments were averaged (n=3) and the error represents SD

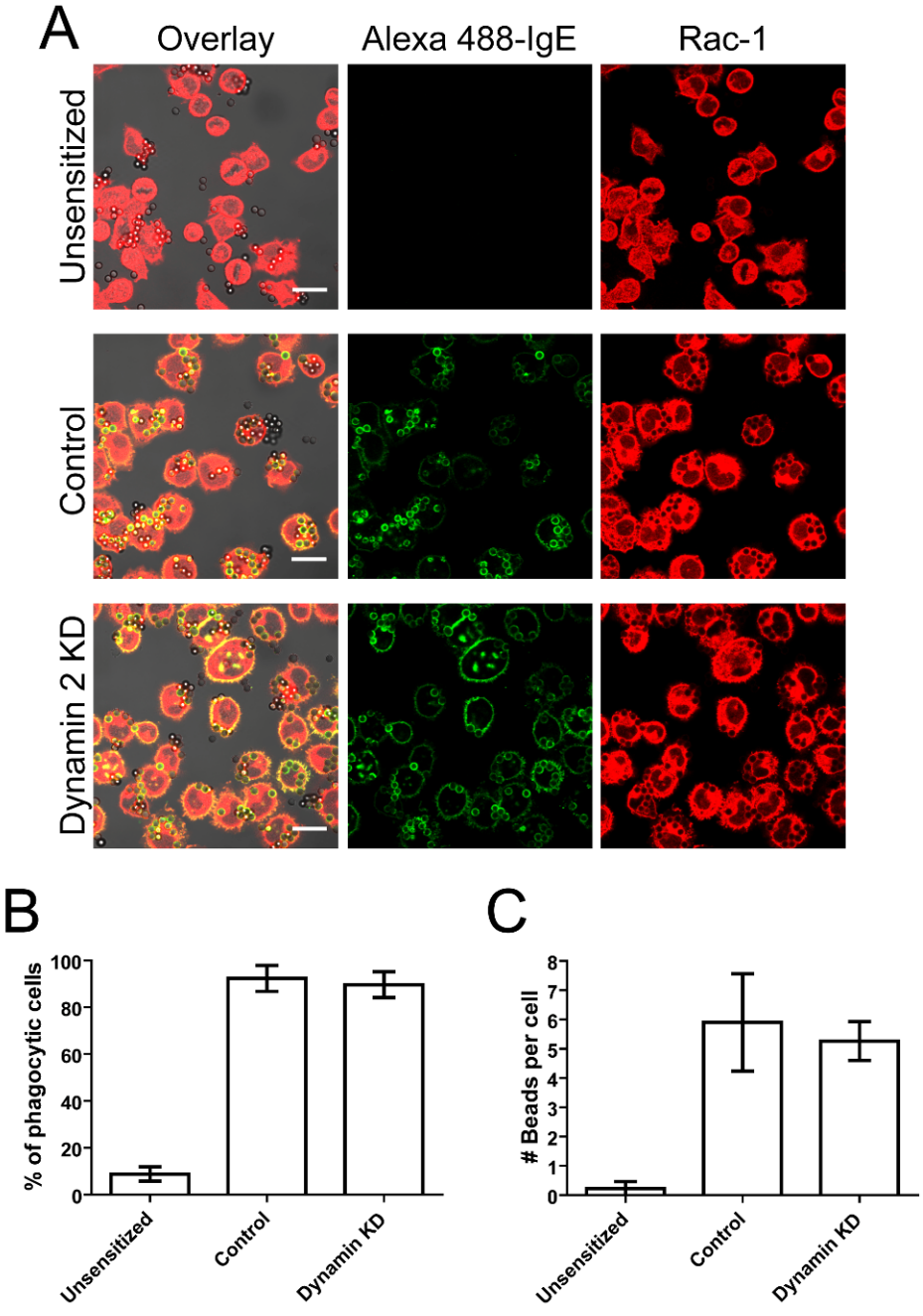
A
Overlay
Alexa 488-IgE
Rac-1
Unsensitized
Control
Dynamin 2 KD
B
% of phagocytic cells
100
80
60
40
20
0
Unsensitized
Control
Dynamin KD
C
Beads per cell
8
7
6
5
4
3
2
1
0
Unsensitized
Control
Dynamin KD

Figure 3.10: Overexpression of the GTPase deficient mutant dynamin 2 K44A-EGFP does not significantly reduce FcεRI-mediated phagocytosis. A) Dynamin-EGFP transfected RBL cells were incubated with DNP conjugated latex beads for 15 min or 30 min at 37°C. Cells were fixed and labeled with Alexa 568 phalloidin to stain actin filaments. In ~20% of cells selective recruitment of dynamin to the bead contact was observed (magenta arrows) and dynamin was also observed in ruffles (cyan box). Althougt the mutant dynamin (K44A) showed accumulation to the bead contact area, it did not prevent actin accumulation to the phagosome and did not reduce phagocytosis of DNP conjugated 4μm latex beads. Scale bars correspond to 20μm. B) The number of internalized beads per cell was quantified and no significant difference was detected between wild type and mutant dynamin 2. The percentage of cells scored as positive obtained from >100 cells from 3 different experiments were averaged (n=3) and the error represents SD.

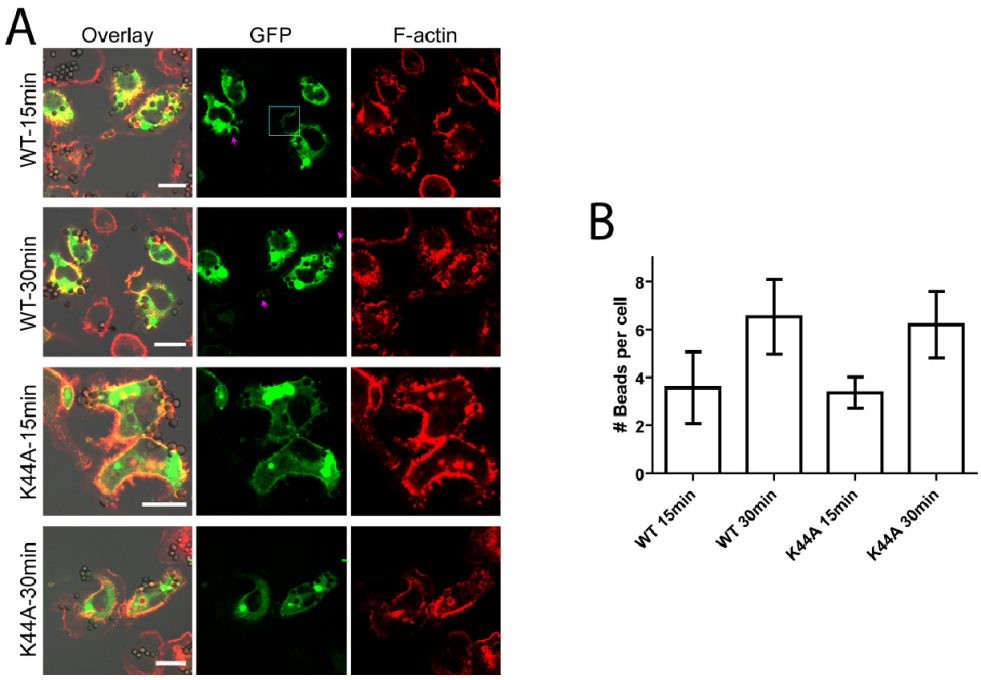
A
Overlay
GFP
F-actin
WT-15min
WT-30min
K44A-15min
K44A-30min
B
Beads per cell
0
2
4
6
8
WT 15min
WT 30min
K44A 15min
K44A 30min

micropatterned ligand arrays to selectively cluster and activate receptors while preventing internalization.

We have characterized different modes of receptor internalization and found that under stimulation conditions (soluble antigen) that form diffraction limited clusters of < 200 receptors per cluster, internalization is dependent on the actin cytoskeleton and dynamin 2 but independent of Rho GTPase and PI3-K regulation (Figure 3.3). In contrast, larger particles of 4μm diameter are rapidly phagocytosed in an actin, Rho GTPase and PI3-K dependent mechanism (Figure 3.5). These observations are consistent with the view that particle size determines the pathway used to internalize activated FcεRI receptors. Both phagocytosis and endocytosis of activated receptors were prevented in the mutant cell line deficient in Syk expression which suggests that signal transduction downstream of Syk is necessary for activating the internalization machinery (Figure 3.3 and 3.5). This mechanism may be a form of receptor down-regulation in response to overstimulation.

Neither clathrin heavy chain knock-down nor simultaneous knock-down of cortactin and its homolog HS1 had any effect on endocytosis of clustered IgE receptors. Cortactin has been found to be important in both clathrin dependent (*28, 53*) and independent (*15*) mechanisms, and it is possible that there is redundancy in the pathway leading to internalization and that reduction in expression levels of protein involved in a specific pathway may lead to up-regulation of a different pathway. This redundancy would complicate the interpretation of results obtained from clathrin and cortactin knock-down. For other cells types protein (dynamin and clathrin) knock-down is sufficient to cause a significant decrease in endocytosis (*22*) (*28*) (*15*), but RBL-2H3 cells may respond differently to such perturbations. The fact that knock-down of dynamin 2 causes only a 35% in endocytosis (Figure 3.6), when others have

found significant reduction by overexpression of dynamin 2 K44A-GFP (*9*), supports this possibility. The use of dominant negative mutant of cortactin or clathrin adapter proteins may prove to be valuable in future investigations to rule out the possibility of up-regulation of alternative pathways caused by protein knock-down.

Based on the selective accumulation of clathrin under clustered IgE-FcεRI using micropatterned ligands, it seems possible that clathrin may have at least a secondary role in receptor internalization (either phagocytosis or endocytosis). For example, clathrin has been implicated in membrane remodeling during phagocytosis (*13*). Although the patterned ligands prevent the formation of phagosomes, receptor clustering at the micron scale may initiate the necessary signals for clathrin activation.

Previously, we reported that several actin binding proteins commonly associated with focal adhesions, such as talin, vinculin and paxillin, were selectively recruited to the micropatterned receptor clusters in the absence of integrins and we hypothesized that these proteins may regulate signaling by working as adapter proteins that could connect F-actin to signaling proteins (e.g. lyn kinase) (*35*). However, another possibility is that these proteins may form part of the machinery responsible for receptor internalization by regulating the actin cytoskeleton. In this regard, these same focal adhesion proteins have been implicated in macrophage Fc-receptor mediated phagocytosis (*58*).

We showed selective accumulation of dynamin 2 by the micro-clustered receptors under conditions that prevent membrane invagination, and this recruitment is correlated to actin polymerization. Disruption of the actin cytoskeleton by Cytochalasin D does not prevent this accumulation of dynamin. In addition, dynamin 2 knock-down caused a significant reduction in the accumulation of actin under the patterned clustered receptor array (Figure 3.8). These results suggest that dynamin 2 recruitment to the membrane is not dependent on actin polymerization but dynamin 2

at the membrane regulates FcεRI dependent actin polymerization. Dynamin 2 regulation of actin dynamics at the membrane may be important in regulating distinct stages of receptor endocytosis. Our results suggest that dynamin 2 recruitment to the membrane is not only at the late stages of receptor endocytosis as commonly viewed, but it appears to be important at the initial stages before membrane invagination. Its accumulation to receptor clusters may be important to recruit other proteins involved in receptor endocytosis including bar domain proteins (*59, 60*) and cytoskeletal proteins.

Contrary to previous reports that show that inhibition of dynamin 2 function prevents macrophage phagocytosis, we found that neither dynamin 2 knock-down or overexpression of the dominant negative mutant dynamin 2-K44A have any effect on phagocytosis for RBL cells. In addition, no reduction of actin polymerization to the nascent phagosome was observed in dynamin knock-down cells incubated with 4μm beads. The fact that dynamin 2 knock-down produced a distinctive effect in F-actin accumulation on cells stimulated with the patterned bilayers and incubated with beads, indicates they represent two different processes. However, since receptor aggregation by micropatterned presents a novel method of cell activation, it is not clear whether it resembles a case of frustrated endocytois, phagocytosis or an intermediate state. We hypothesize that IgE receptor aggregation can elicit ether endocytosis or phagocytosis depending on the particle size and duration of the signaling. Some initial components of the internalization machinery may be partially activated by receptor clustering but the mechanisms of internalization diverge at some stage depending on the characteristics of the antigen. It is possible that stimulation by micropatterned ligands initiates the recruitement of some components of the internalization machinery before the pathway diverges to endocytosis or phagocytosis. The size dependence of the patterned ligands in the type of cellular response elicited is the subject of future

investigation. We have previously used patterned ligand with feature sizes from 1.5 to 4 μm, and we have not detected difference in the recruitment of signaling proteins such as Lyn (*34*), actin (*35*) and dynamin (this report), but based on the differential role for IP3-K and Rho GTPases in phagocytosis and endocytosis, submicron (<500) features may produce different responses.

We observed selective accumulation of dynamin 2-EGFP to phagosomes in a population of the cells (~20%, Figure 3.10), suggesting a possible role for dynamin 2 in receptor internalization by phagocytosis. A recent report showed that polymerized actin surrounding phagocytosed particles function as negative regulator of phagocytosis by acting as a barrier to delay phagosome fusion with lysosomes (*61*). Our data may be explained by a similar mechanism where dynamin-actin interactions are not involved at the initial stages of phagocytosis but are later needed to prevent further particle entry into lysosomal compartment in cargo overloaded cells. This would be consistent with our observations where both dynamin 2 and actin accumulation can be seen around internal particles that were at the late stages of phagocytosis.

In summary, we have shown that receptor endocytosis but not phagocytosis is dependent on the GTPase dynamin 2. Using micropatterned ligands arrays to spatially cluster and activate receptors while preventing internalization, we show that dynamin 2 is recruited to the clustered receptors under conditions that prevent membrane invagination, suggesting that IgE receptor activation is sufficient for the recruitment of dynamin 2 to the plasma membrane. Dynamin 2 knock-down reduces the accumulation of F-actin at the clustered receptors, suggesting a possible role for dynamin 2 in initiation and regulation of FcεRI mediated cytoskeletal interactions important for signaling and/or receptor internalization.

REFERENCES

1. Kraft, S., and Novak, N. (2006) Fc receptors as determinants of allergic reactions, *Trends in Immunology 27*, 88-95.
2. Nimmerjahn, F., Ravetch, J. V., and Frederick, W. A. (2007) Fc-Receptors as Regulators of Immunity, in *Advances in Immunology*, pp 179-204, Academic Press.
3. MacGlashan Jr, D. (2008) IgE receptor and signal transduction in mast cells and basophils, *Current Opinion in Immunology 20*, 717-723.
4. Kalesnikoff, J., and Galli, S. J. (2008) New developments in mast cell biology, *Nat Immunol 9*, 1215-1223.
5. Rivera, J., Fierro, N. A., Olivera, A., and Suzuki, R. (2008) New Insights on Mast Cell Activation via the High Affinity Receptor for IgE, in *Advances in Immunology*, pp 85-120, Academic Press.
6. Liu, H., Rhodes, M., Wiest, D. L., and Vignali, D. A. A. (2000) On the Dynamics of TCR:CD3 Complex Cell Surface Expression and Downmodulation, *Immunity 13*, 665-675.
7. Cheng, P. C., Steele, C. R., Gu, L., Song, W., and Pierce, S. K. (1999) MHC Class II Antigen Processing in B Cells: Accelerated Intracellular Targeting of Antigens, *J Immunol 162*, 7171-7180.
8. Kitaura, J., Xiao, W., Maeda-Yamamoto, M., Kawakami, Y., Lowell, C. A., and Kawakami, T. (2004) Early Divergence of Fcε Receptor I Signals for Receptor Up-Regulation and Internalization from Degranulation, Cytokine Production, and Survival, *J Immunol 173*, 4317-4323.
9. Fattakhova, G. n. V., Masilamani, M., Borrego, F., Gilfillan, A. M., Metcalfe, D. D., and Coligan, J. E. (2006) The High-Affinity Immunoglobulin-E

Receptor (FcεRI) is Endocytosed by an AP-2/Clathrin-Independent, Dynamin-Dependent Mechanism, *Traffic 7*, 673-685.

10. Fattakhova, G. n. V., Masilamani, M., Narayanan, S., Borrego, F., Gilfillan, A. M., Metcalfe, D. D., and Coligan, J. E. (2009) Endosomal trafficking of the ligated FcεRI receptor, *Molecular Immunology 46*, 793-802.
11. Molfetta, R., Gasparrini, F., Peruzzi, G., Vian, L., Piccoli, M., Frati, L., Santoni, A., and Paolini, R. (2009) Lipid Raft-Dependent FcεRI Ubiquitination Regulates Receptor Endocytosis through the Action of Ubiquitin Binding Adaptors, *PLoS ONE 4*, e5604.
12. Doherty, G. J., and McMahon, H. T. (2009) Mechanisms of Endocytosis, *Annual Review of Biochemistry 78*, 857-902.
13. Tse, S. M. L., Furuya, W., Gold, E., Schreiber, A. D., Sandvig, K., Inman, R. D., and Grinstein, S. (2003) Differential Role of Actin, Clathrin, and Dynamin in Fcγ Receptor-mediated Endocytosis and Phagocytosis, *Journal of Biological Chemistry 278*, 3331-3338.
14. Cox, D., Tseng, C.-C., Bjekic, G., and Greenberg, S. (1999) A Requirement for Phosphatidylinositol 3-Kinase in Pseudopod Extension, *Journal of Biological Chemistry 274*, 1240-1247.
15. Sauvonnet, N., Dujeancourt, A., and Dautry-Varsat, A. (2005) Cortactin and dynamin are required for the clathrin-independent endocytosis of γc cytokine receptor, *J. Cell Biol. 168*, 155-163.
16. Fujimoto, L. M., Robyn, R., John, E. H., and Sandra, L. S. (2000) Actin Assembly Plays a Variable, but not Obligatory Role in Receptor-Mediated Endocytosis, *Traffic 1*, 161-171.
17. Pfeiffer, J. R., Seagrave, J. C., Davis, B. H., Deanin, G. G., and Oliver, J. M. (1985) Membrane and cytoskeletal changes associated with IgE-mediated

serotonin release from rat basophilic leukemia cells, *J. Cell Biol. 101*, 2145-2155.

18. Wilson, B. S., Pfeiffer, J. R., and Oliver, J. M. (2002) FcεRI signaling observed from the inside of the mast cell membrane, *Molecular Immunology 38*, 1259-1268.

19. Wilson, B. S., Pfeiffer, J. R., and Oliver, J. M. (2000) Observing FcεRI Signaling from the Inside of the Mast Cell Membrane, *J. Cell Biol. 149*, 1131-1142.

20. Damke, H., Binns, D. D., Ueda, H., Schmid, S. L., and Baba, T. (2001) Dynamin GTPase Domain Mutants Block Endocytic Vesicle Formation at Morphologically Distinct Stages, *Mol. Biol. Cell 12*, 2578-2589.

21. Roux, A. l., Uyhazi, K., Frost, A., and De Camilli, P. (2006) GTP-dependent twisting of dynamin implicates constriction and tension in membrane fission, *Nature 441*, 528-531.

22. Cao, H., Chen, J., Awoniyi, M., Henley, J. R., and McNiven, M. A. (2007) Dynamin 2 mediates fluid-phase micropinocytosis in epithelial cells, *J Cell Sci 120*, 4167-4177.

23. Lee, E., and De Camilli, P. (2002) Dynamin at actin tails, *PNAS 99*, 161-166.

24. Ochoa, G.-C., Slepnev, V. I., Neff, L., Ringstad, N., Takei, K., Daniell, L., Kim, W., Cao, H., McNiven, M., Baron, R., and De Camilli, P. (2000) A Functional Link between Dynamin and the Actin Cytoskeleton at Podosomes, *J. Cell Biol. 150*, 377-390.

25. Bruzzaniti, A., Neff, L., Sanjay, A., Horne, W. C., De Camilli, P., and Baron, R. (2005) Dynamin Forms a Src Kinase-sensitive Complex with Cbl and Regulates Podosomes and Osteoclast Activity, *Mol. Biol. Cell 16*, 3301-3313.

26. Gold, E. S., Underhill, D. M., Morrissette, N. S., Guo, J., McNiven, M. A., and Aderem, A. (1999) Dynamin 2 Is Required for Phagocytosis in Macrophages, *J. Exp. Med. 190*, 1849-1856.

27. Witke, W., Podtelejnikov, A. V., Nardo, A. D., Sutherland, J. D., Gurniak, C. B., Dotti, C., and Mann, M. (1998) In mouse brain profilin I and profilin II associate with regulators of the endocytic pathway and actin assembly, *EMBO J 17*, 967-976.

28. Zhu, J., Zhou, K., Hao, J.-J., Liu, J., Smith, N., and Zhan, X. (2005) Regulation of cortactin/dynamin interaction by actin polymerization during the fission of clathrin-coated pits, *J Cell Sci 118*, 807-817.

29. Kessels, M. M., Engqvist-Goldstein, A. E. Y., Drubin, D. G., and Qualmann, B. (2001) Mammalian Abp1, a Signal-Responsive F-Actin-Binding Protein, Links the Actin Cytoskeleton to Endocytosis via the Gtpase Dynamin, *J. Cell Biol. 153*, 351-366.

30. Mooren, O. L., Kotova, T. I., Moore, A. J., and Schafer, D. A. (2009) Dynamin2 GTPase and Cortactin Remodel Actin Filaments, *Journal of Biological Chemistry 284*, 23995-24005.

31. Schafer, D. A., Weed, S. A., Binns, D., Karginov, A. V., Parsons, J. T., and Cooper, J. A. (2002) Dynamin2 and Cortactin Regulate Actin Assembly and Filament Organization, *Current Biology 12*, 1852-1857.

32. Merrifield, C. J., Perrais, D., and Zenisek, D. (2005) Coupling between Clathrin-Coated-Pit Invagination, Cortactin Recruitment, and Membrane Scission Observed in Live Cells, *Cell 121*, 593-606.

33. Torres, A. J., Wu, M., Holowka, D., and Baird, B. (2008) Nanobiotechnology and Cell Biology: Micro- and Nanofabricated Surfaces to Investigate Receptor-Mediated Signaling, *Annual Review of Biophysics 37*, 265-288.

34. Wu, M., Holowka, D., Craighead, H. G., and Baird, B. (2004) Visualization of plasma membrane compartmentalization with patterned lipid bilayers, *PNAS 101*, 13798-13803.

35. Torres, A. J., Vasudevan, L., Holowka, D., and Baird, B. A. (2008) Focal adhesion proteins connect IgE receptors to the cytoskeleton as revealed by micropatterned ligand arrays,*PNAS 105*, 17238-17244.

36. Pierini, L., Holowka, D., and Baird, B. (1996) Fc epsilon RI-mediated association of 6-micron beads with RBL-2H3 mast cells results in exclusion of signaling proteins from the forming phagosome and abrogation of normal downstream signaling, *J. Cell Biol. 134*, 1427-1439.

37. Larson, D. R., Gosse, J. A., Holowka, D. A., Baird, B. A., and Webb, W. W. (2005) Temporally resolved interactions between antigen-stimulated IgE receptors and Lyn kinase on living cells, *J. Cell Biol. 171*, 527-536.

38. Cao, H., Garcia, F., and McNiven, M. A. (1998) Differential Distribution of Dynamin Isoforms in Mammalian Cells, *Mol. Biol. Cell 9*, 2595-2609.

39. Cao, H., Thompson, H. M., Krueger, E. W., and McNiven, M. A. (2000) Disruption of Golgi structure and function in mammalian cells expressing a mutant dynamin, *J Cell Sci 113*, 1993-2002.

40. Petersen, N. O., Höddelius, P. L., Wiseman, P. W., Seger, O., and Magnusson, K. E. (1993) Quantitation of membrane receptor distributions by image correlation spectroscopy: concept and application, *Biophysical Journal 65*, 1135-1146.

41. Kolin, D., and Wiseman, P. (2007) Advances in Image Correlation Spectroscopy: Measuring Number Densities, Aggregation States, and Dynamics of Fluorescently labeled Macromolecules in Cells, *Cell Biochemistry and Biophysics 49*, 141-164.

42. Costantino, S., Comeau, J. W. D., Kolin, D. L., and Wiseman, P. W. (2005) Accuracy and Dynamic Range of Spatial Image Correlation and Cross-Correlation Spectroscopy, *Biophysical Journal 89*, 1251-1260.

43. Ilic, B., and Craighead, H. G. (2000) Topographical Patterning of Chemically Sensitive Biological Materials Using a Polymer-Based Dry Lift Off, *Biomedical Microdevices 2*, 317-322.

44. Orth, R. N., Wu, M., Holowka, D. A., Craighead, H. G., and Baird, B. A. (2003) Mast Cell Activation on Patterned Lipid Bilayers of Subcellular Dimensions, *Langmuir 19*, 1599-1605.

45. Andrews, N. L., Pfeiffer, J. R., Martinez, A. M., Haaland, D. M., Davis, R. W., Kawakami, T., Oliver, J. M., Wilson, B. S., and Lidke, D. S. (2009) Small, Mobile FcεRI Receptor Aggregates Are Signaling Competent, *Immunity 31*, 469-479.

46. Qualmann, B., and Mellor, H. (2003) Regulation of endocytic traffic by Rho GTPases, *Biochem. J. 371*, 233-241.

47. Menon, A. K., Holowka, D., Webb, W. W., and Baird, B. (1986) Clustering, mobility, and triggering activity of small oligomers of immunoglobulin E on rat basophilic leukemia cells, *J. Cell Biol. 102*, 534-540.

48. Xu, K., Williams, R. M., Holowka, D., and Baird, B. (1998) Stimulated release of fluorescently labeled IgE fragments that efficiently accumulate in secretory granules after endocytosis in RBL-2H3 mast cells, *J Cell Sci 111*, 2385-2396.

49. Field, K. A., Apgar, J. R., Hong-Geller, E., Siraganian, R. P., Baird, B., and Holowka, D. (2000) Mutant RBL Mast Cells Defective in FcεRI Signaling and Lipid Raft Biosynthesis Are Reconstituted by Activated Rho-family GTPases, *Mol. Biol. Cell 11*, 3661-3673.

50. Hong-Geller, E., Holowka, D., Siraganian, R. P., Baird, B., and Cerione, R. A. (2001) Activated Cdc42/Rac reconstitutes FceRI-mediated Ca2+ mobilization and degranulation in mutant RBL mast cells, *PNAS 98*, 1154-1159.

51. Ra, C., Furuichi, K., Rivera, J., Mullins, M. J., Isersky, C., and White, K. N. (1989) Internalization of IgE receptors on rat basophilic leukemic cells by phorbol ester: comparison with endocytosis induced by receptor aggregation, *European Journal of Immunology 19*, 1771-1777.

52. Zhang, J., Berenstein, E. H., Evans, R. L., and Siraganian, R. P. (1996) Transfection of Syk protein tyrosine kinase reconstitutes high affinity IgE receptor-mediated degranulation in a Syk-negative variant of rat basophilic leukemia RBL-2H3 cells, *J. Exp. Med. 184*, 71-79.

53. Cao, H., Orth, J. D., Chen, J., Weller, S. G., Heuser, J. E., and McNiven, M. A. (2003) Cortactin Is a Component of Clathrin-Coated Pits and Participates in Receptor-Mediated Endocytosis, *Mol. Cell. Biol. 23*, 2162-2170.

54. Uruno, T., Zhang, P., Liu, J., Hao, J. J., and Zhan, X. (2003) Haematopoietic lineage cell-specific protein 1 (HS1) promotes actin-related protein (Arp) 2/3 complex-mediated actin polymerization, *Biochem. J. 371*, 485-493.

55. Gomez, T. S., Hamann, M. J., McCarney, S., Savoy, D. N., Lubking, C. M., Heldebrant, M. P., Labno, C. M., McKean, D. J., McNiven, M. A., Burkhardt, J. K., and Billadeau, D. D. (2005) Dynamin 2 regulates T cell activation by controlling actin polymerization at the immunological synapse, *Nat Immunol 6*, 261-270.

56. Orth, J. D., Krueger, E. W., Cao, H., and McNiven, M. A. (2002) The large GTPase dynamin regulates actin comet formation and movement in living cells, *PNAS 99*, 167-172.

57. Baldassarre, M., Pompeo, A., Beznoussenko, G., Castaldi, C., Cortellino, S., McNiven, M. A., Luini, A., and Buccione, R. (2003) Dynamin Participates in Focal Extracellular Matrix Degradation by Invasive Cells, *Mol. Biol. Cell 14*, 1074-1084.

58. Allen, L. A., and Aderem, A. (1996) Molecular definition of distinct cytoskeletal structures involved in complement- and Fc receptor-mediated phagocytosis in macrophages, *J. Exp. Med. 184*, 627-637.

59. Itoh, T., Erdmann, K. S., Roux, A., Habermann, B., Werner, H., and De Camilli, P. (2005) Dynamin and the Actin Cytoskeleton Cooperatively Regulate Plasma Membrane Invagination by BAR and F-BAR Proteins, *Developmental Cell 9*, 791-804.

60. McPherson, V. A., Everingham, S., Karisch, R., Smith, J. A., Udell, C. M., Zheng, J., Jia, Z., and Craig, A. W. B. (2009) Contributions of F-BAR and SH2 Domains of Fes Protein Tyrosine Kinase for Coupling to the FcεRI Pathway in Mast Cells, *Mol. Cell. Biol. 29*, 389-401.

61. Liebl, D., and Griffiths, G. (2009) Transient assembly of F-actin by phagosomes delays phagosome fusion with lysosomes in cargo-overloaded macrophages, *J Cell Sci 122*, 2935-2945.

CHAPTER 4

SUMMARY AND OUTLOOK

4.1 Cytoskeletal regulation of IgE receptor signaling

Regulation of receptor mediated signaling by the cytoskeleton is a common theme in receptor biology. Using a specialized set of tools to spatially control the cell stimulus in combination with biochemical and genetic characterization of intracellular signaling we have investigated the functional implications and the spatial regulation of the cytoskeleton in IgE receptor signaling. Our current knowledge on the functional connection between the cytoskeleton and FcεRI signaling has been based on observed cellular responses after receptor activation in the presence of pharmacological inhibitors of actin polymerization (*1-4*). Such experiments are useful in linking the actin cytoskeleton to FcεRI mediated responses, but fall short in providing enough mechanistic insight into the structural interplay between signaling molecules. Interpretations of such results are also complicated by the possible cross-talk between different signaling pathways that depend on the cytoskeleton. Such interactions between cytoskeletal adapter proteins and immune receptors are typified in T-cells (*5*), where the cytoskeleton coordinates and regulates the interplay between the TCR and integrins at the cell surface to mediate the formations of a supramolecular assembly of proteins called the immunological synapse (*6*).

Using micropatterned ligand arrays containing DNP ligands we identified several actin binding adapter proteins such as paxillin, vinculin and talin, which are selectively recruited to the clustered IgE receptors. Interestingly, these proteins are typically involved in connecting the actin cytoskeleton to the extracellular matrix by means of integrin receptors (*7*). Although these proteins are typically found in actin

rich structures that mediate cell migration, known as focal adhesions, some of these adapter proteins have been implicated in other signaling pathways. For example, the focal adhesion protein talin is responsible for orchestrating several steps that lead to the formation of the immunological synapse (*8*). Considering previous reports where Lyn kinase is co-immunoprecipitated with paxillin in RBL cells(*9*) and other studies that show a role for the paxillin homolog leupaxin in regulation B-cell receptor signaling(*10*), it is conceivable that these focal adhesion proteins act as adapter proteins that connect the cytoskeleton to signaling component involved in IgE receptor mediated cell activation.

The focal adhesion proteins vinculin, paxillin and talin have also been implicated in Fc-receptor mediated phagocytosis that occurs when macrophages come into contact with large (>1μm) opsonized particles (*11*). The presence of these proteins in nacent phagosomes suggests a role for these focal adhesion proteins in Fc-receptor internalization which is independent of integrin activation. Although the main function of mast cells is the release of chemical mediators that lead to systemic responses (e.g. allergic reaction) upon contact with antigen, these cells are capable of engulfing larger sensitized particles by phagocytosis in a process dependent upon FcεRI activation (*12*). The fact that we observe accumulation of the GTPase dynamin 2 to the receptors activated by the micropatterned ligands, support a scenario where activation by the patterned ligands frustrates internalization of the receptor but promotes the assembly of the internalization machinery.

Several proteins that regulate the actin cytoskeleton were identified to be involved in IgE receptor signaling. However the functional role of these proteins has not been successfully addressed. Two possible mechanisms have arisen from this investigation: 1) a direct connection between IgE receptor signaling components and the actin cytoskeleton by focal adhesion proteins and/or 2) dynamin 2 operating as

adapter proteins that coordinate protein-protein interactions and/or regulation of signaling by controlling the machinery responsible for receptor internalization.

Structural connections between focal adhesion proteins are well characterized (*7*). Based on these well known inter-protein interactions, we can envision a mechanism were paxillin binds to the SH2 or SH3 domain of Lyn kinase and vinculin directly links paxillin to the cytoskeleton as shown in Figure 4.1. In this scenario, dynamin could potentially function as a regulator of actin polymerization in coordination with cortactin or other related proteins. It is well established that Lyn can work as both a positive a negative regulator of signaling (*13*). Such connection between Lyn and the actin cytoskeleton by focal adhesion proteins could explain the observed cellular responses in the presence of inhibitors of actin polymerization. The apparent negative regulation of the cytoskeleton in IgE receptor signaling may be mediated by the connection with Lyn kinase.

In a different scenario, the actin cytoskeleton could modulate the machinery necessary for internalization of the activated receptor clusters. Rapid internalization of activated receptor could negatively regulate signaling by reducing the number of cell surface receptors. After receptor activation, the GTPase dynamin 2 is recruited to the clustered receptors where it may induce the selective accumulation of several actin regulating proteins. The formation of a cytoskeletal network controlling contractile forces and membrane tension in combination with bar domain proteins, which regulate membrane curvature, may contribute to the formation of an endocytic structure (Figure 4.2) that leads to the endocytosis of vesicles containing clustered IgE-FcεRI complexes.

Further studies will be needed to elucidate the proposed mechanisms of IgE receptor cytoskeletal regulation. Protein knock-down and over-expression of dominant negative mutants of the identified cytoskeletal proteins will aid in determining the

Figure 4.1: A model for focal adhesion proteins involvement in connecting microfilaments to IgE receptor signaling. Lyn kinase is indirectly connected to the actin cytoskeleton by the adapter proteins paxillin, vinculin and talin, and the cytoskeleton acts as a platform that facilitates interaction between different signaling components.

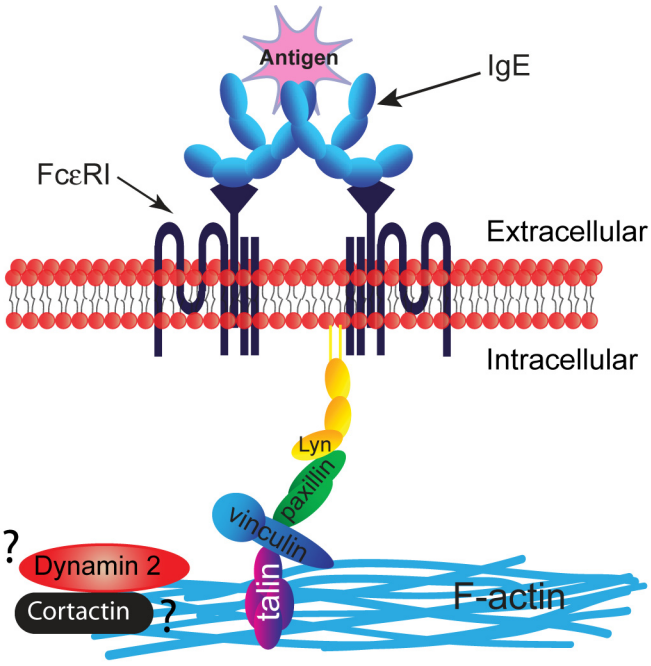
Antigen
IgE
FcεRI
Extracellular
Intracellular
Lyn
paxillin
vinculin
talin
?
Dynamin 2
Cortactin
?
F-actin

Figure 4.2: A model for cytoskeletal regulation of endocytosis mediated by dynamin 2 and actin binding adapter proteins. Dynamin localizes to the the sites of IgE-FcεRI clusters. Dynamin 2 is then responsible for the recruitment of several actin regulating proteins that promote actin assembly. Contractile forces induced by filamentous actin and dynamin interaction in colaboration with bar domain proteins are responsible for the formation of endocytic vessicles containing the activated receptors.

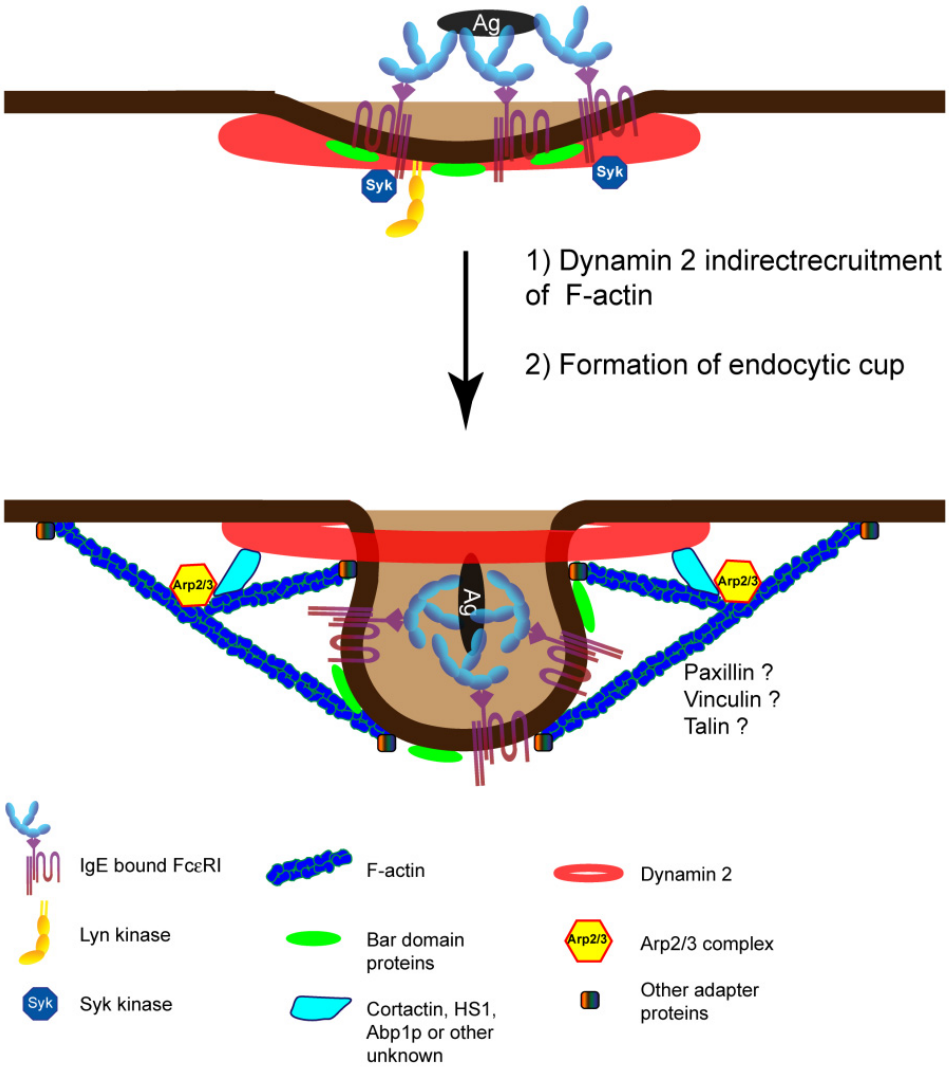
Ag
Syk
Syk
1) Dynamin 2 indirectrecruitment of F-actin
2) Formation of endocytic cup
Arp2/3
Arp2/3
Ag
Paxillin ?
Vinculin ?
Talin ?
IgE bound FcεRI
Lyn kinase
Syk
Syk kinase
F-actin
Bar domain proteins
Cortactin, HS1, Abp1p or other unknown
Dynamin 2
Arp2/3
Arp2/3 complex
Other adapter proteins

functional role of the observed structural reorganization. To differentiate between dynamin-2 and focal adhesion proteins working as adapter proteins in IgE receptor signaling or as regulators of receptor internalization, further biochemical characterizations is needed. Co-immunoprecipitation studies will provide information about the type of protein-protein interactions that occur after receptor activation and the structural connections between dynamin 2, IgE receptor signaling proteins and the actin cytoskeleton.

Furthermore, because the patterned ligands represent a novel method of cell activation, it is not yet clear if this receptor clustering by micropatterned ligands more closely resembles frustrated endocytosis or phagocytosis. Our results indicate a particle (IgE-FcεRI cluster) size dependence in the mechanism of receptor internalization. Based on the observed differential modes of receptor internalization activated by cell stimulation with DNP-conjugated 4 μm beads or DNP-BSA, it is conceivable that the patterned ligand feature size is an important variable for promoting a distinctive cellular response. For example, receptor activation by patterned ligands with a diameter of <500 nm could initiate a cellular response that more closely resembles receptor activation by soluble ligand. Signaling proteins recruited to the sites of receptor activation under these conditions may also be different when compared to feature sizes of >1μm. This size dependence will be the focus of future investigations.

4.2 Spatio-temporal control of cell stimuli by micropatterned ligand arrays: A powerful tool to investigate receptor-mediated signaling.

Unlike physical sciences where researchers can reduce the problem to a set of well defined variables, cell biologists deal with systems of great complexities with little control over the experimental variables. In occasions, such complexities lead to wrong interpretation of experimental result and introduction of artifact by unaccounted

variables. Because of this lack of control, it is not uncommon in cell biology to use multiple approaches to address the same question to establish a mechanism without reasonable doubt.

Over the years, increase cooperation between biologists, physical scientists and engineers have provided the field of cell biology with tools to help get around some of the challenges and complexities found in living cell. From optical microscopes to genetically modified fluorescence proteins, each of these tools have advanced the field incredible ways.

Although the main thrust of our lab in investigation of cellular mechanism in immune cell signaling, we have spent considerable efforts in developing technologies that are useful for our investigation of cellular signaling. One such technology is the development of micropatterned ligand arrays to spatially activate receptor mediated signaling. In addition to the elucidation of cytoskeletal interaction in IgE receptor signaling, we have demonstrated the utility of microfabricated surfaces in the investigation of complicated questions of cell biology in ways not before possible. Lithographic methods and selective surface functionalization schemes to create biocompatible surfaces can be used to control cellular interactions on the micron and sub-micron scales on which cells are organized. Combined with fluorescence microscopy and other approaches of cell biology, our efforts have expanded the toolbox available for cell biologist.

REFERENCES

1. Oka, T., Sato, K., Hori, M., Ozaki, H., and Karaki, H. (2002) FcεRI cross-linking-induced actin assembly mediates calcium signalling in RBL-2H3 mast cells, *136*, 837-846.
2. Torigoe, C., Song, J., Barisas, B. G., and Metzger, H. (2004) The influence of actin microfilaments on signaling by the receptor with high-affinity for IgE, *Molecular Immunology 41*, 817-829.
3. Frigeri, L., and Apgar, J. R. (1999) The Role of Actin Microfilaments in the Down-Regulation of the Degranulation Response in RBL-2H3 Mast Cells, *J Immunol 162*, 2243-2250.
4. Pierini, L., Harris, N. T., Holowka, D., and Baird, B. (1997) Evidence Supporting a Role for Microfilaments in Regulating the Coupling between Poorly Dissociable IgE-FcεRI Aggregates and Downstream Signaling Pathways *Biochemistry 36*, 7447-7456.
5. Smith-Garvin, J. E., Koretzky, G. A., and Jordan, M. S. (2009) T Cell Activation, *Annual Review of Immunology 27*, 591-619.
6. Burkhardt, J. K., Carrizosa, E., and Shaffer, M. H. (2008) The actin cytoskeleton in T cell activation, *Annu. Rev. Immunol. 26*, 233.
7. Critchley, D. R. (2000) Focal adhesions - the cytoskeletal connection, *Current Opinion in Cell Biology 12*, 133-139.
8. Simonson, W. T. N., Franco, S. J., and Huttenlocher, A. (2006) Talin1 Regulates TCR-Mediated LFA-1 Function, *J Immunol 177*, 7707-7714.
9. Minoguchi K, K. H., Nishikata H, Hamawy MM, Siraganian RP. (1994) Src family tyrosine kinase Lyn binds several proteins including paxillin in rat basophilic leukemia cells., *Mol Immunol 31*, 519-529.

10. Chew, V., and Lam, K.-P. (2007) Leupaxin Negatively Regulates B Cell Receptor Signaling, *Journal of Biological Chemistry 282*, 27181-27191.
11. Allen, L. A., and Aderem, A. (1996) Molecular definition of distinct cytoskeletal structures involved in complement- and Fc receptor-mediated phagocytosis in macrophages, *J. Exp. Med. 184*, 627-637.
12. Pierini, L., Holowka, D., and Baird, B. (1996) FcεRI-mediated association of 6-micron beads with RBL-2H3 mast cells results in exclusion of signaling proteins from the forming phagosome and abrogation of normal downstream signaling, *J. Cell Biol. 134*, 1427-1439.
13. Xiao, W., Nishimoto, H., Hong, H., Kitaura, J., Nunomura, S., Maeda-Yamamoto, M., Kawakami, Y., Lowell, C. A., Ra, C., and Kawakami, T. (2005) Positive and Negative Regulation of Mast Cell Activation by Lyn via the FcεRI, *J Immunol 175*, 6885-6892.

APPENDIX[4]

MICROPATTERNED LIGAND ARRAYS TO STUDY SPATIAL REGULATION IN FC RECEPTOR SIGNALING: A PROTOCOL

A.1 Introduction

Cellular receptors for immunoglobulins (Fc-receptors) are widely expressed on the surface of highly specialized cells that form part of the adaptive immune system (*1, 2*). These cells are sensitized by binding of antibodies produced in response to foreign molecules. Receptor activation elicits different cellular responses that depend mainly on the cell and receptor type but also on the presence of other co-stimulatory signals (*3*). Such responses include: release of preformed mediators, de-novo protein synthesis, phospholipid metabolism, changes in cell morphology, endocytosis and phagocytosis. One important class of Fc receptors is the receptor for IgE (FcεRI), which is responsible for the release of chemical mediators that causes inflammatory and allergic reactions (*4*), and is found primarily on mast cells and basophils.

Cross-linking of IgE-FcεRI by multivalent antigen (ligand) triggers intracellular signaling events, leading to multiple cellular responses. In the earliest signaling events, antigen-induced clustering of IgE-FcεRI causes stable association with ordered lipid domains, cytoskeletal redistribution and Lyn kinase phosphorylation of the FcεRI β and γ subunits (*5*). The latter initiates a series of signaling events that induces Ca^{2+} mobilization and other downstream signaling steps leading to degranulation and secretion of preformed mediators (*6*).

Elucidation of signaling pathways involved in receptor signaling are crucial for the development of therapeutics and prevention of immune diseases. Current

[4] This material has been submitted for publication in *Methods in Molecular Biology.*

understanding of FcεRI signaling has been mostly dependent upon biochemical and genetic characterization of protein interactions. Spatial orchestration of these signaling events is a critical aspect, but studies have been limited by these common approaches. We have recently established the use of microfabricated surfaces containing spatially defined ligands to investigate spatial regulation of cell signaling (*7, 8*).

A recent review discussing the applications of micro- and nanofabrication in receptor signaling and cell biology has been published elsewhere (*9*). Herein, we present a detailed description of an approach we developed to investigate spatial regulation in IgE-FcεRI signaling on RBL-2H3 cells by microfabricated surfaces using the polymer lift-off method and 2,4-dinitrophenyl (DNP) ligands. It should be noted that even though the procedure described here is specific for the IgE receptor system, the same principles are applicable to other receptor systems and can be adapted by selecting the appropriate ligands and surface functionalization schemes.

A.2 Materials

A.2.1 Microfabrication

1. Parylene C dimer (Speciality Coating System, Indianapolis, IN)
2. Parylene Deposition System PDS 2010 LABCOTER (Speciality Coating System, Indianapolis, IN)
3. Computer assisted design (CAD) software.
4. Cleaning solution (piranha etch) composed of a freshly prepared mixture of concentrated sulfuric acid and 30% (v/v) hydrogen peroxide solution (3:1 v/v) (see **Note 1**).
5. Silicon wafers containing a ~ 50-100 nm oxide layer or glass wafers (optical quality for microscopy, see **Note 2**).
6. Positive photoresist (see **Note 3**).

7. Resist spinner and hotplates.

8. Chrome coated mask.

9. Developing solutions for dissolving exposed photoresist. The choice of developing solution depends on the photoresist used.

10. Optical pattern generator for mask design (e.g. DWL66 Heidelberg Mask Writer)

11. g-line (435nm) or i-line (365nm) stepper

12. Reactive Ion Etcher (e.g. Oxford PlasmaLab 80+)

A.2.2 RBL-2H3 cell culture

1. Minimum Essential Medium (MEM; Gibco, Invitrogen) supplemented with 20% (v/v) Fetal Bovine Serum (Atlanta Biologicals, GA) and 50µg/mL Gentamicin (Gibco, Invitrogen).

2. Trypsin Solution (Gibco, Invitrogen).

A.2.3. Supported lipid bilayer preparation

1. 1-Palmitoyl-2-Oleoyl-*sn*-Glycero-3-Phosphocholine (16:0-18:1 PC) (POPC; Avanti Polar Lipids, Al).

2. 1,2-Dipalmitoyl-*sn*-Glycero-3-Phosphoethanolamine-N-[6-[(2,4-dinitrophenyl)amino]caproyl] (DNP-Cap-PE; Avanti Polar Lipids, Al).

3. 1,2-Dioleoyl-*sn*-Glycero-3-Phosphoethanolamine-N-(Lissamine Rhodamine B Sulfonyl) (Lissamine Rhodamine PE; Avanti Polar Lipids, Al). Stock solutions of lipids are prepared in chloroform at concentration ranging from 1-25 mg/mL. Store stock solutions in glass vials dessicated at -20°C.

4. Argon or nitrogen gas (Airgas Inc.).

5. Phosphate buffered saline (PBS; 137mM NaCl, 2.7 mM KCl and 10 mM sodium phosphate, pH 7.4) .

6. Acrodisc 25mm syringe filter, 0.2µm HT Tuffryn membrane (Pall Co., NY).

7. Plasma cleaner PDC-32G (115V) (Harrick Plasma, NY) connected to a vacuum pump with a minimum pumping speed of 1.4 m^3/hr and a maximum ultimate total pressure of 200 mTorr.

8. Parafilm M Laboratory Wrapping Film (Fisher Scientific).

A.2.4 Ligand carrier immobilization

1. (3-mercaptopropyl)trimethoxysilane (Sigma-Aldrich), stored under argon in a dessicator at 4°C.

2. 4-Maleimidobutyric acid N-succinimidyl ester, GMBS (Sigma-Aldrich). Prepare a 1M stock solution in Dimethylformamide (DMF) and store at -20°C in small aliquots (stable for weeks in DMF)

3. Toluene (Mallinckrodt Chemicals, NJ)

4. 2,4-dinitrophenylated bovine serum albumin, DNP-BSA (Molecular Probes, Invitrogen), conjugated to a fluorophore (e.g. Alexa 568 or Cy3).

5. Phosphate buffer (0.1M sodium phosphate and 0.15M NaCl, pH 7.3).

A.2.5 Transfection

1. Gene Pulser Xcell electroporator system (Bio-Rad Laboratories)

2. Electroporation buffer (137 mM NaCl, 2.7 mM KCl, 1 $MgCl_2$, 5.6 mM glucose and 20 mM Hepes (pH 7.4))

3. DNA construct encoding for the green fluorescent protein (GFP)-fusion protein of interest.

A.2.6 Cell activation

1. Monoclonal anti-2,4-dinitrophenyl IgE (Sigma-Aldrich).

2. Buffered saline solution, BSS (135 mM NaCl, 5.0 mM KCl, 1.8 mM $CaCl_2$, 1.0 mM $MgCl_2$, 5.6 mM glucose and 20 mM Hepes (pH 7.4)), containing 1 mg/ml BSA

3. 35 x 10 mm tissue culture dish.

4. Micro-patterned substrate.

A.2.7 Fixation and imaging

1. Formaldehyde 3.7%, freshly prepared in PBS from a 37% stock.
2. Bovine serum albumin (BSA)
3. Glass Bottom Culture Dishes, No. 1.5 (MatTek Co., MA)

A.3 Methods

A.3.1 Microfabrication

Due to the highly technical nature of the microfabrication process and the variations in instrumentation between different facilities, specific details are not described. Photolithography instrumentation is expensive and not easily accessible outside dedicated clean room facilities; moreover instrument models vary greatly between facilities, and some procedures will need to be adapted and/or optimized depending on the available instrumentation.

Many universities have access to clean room facilities and technical staff who train in the fabrication process. We suggest initial collaborations with groups with experience in microfabrication. The fabrication procedure described here is straightforward and can be easily followed by a person with basic knowledge in the field. Alternatively, some companies or facilities may be able to process custom orders.

The fabrication of the patterned substrate involves a series of steps that are summarized in Figure A.1. Once the patterned parylene wafers are prepared, they can be stored for several months (in a dessicator) for further use. Immobilization of the biomaterial is then performed in the laboratory.

1. Design pattern with desired feature size and shape in a computer assisted design (CAD) software. The pattern size and spacing should be enough to include several features per biological cell and large enough (>500nm) for efficient visualization using fluorescence microscopy.

Figure A.1: **Schematic diagram of patterned surface micro-fabrication and deposition of biological material (e.g. ligand).**

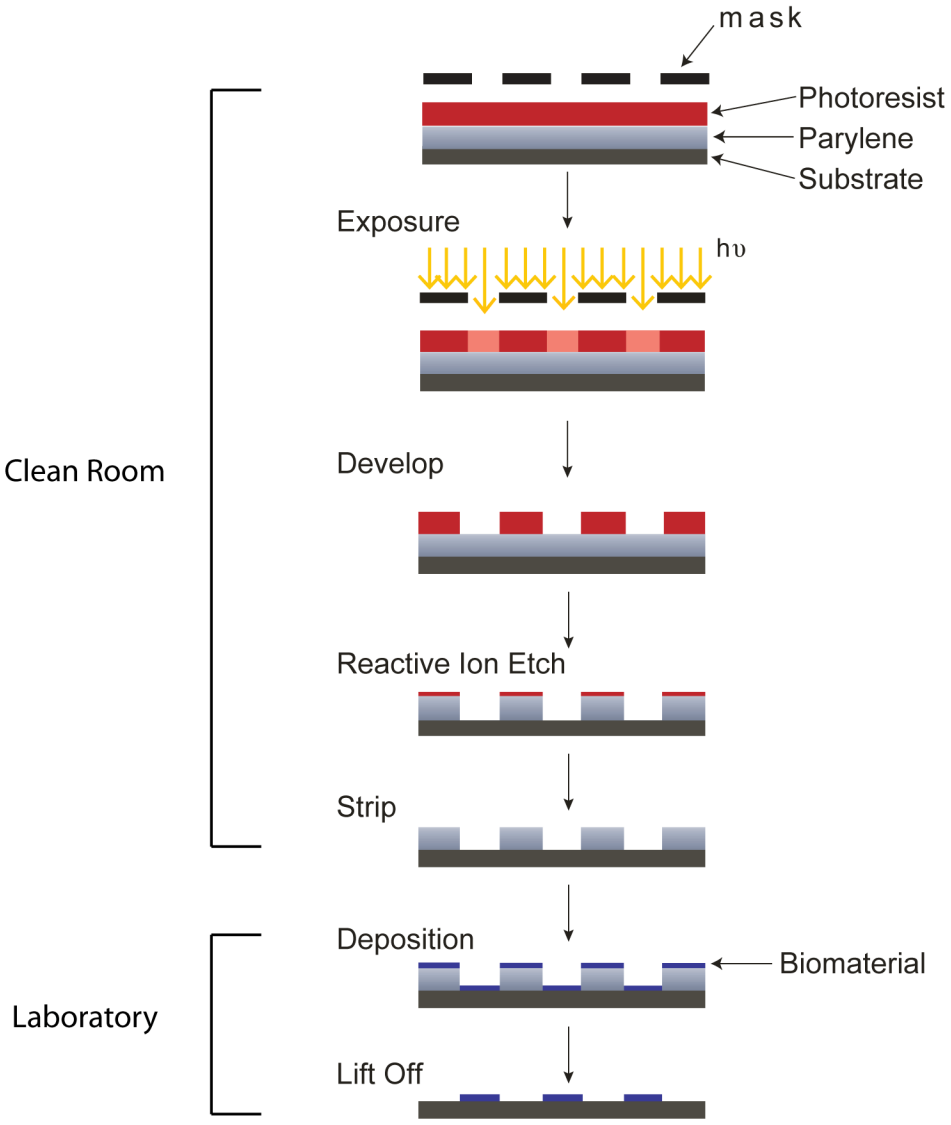
mask
Photoresist
Parylene
Substrate
Exposure
hυ
Develop
Reactive Ion Etch
Strip
Deposition
Biomaterial
Lift Off
Clean Room
Laboratory

2. Design chrome mask. The mask is fabricated by transferring the CAD pattern using an optical pattern generator on a chrome (~80 nm layer) evaporated glass plate (5'' by 5'') coated with photoresist. After light exposure and photoresist development, the chrome is removed from areas unprotected by photoresist by using acid etch. Once prepared, the same mask can be used indefinitely for the photolithographic preparation of the patterned wafers and can be stored for years without significant lost of quality.

3. Clean wafer with piranha solution.

4. Coat the wafers with a thin layer (~1μm) of Parylene C polymer using the Parylene Coating System. The amount of parylene dimer loaded into the system and other instrument settings will have to be optimized to achieve the desired layer thickness.

5. Spin-coat wafers with photoresist to get a uniform layer of ~1.6-2.0 μm and place wafers on a hot plate for ~0.5-2 min (soft-bake) to evaporate any excess solvent and promote adhesion of the resist to the wafer. Soft-bake conditions (baking time and temperature) will depend on the choice of photoresist.

6. Expose photoresist coated wafer to electromagnetic radiation through the mask (prepared previously as depicted in steps #1-2) by using a 5X g-line (435nm) or 10x i-line (365nm) stepper. The optimal focus and exposure time should be determined experimentally.

7. Place exposed wafers on a hot plate for ~0.5-2 min (post-bake) to anneal the surface. Post-bake conditions will depend on the choice of photoresist.

8. Dissolve the exposed photoresist (develop) using the appropriate solvent for the photoresist and characterize the photoresist film thickness. Some facilities have automatic instrumentation for wafer development such as the Hamatech-Steag wafer processors.

9. Etch wafer using reactive ion etcher (RIE) with oxygen as the reactive specie **(see Note 4)**.

10. Dissolve remaining photoresist with acetone while spinning the wafer using a spin-coater.

11. Store wafer for future use.

12. Before ligand immobilization on the surface, cut silicon wafers into 8 x 8mm pieces. These small pieces are used for cell experiments (see **Note 5**). When working with glass wafer, cut wafer into 22 x 22 mm pieces by scratching the surface on the side opposite to the parylene layer using a diamond scribing tool with the help of a rubber ruler. Carefully detach coverslip from a glass bottom culture dish (No. 1.5) and replace with patterned parylene glass piece by using an adhesive, such as Sylgard 182 silicone elastomer (Dow Corning), with the parylene layer facing the interior of the dish.

A.3.2 Ligand immobilization using supported membranes

Two different methods for immobilizing 2,4-dinitrophenyl (DNP) ligand to the patterned substrates are presented here. The first method requires supported lipid bilayers for ligand presentation while the other alternative method involves covalent coupling of a ligand carrier to the surface (see Figure A.2). Both immobilization schemes are equivalent in their ability to induce receptor clustering. However, we find that supported lipid bilayers provide some significant advantages. Supported lipid bilayers tend to be inert and more resistive to nonspecific protein absorption, in contrast to the SiO_2 surface which is more prone to protein absorption and cell adhesion (*10, 11*). Our experimental system uses IgE antibodies specific to DNP groups. Cells are sensitized with anti-DNP IgE antibodies where they form tight complexes (high affinity, low dissociation) with FcεRI receptor on the cell surface. IgE-FcεRI clustering and activation by the immobilized ligands recruits a series of signaling proteins that, if labeled, can be visualized with fluorescence microscopy

Figure A.2: Micro-patterned ligand array after polymer lift-off. A) Array of immobilized fluorescent BSA visualized after partially peeling the parylene layer. Nonspecific bound material is removed with the polymer, leaving a surface with clearly defined features and low background fluorescence. B) Cartoon showing possible ligand immobilization schemes. The ligand of interest (e.g. DNP) can be incorporated into a supported lipid bilayer (top) or covalently attached to the surface via a protein carrier such as BSA (bottom).

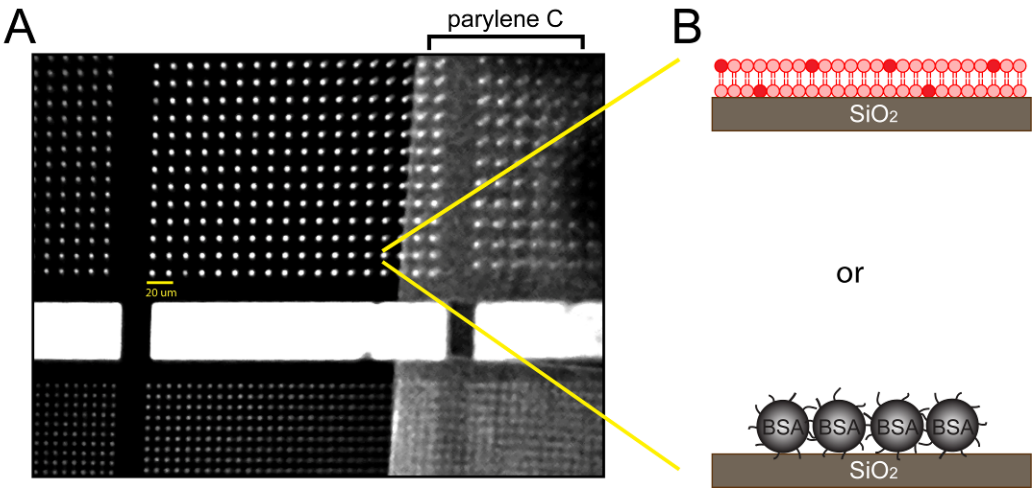
A
parylene C
20 um
B
SiO2
or
BSA
BSA
BSA
BSA
SiO2

(Figure A.3). For other experimental systems, the choice of ligand and immobilization scheme may need to be adapted (see ref. (*9*)). For example, biotin-streptavidin interaction can be used to tether biotinylated proteins on a surface modified with biotin groups attached to streptavidin (*12*).

1. Prepare a solution containing 89 mol% POPC, 10 mol% DNP-cap-PE and 1 mol% lissamine rhodamine PE by mixing stock solutions in chloroform (see **Note 6**). The amount of lipids used should amount to a total lipid concentration of 1mM after reconstitution in buffer (see step 3). Use a glass vial to mix the lipids.

2. Evaporate solvent with a stream of argon or nitrogen gas to create thin lipid film in a glass vial. Lipid films may be stored under argon for weeks at -20°C in a dessicator.

3. Hydrate film by adding ~2mL of PBS for 5min. The temperature of the buffer should be above the gel-liquid crystal transition temperature of the major lipid and should be maintained during the hydration period. The effects of buffer pH and ionic strength on supported lipid bilayer formation and stability are addressed in reference (*13*).

4. Vortex for 30s to create large multilamellar vesicles (LMV).

5. Sonicate the samples with a probe sonicator with suspension at ~10°C higher than the transition temperature of major lipids until the suspension becomes clear corresponding to unilamellar vesicles (between 5-10 min). Use water bath to control temperature and prevent overheating.

6. Filter the liposome suspension through a 0.2 μm filter (Acrodisc) to remove particles deposited during sonication.

7. Plasma clean substrate (parylene patterned surface) for ~10s to make surface hydrophilic.

Figure A.3: Cell activation with the patterned lipid bilayers containing DNP ligands. A) Cartoon representing RBL mast cells interacting with the patterned ligand array. FcεRI-IgE binding and clustering by the immobilized DNP molecules causes localized recruitment of signaling proteins such as Lyn kinase (zoomed box). B) Confocal images of RBL cells stimulated by ligand containing lipid patterns at 37°C for ~30 min. Distinctive local accumulation of Lyn kinase (upper) and actin (lower) shown in green can be visualized under the clustered FcεRI-IgE. Supported membranes (red) are labeled by adding 1 mol% Lissamine Rhodamine PE to the lipid mixture. Scale bar corresponds to 20 μm.

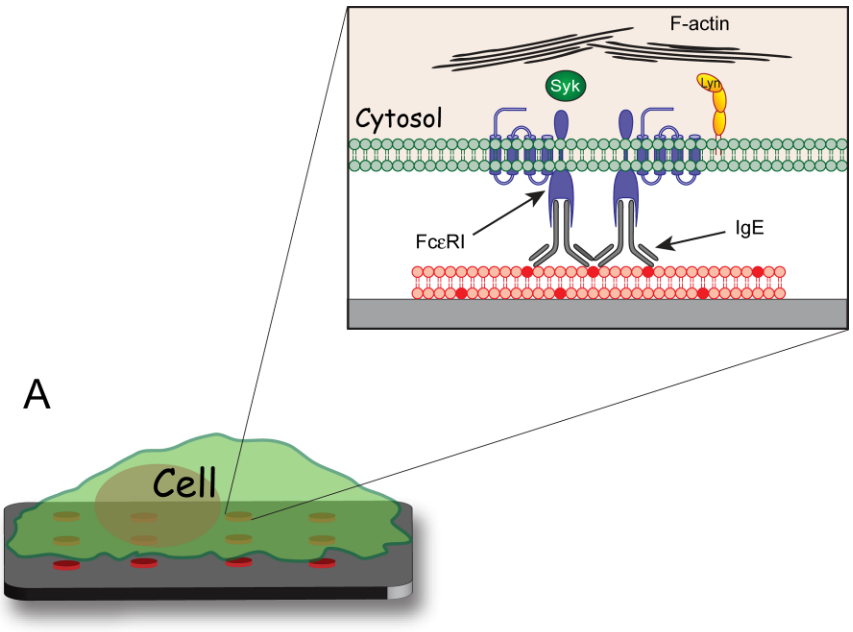
A
Cell
F-actin
Syk
Lyn
Cytosol
FcεRI
IgE

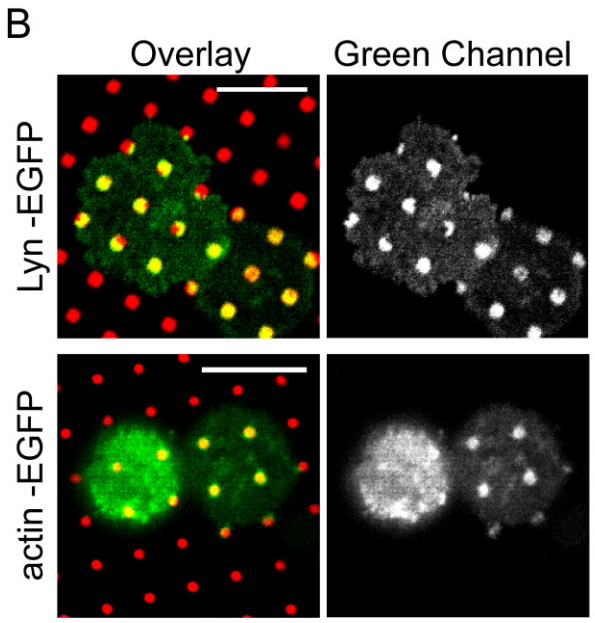
B
Overlay
Green Channel
Lyn -EGFP
actin -EGFP

8. Cut a piece of Parafilm M and place the patterned parylene substrate on the film, add lipid suspension, and incubate for ~10min. The hydrophobicity of the parafilm will cause the solution to remain on the substrate.

9. Fill four 100 x 50 mm crystallizing dishes with distilled de-ionized water.

10. Rinse the substrate vigorously in water iteratively in each of the crystallizing dishes. Use a small (35 x 10 mm or smaller) dish to transfer the substrate from each crystallizing dish to the other to avoid drying the surface and hence destroying the bilayer. After the second rinse, mechanically peel of the parylene layer with tweezers. This will yield supported lipid bilayers patterned on the substrate. Rinse once more with water (see **Note 7**).

11. Place the patterned substrate on the 35 x 10mm culture dish and replace water with BSS. Keep the substrate hydrated at all times.

12. Experiment with cells should ideally be done same day as lipid preparation (see **Note 8**).

A.3.3 Covalent ligand (attached to carrier protein) immobilization using silane chemistry (alternative method)

1. Rinse patterned parylene substrate gently with acetone and dry with nitrogen gas in a glass dish.

2. Prepare a 2% (v/v) solution of (3-mercaptopropyl)trimethoxysilane (MPTS) in toluene. Aminosilanes and their fumes are irritants and highly corrosive. The reactions must be done carefully in a chamical hood.

3. Incubate patterned parylene substrate with the MPTS solution for 20-30 minutes in the hood at room temperature in a glass dish to functionalize the surface with thiol groups. Rinse surface with acetone and dry using nitrogen or argon gas. When working with glass wafers, this reaction should be carried out before using adherents to attach the glass piece to the plastic dish (as described in step 3.1.13)

4. Rinse the surface with absolute ethanol and add the 2mM of the GMBS cross-linker solution in absolute ethanol for 1 hour (see **Note 9**).

5. Rinse substrate with phosphate buffer.

6. Immediately incubate patterned parylene substrate with 25-100 μg/ml of protein (DNP-BSA) in phosphate buffer for 2 hours (up to overnight).

7. Rinse with phosphate buffer to remove unbound protein.

8. Mechanically peel-off parylene under buffer to reveal the patterned protein and rinse the surface with buffer.

9. Block surface with PBS containing 10mg/mL BSA for 2 hours (up to overnight) to minimize nonspecific binding.

A.3.4 RBL-2H3 cell culture

1. Grow adherent RBL-2H3 cells in media to pre-confluence in 25 cm^2 flask in a 5% CO_2 incubator.

2. Harvest cells using trypsin solution to detach cells from the flask and resuspend in media or BSS at 0.5 x 10^6 cells/mL.

A.3.5 Cell transfection

1. Harvest the cells and resuspend at 1×10^7 cells per ml in electroporation buffer.

2. Mix ~5-10 μg of plasmid DNA with 500 μL cells suspension.

3. Electroporate cells by using an exponential pulse of 280 V and 950 μF in a 4-mm cuvette by using a Gene Pulser Xcell electroporator system.

4. Recover electroporated cells (avoid floating dead cell debris formed during electroporation), plate cells in medium at ~60% confluency and incubate at 37°C for 24 h (see **Note 10**).

A.3.6 Cell activation with patterned ligand

1. Sensitize cells by adding IgE to a final concentration of ~0.5 ug/mL and incubate for 1 hour keeping cells in suspension at 37°C (overnight incubation of attached cells

with IgE is also possible). Remove excess IgE by washing and resuspension in BSS containing 1 mg/mL BSA and resuspend cells at a concentration of ~0.5 x 10^6 cells/mL.

2. Place patterned substrate on 35 x 10 mm tissue culture dish and add ~ 1mL of cell suspension (see **Note 11**).

3. Incubate cells with the patterned substrate for 15-45 min at 37°C. It will take about 5 minutes for the cells to settle and begin attaching to the surface. For live cell imaging, skip steps 5-7 and immediately image cell using fluorescence microscope.

4. After the appropriate incubation time, rinse the cells with BSS to remove cells that are still in suspension.

5. Fix cells by adding 3.7% formaldehyde (in PBS) and incubate for 10 min. Remove fixative and quench reaction by adding PBS containing 10mg/mL BSA and incubate for 5min.

6. Rinse cells with PBS. Fixed cells can be stored at 4°C in PBS with 0.01% (w/v) NaN_3, to prevent microbial growth, for weeks.

7. Image cells using fluorescence microscope. If using inverted fluorescence microscope and patterned silicon substrate, turn substrate upside down inside a glass bottom dish filled with PBS buffer to visualize fluorescence features (see **Note 12**).

A.4 Notes

1. Piranha solution is extremely corrosive and reactive, and handling and disposal should be done with extreme caution (always use a hood and protective equipment). Some facilities may have access to automated wafer cleaning instrumentation such as the Hamatech Wafer Processor that are useful for reducing exposure to dangerous chemicals.

2. Fabrication on glass wafer is desired when a transparent substrate is required. For example, total internal reflection fluorescence microscopy (TIRFM) requires a transparent substrate for propagation of an evanescent wave. Fabrication of glass wafers involves the same steps as silicon wafers but can be more difficult because of the fragility and thickness of optical glass wafers, which are much thinner (0.16-0.19 mm) than standard silicon wafers (>0.4 mm). For confocal and epifluorescence imaging, silicon wafers are sufficient. In some confocal systems scattered light from the silicon surface can be visualized as background noise. This background noise is small compared to the signal obtained from the labeled cells and can be improved by collecting fluorescence from wavelength far from the excitation wavelength.
3. Many different options are available for photoresist and the choice will mainly depend on the desired feature size and the available instrumentation (i.e. i-line or g-line stepper). We found that both SPR 220-3.0 (i-line or g-line) and SPR 955 cm-2.1 (i-line) (Rohm and Haas Electronic Materials LLC, MA) work well with our fabrication scheme.
4. The optimal time for oxygen etching should be optimized experimentally. Ideally the majority of the ~1.6-2.0 μm photoresist layer should be consumed without exposing the parylene layer. This step is important because under etching will leave residual parylene on the patterns and over etching will consume the parylene layer. After etching the remaining thickness of the palylene features should be confirmed with a profilometer.
5. The lattice structure of the silicon wafers is responsible for its brittle nature. This property allows easy cutting of wafers by slightly scratching a corner with a diamond scribing tool and applying small pressure on both side of the scratch.

6. The ligands are chosen to be specific for the experimental setting. For other receptors the lipid composition may be changed, and other lipids with modified head groups may also be used for ligand presentation. For example, avitin-biotin interactions exploited by using biotinilated lipids. As an alternative to ligand presentation with supported lipid bilayers, an alternate method for covalently immobilizing ligands is presented in section 3.3.
7. Once the supported lipid bilayer has formed it is important to keep it hydrated. Exposure to air will destroy the supported lipid bilayer (*13*).
8. Although it may be possible to use the supported membranes days after preparation, it is recommended to use them within a few hours of preparation. Supported membranes tend to expand within hours of preparation in a pH and ionic strength dependent manner (*13*), and this will affect the quality of the patterned ligands.
9. After the MPTS covalently attaches to the silicon dioxide surface, its thiol group reacts specifically with the maleimide moiety on the GMBS cross-linker. This activates the surface with succinimide residues that can react with amine groups of an antibody or other protein to form stable amide bonds (*14, 15*).
10. Chemical tranfection methods may also be use to introduce GFP encoding DNAs into the cells. We chose to describe electroporation for its simplicity.
11. Although supported lipid bilayers are usually a better choice for preventing non-specific interactions, one advantage of covalent immobilization of proteins is that the modified surfaces can be stored for weeks at 4°C without significant loss of functionality and short periods of drying do not affect the immobilized ligand.
12. In cases where the protein to be investigated is not available as GFP fusion protein immunofluorescence microscopy can be used to detect proteins. In

such cases, fluorescent lipids cannot be used to visualize the patterned features because the detergent used to permeabilize cells (Triton X-100) partially dissolves the supported lipid bilayers. To overcome this technical limitation, fluorescently labeled anti-DNP IgE can be used to sensitize the cells and hence visualize the clustered receptors (see ref. (*11*) for example). Covalently immobilized protein carriers are not affected by permeabilizing reagents.

REFERENCES

1. Bruhns, P., Frémont, S., and Daëron, M. (2005) Regulation of allergy by Fc receptors, *Current Opinion in Immunology* ***17***, 662-669.
2. Nimmerjahn, F., Ravetch, J. V., and Frederick, W. A. (2007) Fc-Receptors as Regulators of Immunity, *Advances in Immunology* ***96***, 179-204, Academic Press.
3. Kraft, S., and Novak, N. (2006) Fc receptors as determinants of allergic reactions, *Trends in Immunology* ***27***, 88-95.
4. Kinet, J.-P. (1999) THE HIGH-AFFINITY IgE RECEPTOR (FceRI): From Physiology to Pathology, *Annual Review of Immunology* ***17***, 931-972.
5. Holowka, D., Gosse, J. A., Hammond, A. T., Han, X., Sengupta, P., Smith, N. L., Wagenknecht-Wiesner, A., Wu, M., Young, R. M., and Baird, B. (2005) Lipid segregation and IgE receptor signaling: A decade of progress, *Biochimica et Biophysica Acta (BBA) - Molecular Cell Research* ***1746***, 252-259.
6. Rivera, J., Fierro, N. A., Olivera, A., and Suzuki, R. (2008) New Insights on Mast Cell Activation via the High Affinity Receptor for IgE, *Advances in Immunology* ***98***, 85-120, Academic Press.
7. Orth, R. N., Wu, M., Holowka, D. A., Craighead, H. G., and Baird, B. A. (2003) Mast Cell Activation on Patterned Lipid Bilayers of Subcellular Dimensions, *Langmuir* ***19***, 1599-1605.
8. Wu, M., Holowka, D., Craighead, H. G., and Baird, B. (2004) Visualization of plasma membrane compartmentalization with patterned lipid bilayers, *PNAS* ***101***, 13798-13803.

9. Torres, A. J., Wu, M., Holowka, D., and Baird, B. (2008) Nanobiotechnology and Cell Biology: Micro- and Nanofabricated Surfaces to Investigate Receptor-Mediated Signaling, *Annual Review of Biophysics* ***37***, 265-288.

10. Kam, L., and Boxer, S. G. (2001) Cell adhesion to protein-micropatterned-supported lipid bilayer membranes, *Journal of Biomedical Materials Research* ***55***, 487-495.

11. Torres, A. J., Vasudevan, L., Holowka, D., and Baird, B. A. (2008) Focal adhesion proteins connect IgE receptors to the cytoskeleton as revealed by micropatterned ligand arrays, *PNAS* ***105***, 17238-17244.

12. Doh, J., and Irvine, D. J. (2006) Immunological synapse arrays: Patterned protein surfaces that modulate immunological synapse structure formation in T cells, *PNAS****103***, 5700-5705.

13. Cremer, P. S., and Boxer, S. G. (1999) Formation and Spreading of Lipid Bilayers on Planar Glass Supports, *The Journal of Physical Chemistry B* ***103***, 2554-2559.

14. Shriver-Lake, L. C., Donner, B., Edelstein, R., Breslin, K., Bhatia, S. K., and Ligler, F. S. (1997) Antibody immobilization using heterobifunctional crosslinkers, *Biosensors and Bioelectronics* ***12***, 1101-1106.

15. Vijayendran, R. A., and Leckband, D. E. (2000) A Quantitative Assessment of Heterogeneity for Surface-Immobilized Proteins, *Analytical Chemistry* ***73***, 471-480.